



Rational Formulation Design of Topical Tazarotene a Third-Generation Retinoid

Solomon Sherif

March 2023

**This thesis is submitted in accordance with the requirements of the
UCL School of Pharmacy for the degree of Doctor of Philosophy**

UCL School of Pharmacy

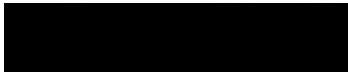
29-39 Brunswick Square

London WC1N 1AX

Declaration

This thesis describes research conducted at the University College London School of Pharmacy under the supervision of Dr Majella E. Lane. I, Solomon Sherif, confirm that the work presented in this thesis is my own. Where information has been derived from other sources, I confirm that this has been indicated in the thesis. I also certify that I have written all the text herein and have indicated by suitable citation any part of this dissertation that has already appeared in a publication.

Signature:

A solid black rectangular box used to redact the author's signature.

Date: 31/03/2023

Abstract

The skin acts as an essential barrier to the outside world through a complex structure of lipids and proteins making topical drug delivery a major challenge for formulation scientists. Retinoids are compounds that provide therapeutic benefits for a range of dermatological conditions by actioning on the retinoic acid receptor (RAR). First- and second-generation retinoids however are associated with unwanted side effects as a consequence of indiscriminate RAR targeting. Tazarotene was developed as a third-generation selective retinoid binding predominantly to the RAR- γ subunit, which is the primary target of retinoid therapy to increase efficiency and reduce the severity of or eliminate unwanted side effects. The lipophilic nature of tazarotene however prevents it from effectively penetrating the skin to exert its full effects. In this thesis, the physicochemical properties of tazarotene in a range of CPEs were characterised before using them to study the delivery of tazarotene into the skin both *in-vitro* and *in-vivo*. Franz diffusion cell studies were conducted with single solvents and a combination of binary or ternary solvent systems. Tape stripping of human volunteers using the best-performing formulations was performed. A novel Confocal Raman Spectroscopy (CRS) technique was used to non-invasively quantify tazarotene and detect CPE deposition in the skin.

Impact statement

Academic research should ideally contribute to the economy and wider society beyond academia, having an impact on the outside world. This can occur in several ways for example through the innovation of new products and diagnostic tools, enhancing the quality of life and health of a population or improving current public services and policy. The research presented in this thesis has demonstrated how the commercially available Zorac[®] gel formulation containing the API tazarotene can be reformulated into a new gel to enhance the topical drug delivery of tazarotene into the skin. This enhanced drug delivery could improve the efficiency of tazarotene in the clinic for a range of dermatological conditions including psoriasis, acne and photoaging as well as reduce or eliminate the occurrence of unwanted side effects typically associated with retinoid therapy. A pioneering CRS method was developed to non-invasively quantify tazarotene and detect CPE deposition into the skin in real-time. The revolutionary CRS technique used to develop this new method could be utilised by clinicians to non-invasively assess drug and/or excipient penetration into the skin from other topically applied formulations to study their effects on dermatological conditions in real-time. This could ultimately reduce the time, cost and discomfort of *in-vivo* skin analysis associated with more established invasive techniques such as tape-stripping.

Acknowledgements

Ever since I was a first-year pharmacy undergraduate student at the School of Pharmacy many years ago, I aspired to pursue a PhD research project not fully knowing the amount of hard work, dedication and persistence required. My PhD journey at times felt like a never-ending roller coaster ride but fortunately for me, there were many more highs than lows. I lived, laughed, learnt, and loved along the way with the help of some very special people. I'd like to first thank Dr Majella Lane for allowing me to pursue a PhD research project in her group and for her continuous support. Without her and Professor Jonathan Hadgraft's expert knowledge, this could not have been possible. I would also like to thank Professor Kevin Taylor, Professor Alex Thompson, Professor Ijeoma Uchegbu, Professor Anthony Smith and Dr Andrew Wilderspin for their invaluable guidance over the years at the School of Pharmacy. It was a pleasure being part of the UCL skin research group in lab 322 where I was fortunate enough to have amazing colleagues to work with and learn from. A special mention goes out to Fotis, Monjur, Ken, Yanling and Bruno for all the interesting scientific conventions we had, I will miss going to Skin Forum and other research conferences together. I want to thank all the staff at the UCL School of Pharmacy for doing a fantastic job supporting me and all the other PhD students, the School of Pharmacy could not function without you all.

Table of Contents

Declaration.....	2
Abstract.....	3
Impact statement.....	4
Acknowledgements.....	5
Table of Contents.....	6
List of Figures.....	10
List of Table.....	15
List of Symbols and Abbreviations.....	16
Symbols.....	16
Abbreviations.....	19
Chapter One.....	23
Introduction to retinoids, skin permeation and analysis.....	23
1.1 Skin physiology.....	23
1.1.1 Epidermis.....	24
1.1.2 Dermis.....	27
1.1.3 Hypodermis.....	28
1.1.4 Skin appendages.....	28
1.2 Skin disorders.....	29
1.2.1 Acne.....	29
1.2.2 Psoriasis.....	30
1.2.3 Photoaging.....	32
1.3 Retinoic acid receptor.....	32
1.4 Tazarotene: a third-generation topical retinoid.....	36
1.5 Pathways of percutaneous absorption.....	39
1.6 Passive enhancement strategies in topical delivery.....	44
1.7 Franz diffusion cell permeation and mass balance studies.....	46
1.8 Tape-stripping for drug penetration and SC protein analysis.....	50
1.9 Raman scattering and Confocal Raman Spectroscopy for non-invasive analysis.....	55
1.10 Aims and objectives.....	62

Chapter Two.....	65
Physiochemical characterisation and <i>in-vitro</i> HPLC evaluation of topical tazarotene formulations	65
2.1 Introduction	65
2.2 Materials and methods	68
2.2.1 Materials	68
2.2.2 Molecular modelling	69
2.2.3 HPLC method development and validation for tazarotene analysis	69
2.2.4 Solubility studies of tazarotene	71
2.2.5 Stability studies of tazarotene	72
2.2.6 Miscibility studies of CPEs.....	72
2.2.7 Tazarotene formulation preparation	73
2.2.8 Porcine skin preparation	74
2.2.9 Receptor fluid preparation.....	74
2.2.10 Mass balance validation.....	75
2.2.11 In-vitro infinite dose permeation studies of topical tazarotene formulations	76
2.2.12 Mass balance of topical tazarotene formulations	77
2.2.13 Data collection and statistical analysis of <i>in-vitro</i> results.....	78
2.3 Results and discussion	78
2.3.1 Molecular modelling calculations	78
2.3.2 HPLC method development and validation	83
2.3.3 Saturation solubility of tazarotene	92
2.3.4 Stability of tazarotene.....	96
2.3.5 Miscibility of CPE.....	97
2.3.6 Mass balance development and validation	101
2.3.7 Mass balance of topical tazarotene formulations	103
2.4 Conclusions	108
Chapter Three	111
In-vitro Confocal Raman Spectroscopy evaluation of topical tazarotene formulations.....	111
3.1 Introduction	111
3.2 Materials and methods.....	115
3.2.1 Materials	115
3.2.2 CRS instrument	115
3.2.3 Raman reference spectra collection and calibration	117

3.2.4 Tazarotene formulation preparation	118
3.2.5 Porcine skin preparation	118
3.2.6 <i>In-vitro infinite dose permeation</i> studies of topical tazarotene formulations.....	119
3.2.7 Data collection and statistical analysis of <i>in-vitro</i> results	120
3.3 Results and discussion	121
3.3.1 Raman reference spectra and calibration.....	121
3.3.2 Water content measurements and SC thickness.....	125
3.3.3 CRS studies of topical tazarotene formulations.....	128
3.4 Conclusions	144
Chapter Four	147
In-vitro LC-MS evaluation of topical tazarotene formulations	147
4.1 Introduction	147
4.2 Material and methods	150
4.2.1 Materials	150
4.2.2 LC-MS method development and validation for tazarotene analysis.....	150
4.2.3 Tazarotene formulation preparation	153
4.2.4 Human skin preparation	154
4.2.5 Receptor fluid preparation	155
4.2.6 Human skin integrity measurements.....	155
4.2.7 <i>In-vitro</i> finite dose permeation studies of topical tazarotene formulations	156
4.2.8 Mass balance of topical tazarotene formulations	157
4.2.9 Residence time studies of topical tazarotene gel formulations	158
4.2.10 Data collection and statistical analysis of <i>in-vitro</i> results	159
4.3 Results and discussion	159
4.3.1 LC-MS method developed & validation for tazarotene analysis	159
4.3.2 Mass balance of topical tazarotene formulations	165
4.4 Conclusions	176
Chapter Five	180
<i>In-vivo</i> LC-MS & CRS evaluation of topical tazarotene formulations.....	180
5.1 Introduction	180
5.2 Materials and methods.....	184
5.2.1 Materials	184
5.2.2 Volunteer recruitment	184

5.2.3 Tazarotene formulation preparation	185
5.2.3 Application of topical tazarotene formulations.....	186
5.2.4 Tape stripping procedure.....	186
5.2.5 TEWL measurements	186
5.2.6 SC Protein content measurements	187
5.2.8 LC-MS quantification of tazarotene on tape strips.....	188
5.2.9 CRS instrument	188
5.2.10 Data collection and statistical analysis of the <i>in-vivo</i> results.....	189
5.3 Results and discussion	190
5.3.1 Tape stripping of topical tazarotene formulations	190
5.3.2 CRS of topical tazarotene formulations	195
5.4 Conclusions	203
Chapter Six	207
6.1 Overall conclusions	207
6.2 Future work.....	211
References	213

List of Figures

Figure 1.1 Anatomy of the skin, epidermis, dermis, appendices, and subcutaneous tissue.....	23
Figure 1.2 Schematic illustration of the different layers found within the epidermis.....	24
Figure 1.3 The three routes of permeation, appendageal, intercellular and transcellular.....	38
Figure 1.4 Partition and diffusion during percutaneous absorption of a solute through the SC.....	39
Figure 1.5 Schematic representation of the vertical Franz diffusion cell for <i>in-vitro</i> studies.....	45
Figure 1.6 A complete Confocal Raman instrumentation set-up used for real-time <i>in-vivo</i> skin measurements.....	57
Figure 2.1 HPLC Linear calibration curve of tazarotene.....	81
Figure 2.2 Saturation solubility of tazarotene in a range of vehicles.....	90
Figure 2.3 Saturation solubility of tazarotene in PBS, BSA + PBS and BrijO20 [®] + PBS.....	92
Figure 2.4 Saturation solubility of tazarotene in BrijO20 [®] + PBS at increasing concentrations.....	93
Figure 2.5 Stability of tazarotene in a range of vehicles over 24 h.....	94
Figure 2.6 Stability of tazarotene in methanol over 24 h.....	98
Figure 2.7 Mass balance validation of tazarotene.....	99
Figure 2.8 Infinite dose mass balance study of single solvents containing tazarotene applied to porcine skin after 24 h	101
Figure 2.9 Infinite dose mass balance study of the commercial Zorac [®] gel formulation and binary solvent systems containing tazarotene applied to porcine skin after 24 h.....	102
Figure 2.10 Infinite dose mass balance study of the commercial Zorac [®] gel formulation, ternary and quaternary solvent systems containing tazarotene applied to porcine skin after 24 h.....	103

Figure 3.1 Raman fingerprint region spectra of keratin in porcine skin.....	118
Figure 3.2 Raman fingerprint region spectra of HG, PG, TC, IPM and IPA.....	119
Figure 3.3 Raman fingerprint region spectra of tazarotene in ethanol at 0.1%, 0.3%, 0.5%, 0.8% and 1%.....	120
Figure 3.4 Raman ratio vs mass ratio of tazarotene calibration curve.....	122
Figure 3.5 Raman high wavelength region spectra of water and protein bands in porcine skin.....	123
Figure 3.6 Water content profile of porcine skin with model fitting SC thickness....	124
Figure 3.7 Semi-quantitative depth profiles of tazarotene in the commercial Zorac [®] gel formulation, HG:TC, PG:TC, HG:PG, HG:PG:TC and HG:IPM:IPA.....	126
Figure 3.8 Normalised SC depth profiles of tazarotene in the commercial Zorac [®] gel formulation, HG:TC, PG:TC, HG:PG, HG:PG:TC and HG:IPM:IPA	126
Figure 3.9 Quantitative mass ratio depth profiles of tazarotene in the commercial Zorac [®] gel formulation, HG:TC, PG:TC, HG:PG, HG:PG:TC and HG:IPM:IPA	127
Figure 3.10 Concentration depth profiles of tazarotene in the commercial Zorac [®] , HG:TC, PG:TC, HG:PG, HG:PG:TC and HG:IPM:IPA	128
Figure 3.11 Normalised AUC of tazarotene in the skin from the commercial Zorac [®] , HG:TC, PG:TC, HG:PG, HG:PG:TC and HG:IPM:IPA.....	129
Figure 3.12 Proportion of tazarotene above and below a skin depth of 7 μ m from the commercial Zorac [®] , HG:TC, HG:PG, PG:TC, HG:PG:TC, and HG:IPM:IPA	130
Figure 3.13 Semi-quantitative depth profiles of HG in the commercial Zorac [®] , HG:TC, HG:PG, HG:PG:TC, and HG:IPM:IPA	132
Figure 3.14 Normalised depth profiles of hexylene glycol in the commercial Zorac [®] , HG:TC, HG:PG, HG:PG:TC and HG:IPM,	133
Figure 3.15 Normalised AUC of HG in the SC from the commercial Zorac [®] , HG:TC, HG:PG, PG:TC, HG:PG:TC and HG:IPM:IPA	133
Figure 3.16 Proportion of HG above and below a skin depth of 7 μ m from the commercial Zorac [®] gel formulation, HG:TC, HG:PG, HG:PG:TC and HG:IPM:IPA	134

Figure 3.17 Correlations between the amount of tazarotene and HG found in the SC	135
Figure 3.18 Semi-quantitative depth profiles of propylene glycol in PG:TC, HG:PG, and HG:PG:TC	137
Figure 3.19 Normalised depth profiles of PG in PG:TC, HG:PG, and HG:PG:TC	137
Figure 3.20 Normalised AUC of PG in the SC from PG:TC, HG:PG, PG:TC, and HG:PG:TC	138
Figure 3.21 Proportion of PG above and below a skin depth of 7 μm from PG:TC, HG:PG and HG:PG:TC	139
Figure 3.22 Correlation of normalised AUC of PG and tazarotene vehicle depth profiles.....	140
Figure 4.1 LCMS Linear calibration curve of tazarotene.....	157
Figure 4.2 Finite dose mass balance study of binary solvent systems containing tazarotene compared with commercial formulation from human epidermal skin after 24 h permeation experiments.....	162
Figure 4.3 Permeation profile of tazarotene from the commercial Zorac [®] gel formulation and binary solvent systems PG:TC and HG:TC after application to human epidermal skin.....	163
Figure 4.4 Percentage of tazarotene permeated through the skin from the commercial Zorac [®] gel formulation and binary solvent systems PG:TC and HG:TC after application to human epidermal skin.....	164
Figure 4.5 Finite dose mass balance study of ternary solvent systems containing tazarotene compared with the commercial Zorac [®] gel formulation from human epidermal skin after 24 h permeation experiments.....	165
Figure 4.6 Permeation profile of tazarotene from the commercial Zorac [®] gel formulation and ternary solvent systems after application to human epidermal skin.....	166
Figure 4.7 Percentage of tazarotene permeated through the skin from the commercial Zorac [®] gel formulation and ternary solvent systems HG:IPM:IPA and HG:PG:TC after application to human epidermal skin.....	167
Figure 4.8 In-vitro correlation of LC-MS human skin extractin amounts and the total amount of tazarotene detected in porcine skin by CRS from the commercial Zorac [®] gel formulation, PG:TC, HG:TC, HG:PG:TC and HG:IPM:IPA.....	167

Figure 4.9 Finite dose mass balance study of an in-house gel containing HG:TC and tazarotene compared with the commercial Zorac [®] gel formulation formation from human epidermal skin after 24 h permeation experiments.....	168
Figure 4.10 Permeation profile of tazarotene from the commercial Zorac [®] gel formulation and in-house gel formulations after application to human epidermal skin.....	169
Figure 4.11 Percentage of tazarotene permeated through the skin from the commercial Zorac [®] gel formulation and in-house gel formulations after application to human epidermal skin.....	170
Figure 4.12 Percentage weight loss of the commercial Zorac [®] gel formulation and in-house gel under static conditions 50% RH and 32°C after application of 5µL on a quartz pan over 24 h.....	171
Figure 5.1 Concentration of tazarotene delivered into the SC from HG:TC solution and in-house gel.....	186
Figure 5.2 Changes in TEWL of tape-stripped healthy volunteers' forearms after application of the HG:TC solution and in-house gel.....	187
Figure 5.3 Amount of SC protein removed from the forearm of healthy volunteers after application of HG:TC solution and in-house gel.....	188
Figure 5.4 Pooled amount of SC protein removed from the forearm of healthy volunteers after application of HG:TC solution and in-house gel.....	189
Figure 5.5 Correlation between the concentration of tazarotene and amount of SC removed from the forearm of healthy volunteers after application of HG:TC solution and in-house gel.....	190
Figure 5.6 Water content profile from the forearm of a healthy volunteer with model fitting to calculate SC thickness.....	191
Figure 5.7 Quantitative depth profiles of tazarotene in the HG:TC solution and in-house gel from the forearm of a healthy volunteer.....	192
Figure 5.8 Concentration depth profiles of tazarotene in the HG:TC solution and in-house gel from the forearm of a healthy volunteer.....	193
Figure 5.9 Normalized depth profiles of tazarotene in the HG:TC solution and in-house gel from the forearm of a healthy volunteer.....	194
Figure 5.10 Proportion of tazarotene above and below a skin depth of 7 µm in the HG:TC solution and in-house gel from the forearm of a healthy volunteer.....	195

Figure 5.11 Total amount of tazarotene delivered into the forearm of a healthy volunteer from the HG:TC solution and in-house gel.....196

Figure 5.12 Correlation between the amount of tazarotene in the SC detected in-vivo by CRS and LC-MS delivered from the HG:TC solution and in-house gel197

List of Table

Table 1.1 Physicochemical properties of tazarotene.....	36
Table 2.1 Hildebrand and Hansen solubility parameters for tazarotene.....	77
Table 2.2 Hildebrand and Hansen solubility parameters for a range of vehicles.....	78
Table 2.3 HPLC peak areas of tazarotene at different concentrations.....	81
Table 2.4 HPLC accuracy results for tazarotene.....	83
Table 2.5 HPLC Interday variability results for tazarotene.....	85
Table 2.6 HPLC Intraday variability results for tazarotene.....	85
Table 2.7 Robustness results for varied HPLC conditions.....	86
Table 2.8 HPLC System suitability results for tazarotene.....	89
Table 2.9 Miscibility of PG with TC, PGMC, PGML, PGDC, MTC, IPM, DiPG in 0.1% tazarotene at room temperature.....	97
Table 2.10 Miscibility of HG with TC, PGMC, PGML, PGDC, MTC, IPM, DiPG in 0.1% tazarotene at room temperature.....	97
Table 4.1 LC-MS peak areas of tazarotene at different concentrations.....	157
Table 4.2 LC-MS accuracy results for tazarotene.....	158
Table 4.3 LC-MS Intra-day variability results for tazarotene.....	159
Table 4.4 LC-MS Inter-day variability results for tazarotene.....	159
Table 4.5 Robustness results for varied LC-MS conditions.....	160
Table 4.6 LC-MS System suitability results for tazarotene.....	161

List of Symbols and Abbreviations

Symbols

\bar{x}	Arithmetic mean of a sample
$C_{\text{BSA:protein}}$	BSA:protein proportionality constant
$C_{\text{BSA:water}}$	BSA:water proportionality constant
∂C	Change in concentration of permeant
ΔH_m	Change in enthalpy
∂x	Change in membrane thickness
γ_A	Concentration of material A
k_p	Coefficient of permeability
γ_{protein}	Concentration of protein
C_{app}	Concentration of solute applied to the skin
$\gamma_{\text{Tazarotene}}$	Concentration of tazarotene
$^{\circ}\text{C}$	Degree Celsius
ρ_i	Density
$\rho_{\text{dry SC}}$	Density of dry stratum corneum
ρ_{water}	Density of water
A	Diffusion area
D	Diffusion coefficient
h	Diffusion path length or hour
c_D	Donor compartment API concentration
$V_{\text{day SC}}$	Dry stratum corneum volume
ΔS_m	Entropy of mixing components
$C_{\text{ethanol:water}}$	Ethanol:water proportionality constant

J	Flux of the permeant
ΔG_m	Gibbs free mixing enthalpy
ΔH_v	Heat of vaporization
RT	Ideal gas constant
x_i	i^{th} observation of the variable X
t_{lag}	Lag time
$m_{\text{dry SC}}$	Mass of dry stratum corneum
m_{material}	Mass of material
m_A	Mass of material A
m_{protein}	Mass of protein
m_{solvent}	Mass of solvent
m_{water}	Mass of water
γ_{material}	Material concentration
$C_{\text{material:solvent}}$	Material:solvent proportionality constant
V	Measurement volume
T_0	Melting point of API
X_2	Molar fraction
ΔH_f	Molar heat of fusion
V_m	Molar volume
V_2	Molar volume of API
$K_{o/w}$	Octanol/water partition coefficient
K	Partition coefficient
C_{Protein}	Protein content
R_{material}	Raman material signal
R_{protein}	Raman protein signal
R_{Solvent}	Raman solvent signal

$R_{\text{Tazarotene}}$	Raman tazarotene signal
c_R	Receptor compartment API concentration
S	Slope of the calibration curve
δ	Solubility parameter
δ_d	Solubility parameter of dispersion
δ_p	Solubility parameter of electrostatic forces
δ_h	Solubility parameter of hydrogen bonding
γ_{solvent}	Solvent concentration
σ	Standard deviation
J_{ss}	Steady-state flux of the permeant
$\sum_{i=1}^N$	Summation of all X_i values in a sample
$C_{\text{tazarotene:ethanol}}$	Tazarotene:ethanol proportionality constant
T	Temperature in degrees Kelvin
M_A	Total amount of material A per skin surface area
M_A	Total amount of material A per unit area
M_{water}	Total amount of water per unit area
R	Universal gas constant
Φ_1	Volume fraction of vehicle
W_{water}	Water concentration
γ_{water}	Water concentration in the stratum corneum
V_{water}	Water volume

Abbreviations

AU	Absorbance unit
ACN	Acetonitrile
AP-1	Activator protein-1
API	Active Pharmaceutical Ingredient
ANOVA	Analysis of variance
AUC	Area under the curve
BL	Basal lamina
BSA	Bovine serum albumin
BG	Butylene glycol
CRABR	Cellular retinoic binding receptor
cm	Centimetre
CCD	Charge coupled device
CPE	Chemical penetration enhancer
CRS	Confocal Raman Spectroscopy
R ²	Correlation coefficient
Da	Dalton
DNA	Deoxyribonucleic acid
DSC	Differential scanning calorimetry
DiPG	Dipropylene glycol
DVS	Dynamic vapour sorption
EtOH	Ethanol
GC	Gas chromatography
g	Gram
HG	Hexylene glycol

HPLC	High-performance liquid chromatography
IRD	Infrared densitometry
IPA	Isopropyl alcohol
IPM	Isopropyl myristate
kΩ	Kiloohm
LOD	Limit of detection
LOQ	Limit of quantification
LCMS	Liquid chromatography-mass spectrometry
log	Logarithm
MS	Mass spectrometry
MTC	Medium chain triglycerides
MP	Melting point
MeOH	Methanol
μg	Microgram
μL	Microliter
μm	Micrometre
mg	Milligram
mL	Millilitre
min	Minute
M	Molar
mol	Mole
MW	Molecular weight
ng	Nanogram
nm	Nanometre
NMF	Natural Moisturizing Factor
pKa	Negative logarithm of the acid dissociation constant

P	Partition coefficient
PBS	Phosphate buffered saline
BrijO	Polyoxyethylene oleyl ether
PTFE	Polytetrafluoroethylene
pH	Potential of hydrogen
p	Probability value
PG	Propylene glycol
PGDC	Propylene glycol dicaprylocaprate
PGMC	Propylene glycol monocaprylate
PGML	Propylene glycol monolaurate
RSD	Relative standard deviation
RAR	Retinoic acid receptor
RXR	Retinoid X receptor
rpm	Revolutions per minute
n	Sample size
SB	Stratum basale
SC	Stratum corneum
SG	Stratum granulosum
SS	Stratum spinosum
TC	Transcutol
TEWL	Transepidermal water loss
UHPLC	Ultra-High-Performance Liquid Chromatography
UV	Ultraviolet
UV-VIS	Ultraviolet-visible
v/v	Volume per volume
w/v	Weight per volume

Chapter One:

Introduction to retinoids,
skin permeation and analysis

Chapter One

Introduction to retinoids, skin permeation and analysis

1.1 Skin physiology

The skin is the largest organ in the human body with an average surface area of 1.8 m² representing approximately 10% of its total mass. It consists of three distinct layers, the epidermis, dermis, hypodermis or subcutaneous tissue, and several appendices such as hair follicles, sebaceous glands, eccrine and apocrine sweat glands illustrated in figure 1.1 (Wickett and Visscher 2006, Hadgraft and Lane 2011).

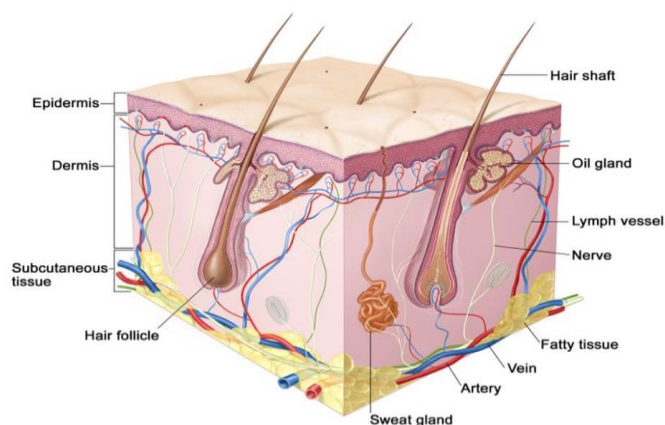


Figure 1.1 Anatomy of the skin, epidermis, dermis, appendices, and subcutaneous tissue. © 2008 Terese Winslow

The skin controls the inward and outward passage of water and electrolytes, regulates body temperature and blood pressure, and serves as a significant sensory organ mediating external stimuli in the form of pressure, injury, discomfort, pain and temperature and humidity changes. Additionally, the skin's main function is to act as a barrier between the "internal" and "external" environment of a human being, protecting against microorganisms, UV radiation, and unwanted xenobiotics.

However, this function, as it will be discussed later, also makes drug delivery to and through this organ a major challenge.

1.1.1 Epidermis

The epidermis, the skin's outer layer, is a stratified avascular tissue that varies in thickness, going from 0.8 mm on the palms, to 0.06 mm on the eyelids. The epidermis's main cell type is the keratinocyte, which undergoes a maturation process involving migration from the proliferative to the outermost epidermal layer (Menon, Cleary et al. 2012).

Figure 1.2 illustrates how the four histologically different layers can be characterized based on the various stages of keratinocyte maturation in the epidermis.

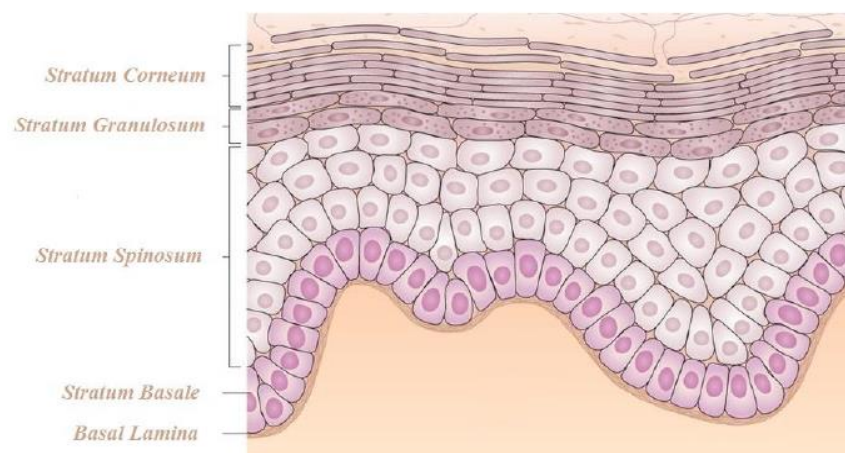


Figure 1.2 Schematic illustration of the different layers found within the epidermis (Solanas and Benitah 2013).

The stratum basale (SB), or basal layer, is directly attached to the basal lamina (BL). It is the innermost layer of the epidermis and consists mainly of columnar keratinocytes, which receive regulatory signals from the basal lamina via connections known as hemidesmosomes. Basal cell mitosis causes keratinocytes to

progressively migrate to the surface of the skin. This process is important for epidermal turnover and is balanced by corneocyte loss from the stratum corneum (SC) to maintain a consistent thickness in healthy skin. A small proportion of the basal layer is comprised of melanin-producing cells, melanocytes. Melanin accumulates in melanosomes that are then transferred to adjacent keratinocytes, which provide pigmentation and protection against UV light (Wickett and Visscher 2006).

Langerhans cells are also present in the SB. These are dendritic cells derived from the bone marrow that can come into contact with antigens, migrate and present to T lymphocytes in the lymph nodes of the skin, thus becoming involved in contact sensitization (Walters 2002). The keratinocytes change their shape from columnar to polygonal in the stratum spinosum (SS) or prickle cell layer and maintain their cell-to-cell connections through a high number of desmosomes, thus giving them a spiny appearance. The synthesis of cellular keratin filaments begins in the SB with the first lipid-enriched lamellar bodies beginning to appear. The keratinocytes in the upper part of the SS begin to flatten and elongate, indicating the transition to a stratum granulosum (SG) that further increases protein and lipid production (Menon 2002, Wickett and Visscher 2006).

The SG, or granular layer, is mainly defined by the existence of multiple keratohyalin granules comprising of hydrolytic enzymes, loricrin, profilaggrin and keratin. As the keratinocytes move upward, the lipid-enriched lamellar bodies, comprising primarily of phospholipids, glycolipids, cholesterol and lipases, merge with the cell membrane and discharge their contents into the intercellular space where the lipase's enzymatic activity contributes to the development of a mixture of ceramides, cholesterol, and

fatty acids. The release of lysing enzymes allows the nuclei and other keratinocyte cytoplasmic organelles to weaken and thus become more flattened and compacted (Wertz 2000, Menon 2002).

The result of keratinocyte differentiation is the SC or horny layer, the outermost layer of the skin, which is the one responsible for its barrier properties. The SC consists of flattened, anucleate, non-viable, polygonal, terminally differentiated corneal keratinocytes, known as corneocytes, which are tangentially piled to the surface of the skin, of 15 - 25 layers forming an approximately 15 - 20 μm thick barrier, depending on the anatomical location of the body (Bommannan, Potts et al. 1990). Corneocytes are composed of approximately 70% keratin and 20% lipids, bound by corneodesmosomes and enclosed in highly cross-linked corneal envelopes. These resistant structures replace cell membranes and consist mainly of loricrin from keratohyalin granules interconnected to other intracellular proteins such as involucrin, small proline – rich protein and keratin, and ceramide on its surface (Bommannan, Potts et al. 1990, Wickett and Visscher 2006, Menon, Cleary et al. 2012).

Corneocytes also contain several low molecular weight, hygroscopic and water-soluble amino acids, amino acid derivatives and salts called the natural moisturizing factor (NMF), derivatives from filaggrin degradation. NMF is unique in the stratum corneum and can represent up to 10 % of the dry weight of the corneocyte. Its primary role is to act as a moisturizer, absorb atmospheric water and maintain the corneal hydration of the stratum, thereby maintaining its strength and providing an aqueous environment needed for enzymatic activity (Rawlings, Scott et al. 1994, Kezic, Kemperman et al. 2008).

Although the SC is made up of nonviable cells, it should not be considered to be inert since multiple enzymatic metabolic interactions occur within this layer. The highly effective barrier function of the SC is a function of its components, which are mainly proteins on a dry weight basis, accounting for approximately 75 - 80% of the composition, and a complex lipid mixture (MaoQiang, Feingold et al. 1996). The largest proportion of protein content in the SC consists of corneocyte intracellular proteins and the cornified envelopes discussed above. The intercellular lipid mixture is organised in multiple bilayers characterised by the absence of phospholipids and triglycerides and mainly composed of ceramides (37-41%), cholesterol (27-32%), cholesteryl esters (10 - 15%), and fatty acids (9-16%) (Downing, Stewart et al. 1987, Norlen, Nicander et al. 1999).

The composition of the SC lipid also shows site-dependent and wide inter-individual variations. A simplistic two-phased model, which is described as a distribution of hydrophilic protein in a continuous lipid matrix, may be used to describe the structure of the stratum corneum. This concept was the first to compare the stratum corneum with a brick wall, where the corneocytes are the bricks embedded in a mortar of intercellular lipids (Lampe, Williams et al. 1983, Norlen, Nicander et al. 1999)

1.1.2 Dermis

The corneum or dermis lies between the basal lamina and the hypodermis and is about 1-5 mm thick and about 20-30 times thicker than the epidermis it supports. It is an extremely vascularized tissue that regulates blood pressure and temperature, provides oxygen and skin nutrients, removes waste materials, mounts immune responses, and manages wound healing. It consists mainly of collagen, elastin and

glycosaminoglycan, a hard and supportive matrix which is collectively referred to as the extracellular matrix and produced by the fibroblasts, the principal cells of the layer (Menon 2002). Lymph and blood vessels, nerve cells and fibres, skin appendages and small amounts of muscle are embedded within the extracellular matrix. The dermis is divided into a thin papillary layer and a thick reticular layer. The papillary layer lies beneath the epidermis and connects it to the dermis. It contains thin, loosely arranged fibres of collagen. In the deeper reticular layer, thicker bundles of collagen run parallel to the skin surface, extending from the base of the papillary layer to the subcutaneous tissue (Menon 2002, Walters 2002).

1.1.3 Hypodermis

The skin's innermost layer is the hypodermis or subcutaneous tissue. Except for the eyelids and male genitalia, it is present all over the body. Its cells produce and accumulate large amounts of lipids and are organized into lobules that are supported by bundles of collagen fibres so that the underlying structure and the overlying skin layers are flexibly linked. The principal functions of the subcutaneous tissue are heat insulation and mechanical shock absorption, as well as the storage of a readily available caloric source (Menon 2002, Walters 2002).

1.1.4 Skin appendages

Several appendages are found in human skin, including hair follicles, sebaceous glands, eccrine and apocrine sweat glands, and nails. Except on palms, soles and lips, the hair follicles are distributed throughout the surface of the skin. Epidermal invagination occurs in the dermis where the hair shaft is formed, composed of tightly bonded horny cells with high keratinisation. Each hair follicle is associated with a

smooth muscle, which can build the hair shaft in response to external stimulation, and sebaceous glands (Menon 2002, Walters 2002).

Sebaceous glands are located primarily on the chest, back, face and scalp, and lubricate the surface of the skin with a mixture of lipids, known as sebum, consisting mostly of free fatty acids and triglycerides. Eccrine sweat glands are found on the whole surface of the skin and are situated in the dermis where they secrete a dilute saline solution that reaches the surface of the skin via a duct. Secretion is stimulated by factors relating to body temperature control and emotional stress (Menon 2002, Walters 2002). Apocrine sweat gland distribution is limited to the armpits, nipples, and anal and genital areas. Usually associated with hair follicles, they are activated by emotional stresses that induce the secretion of fluid rich in proteins, lipids, and sugars that are metabolized by surface bacteria.

Nails are comprised of flattened, highly keratinized cells which are strongly connected to form dense elastic plates. These cells are derived from the reproductive matrix and are spread distally to the nail bed, rich in blood and nerve supply and protecting it from injuries (Menon 2002, Walters 2002).

1.2 Skin disorders

1.2.1 Acne

Acne vulgaris is the most common dermatological condition with a prevalence of 80–85% among adolescents. Acne develops in a pilosebaceous unit and involves several processes. The exact sequence of events leading to acne progression is still

not fully understood, but the most significant pathophysiological factors include sebaceous hyperplasia with hyperseborrhea, changes in growth and differentiation of follicular keratinocytes, cutibacterium acnes follicular colonisation, and immune reactions. These processes impair the functioning of the pilosebaceous unit, leading to the formation of microcomedones, comedones and inflammatory lesions (Bhate and Williams 2013, Byrd, Belkaid et al. 2018).

Retinoids play a vital role in the treatment of acne because they inhibit the formation and decrease the number of non-inflammatory microcomedones that are precursors to inflammatory acne lesions. They do this by normalizing follicular differentiation and by preventing the hyperkeratotic blockage of the pilosebaceous duct (Anja, B. et al. 2008, Thielitz and Gollnick 2008, Leyden, Stein-Gold et al. 2017). Tazarotene has shown excellent efficacy in the treatment of acne but is currently only licenced in the USA (Gregoriou, Kritsotaki et al. 2014)

1.2.2 Psoriasis

Psoriasis is a genetic disease of the immune system that affects people of every age. The most common form of the disease, representing approximately 90% of all cases, is psoriasis vulgaris also known as plaque psoriasis. The hallmark of vulgar psoriasis is elevated, red and scaling lesions known as plaques. Plaques are usually 2-3 mm higher over the surface of the skin, and psoriasis has a well-defined border,

unlike other inflammatory lesions. Any skin site can be affected; however, typical locations include the extensor surfaces of the forearm and shins, perianal, periumbilical, and retro-auricular regions and the scalp (Krueger and Bowcock 2005, Boehncke and Schön 2015).

Plaques can be localized in small areas or extend over the entire body in the most extreme cases. Patients experience pain, itch and sometimes even bleeding. In the psoriatic epidermis, keratinocyte proliferation and maturation occur so rapidly that terminal differentiation is incomplete. Therefore, keratinocytes retain intact nuclei and release very few extracellular lipids normally used as the “mortar” between corneocytes for adhesion. A poorly formed SC barrier results in the characteristic scales or flakes seen in psoriatic lesions. In Europe and North America, psoriasis prevalence is roughly 2% where approximately 70-80% of patients have mild forms of the disease which can be managed by topical treatments alone (Krueger and Bowcock 2005, Boehncke and Schön 2015).

Topical retinoid treatments have proven to be particularly effective in managing plaque psoriasis as a monotherapy. The use of first- generation retinoids, namely all-trans retinoic acid (tretinoin) and 13-cis-retinoic acid (isotretinoin) have shown efficacy in plaque psoriasis, however, due to their non-specific interactions with

retinoic acid receptors they have been associated with a substantial amount of unwanted side effects (Warren and Khanderia 1989, van de Kerkhof 2006).

Tazarotene is the first of a new generation of selective retinoids developed for the topical treatment of psoriasis. Tazarotene has been shown to modulate major pathogenic factors in psoriasis, including abnormal keratinocyte differentiation, keratinocyte hyperproliferation, and dermal and epidermal inflammatory infiltration (Weinstein 1997, Koo, Behnam et al. 2003, Weindl, Roeder et al. 2006).

1.2.3 Photoaging

UV irradiation from the sun has deleterious effects on human skin, including sunburn, immune suppression, cancer, and premature ageing. Sunburn and immune suppression occur acutely in response to excessive exposure to the sun, whereas skin cancer and photoaging result from accumulated damage caused by repeated exposures. skin cancer, the most prevalent form of cancer in humans, typically occurs in skin that is photoaged. Photoaged skin is characterized by wrinkles, laxity, uneven pigmentation, brown spots, and a leathery appearance. In contrast, chronologically aged skin that has been protected from the sun is thin and has reduced elasticity but is otherwise smooth and unblemished. Histologic and ultrastructural studies have shown that alterations in photoaged skin are found in dermal connective tissue (Han, Chien et al. 2014, Poon, Kang et al. 2015)

The dermis lies below and provides mechanical support for the outer, protective layer of skin, the epidermis. The extracellular matrix in the dermis is composed

primarily of type I collagen, with lesser amounts of type III collagen, elastin, proteoglycans, and fibronectin. Collagen fibrils are responsible for the strength and resiliency of the skin. Dermal damage induced by ultraviolet irradiation is principally manifested histologically as the disorganization of collagen fibrils and the accumulation of abnormal elastin-containing material(Han, Chien et al. 2014). From the molecular level UV-A radiation triggers activator protein-1(AP-1) to be produced resulting in the upregulation of Matrix metalloproteinases (MMPs) which then degrades collagen and other extracellular matrix components to produce wrinkles. Biochemical evidence of connective tissue alterations in photoaged skin includes reduced levels of types I and III collagen precursors and cross-links, an increased ratio of type III to type I collagen, and an increased level of elastin(Tanveer, Rashid et al. 2023).

This has led to the belief that the aged appearance of sun-exposed skin results from alterations in the structure and composition of collagen and elastin in the dermal extracellular matrix. Topical retinoids can improve photoaging by stimulating an increase in epidermal proliferation causing epidermal thickening, tightening the packing of stratum corneum proteins and promoting the biosynthesis and deposition of the glycosaminoglycans. Tazarotene has demonstrated its ability to strongly antagonize AP-1 production and subsequent upregulation of MMPs. Tazarotene also inhibits ornithine decarboxylase and activates tazarotene-inducible genes (TIGs) tumour suppressor genes that promote activation of G protein-coupled receptor kinase 5 (GRK5). As a result, it improves fine wrinkles, epidermal thickness, elastosis, lentiginos and hyperpigmentation with only mild adverse events at higher concentrations(Riahi, Bush et al. 2016, Pedersen, Voorhees et al. 2019).

1.3 Retinoic acid receptor

Retinoids exert their actions through hormone-like receptors located in the cytoplasm via the cellular retinoic acid binding receptor (CRABR) and two types of nuclear hormone receptors, retinoid acid receptors (RARs) and retinoid X receptors (RXRs). The binding of retinoids to CRABR is however not required to produce biological effects such as keratinocyte differentiation. Instead, CRABR binding may regulate the intracellular quantity of retinoic acid or act as a retinoic acid feedback mechanism. RARs and RXRs are further classified into three distinct subunits α , β and γ . In human skin, RAR- β is mainly located in the dermis whereas both RAR- γ and RAR- α are found primarily in the epidermis (Blomhoff and Blomhoff 2006, Zasada and Budzisz 2019). Retinoic acid (RA) signalling is reliant on cells that can metabolize retinol to RA. RA is released from RA-generating cells resulting in their uptake by neighbouring cells. Signalling is considered to be paracrine, even though RA functions itself is autocrine during spermatogenesis. During RA signalling the transduction involves binding of RA to a nuclear RAR that forms a heterodimer complex with retinoid X receptor (RXR). Both RAR and RXR display a high degree of cooperativity in binding to target DNA. RARs are required to bind with RXRs to ensure effective DNA binding and function. In addition, RXRs can form homodimers in addition to stable heterodimers with hormone receptors other than RARs, such as

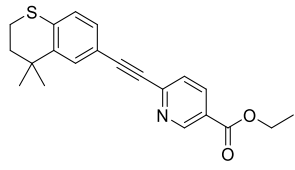
thyroid hormone receptors and vitamin D₃ receptors (Blomhoff and Blomhoff 2006, Zasada and Budzisz 2019). Activation of RARs or RXRs regulates gene transcription by binding directly to promoter regions of specific genes. RAR–RXR controls transcription by binding to DNA at an RA response element (RARE) located in enhancer regions specific to RA target genes (Cunningham and Duester 2015). Almost all retinoid-induced differentiation is associated with this mechanism. Alternatively, retinoid binding to RARs or RXRs can result in an inactive complex blocking the transcriptional effect of nuclear transcription factors such as AP1. AP1 regulates the transcription of many genes relating to proliferation and inflammation. The anti-proliferative and anti-inflammatory effects of retinoids are primarily mediated by this mechanism(Blomhoff and Blomhoff 2006, Zasada and Budzisz 2019). RARs function by enhancing the transcription of specific genes in the presence of retinoic acid or other retinoid agonists. The RA receptors influence a wide range of physiological responses via several hormonal signalling pathways. Due to the multiplicity of retinoid pathways, there are both therapeutic opportunities and problems associated with retinoid therapy. In the human epidermis, RAR- γ predominates and consequently is the primary molecular target of retinoid action in human skin. The wide array of biological effects mediated by the different pathways allows retinoid therapy to be used for many diseases. The indiscriminate activation of these pathways by non-specific retinoids, however, results in a range of unwanted

toxic side effects that accompany their therapeutic efficacy (*de Lera, Bourguet et al. 2017*).

1.4 Tazarotene: a third-generation topical retinoid

Tazarotene and its free acid metabolite tazarotenic acid belong to a novel family of retinoids known as acetylenic retinoids. The development of tazarotene was based on all-trans retinoic acid, which is a very flexible molecule. Due to all-trans retinoic acid's structure of alternating double and single bonds, all-trans retinoic acid interacts non-selectively with both RARs and RXRs. To develop receptor specificity, the rotational mobility of all-trans retinoic acids was restricted. Replacing its polyene chain double bonds with two-ring structures and incorporating a linear triple bond achieved this. Other structural modifications included (i) converting its free acid group into an ethyl ester prodrug form to improve its therapeutic index, (ii) the addition of a nicotinic acid moiety ensuring rapid metabolism into its active free-acid form, reducing the uptake in adipose tissue and incorporating a sulphur atom into the lipophilic ring facilitating a rapid oxidative deactivating metabolism (Chandraratna 1996).

Table 1.1 Physicochemical properties of tazarotene

Chemical structure	 <p style="text-align: center;">$C_{21}H_{21}NO_2S$ *</p>
Molecular mass	351.46 g mol ⁻¹ *
Melting range	103 -105°C *
Log P	5.22 **
pK_a	1.23 **

* (Frigoli, Fuganti et al. 2005)

** ChemAxon, Marvin version 18.19

As metabolite tazarotenic acid does not contain any isomers, Tazarotene cannot be converted into other forms that activate alternative retinoid receptors and is thus unable to bind to any retinoic acid receptors other than those specific to the RAR family. The molecular effects of tazarotene are achieved by activating gene transcription primarily through RAR-β and RAR-γ binding. The ranked order of tazarotenic acid binding affinity to RARs is RAR-β > RAR-γ >> RAR-α (Chandraratna 1996, Chandraratna 1998).

In-vivo studies reveal that systemic absorption of tazarotene following topical administration to the skin is limited in both healthy individuals and patients with psoriasis, as less than 1% of the applied dose is found in the urine and faeces over a

7-day recovery period. Plasma protein binding of tazarotene is >99% with albumin being the main binding protein identified (Menter 2000).

Tazarotene is a prodrug and upon penetration across the SC after topical administration, it is quickly metabolized by esterases in the skin to its active metabolite, the more water-soluble free acid, tazarotenic acid. Tazarotene has an elimination half-life, between 17-18 hours following topical administration, suggesting that percutaneous absorption of tazarotene into the skin is the rate-limiting step. Topical application of tazarotene is safer than oral administration, as the percutaneous absorption and pharmacokinetics of the drug help minimise its systemic exposure, limiting the potential for adverse events (Tang-Liu, Matsumoto et al. 1999, Menter 2000).

1.5 Pathways of percutaneous absorption

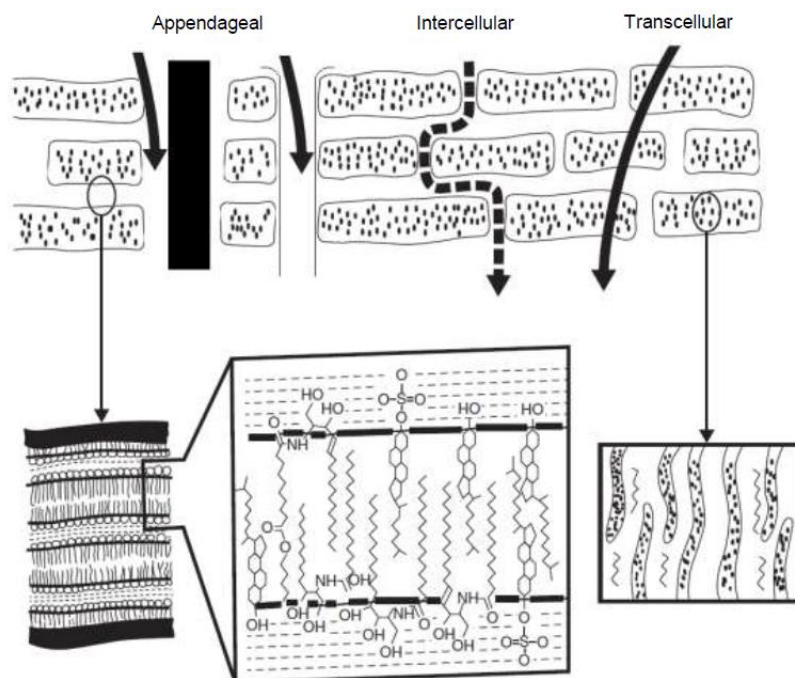


Figure 1.3 The three routes of permeation, appendageal, intercellular and transcellular (Benson 2012).

Overcoming the barrier properties of the SC is the rate-limiting step for most actives that need to penetrate the skin. Transport across the SC is largely a passive process believed to occur via three routes: intercellular, through the lipid matrix; transcellular, through corneocytes; or transappendageal, down the hair shaft or through sebaceous or sweat glands. Experimental evidence suggests that, under normal circumstances, the predominant route of penetration for small molecules is through the intercellular spaces between corneocytes (Moser, Kriwet et al. 2001, Touitou 2002). As the intercellular spaces contain structured lipids and proteins, an API must

therefore cross a variety of lipophilic and hydrophilic regions before it reaches the junction between the SC and the viable epidermis. The diffusional path length through the SC is much longer than the actual thickness of the SC and is estimated to be over 500 μm . Actives must therefore travel a tortuous path before penetrating the SC to reach the viable epidermis (Hadgraft 2004).

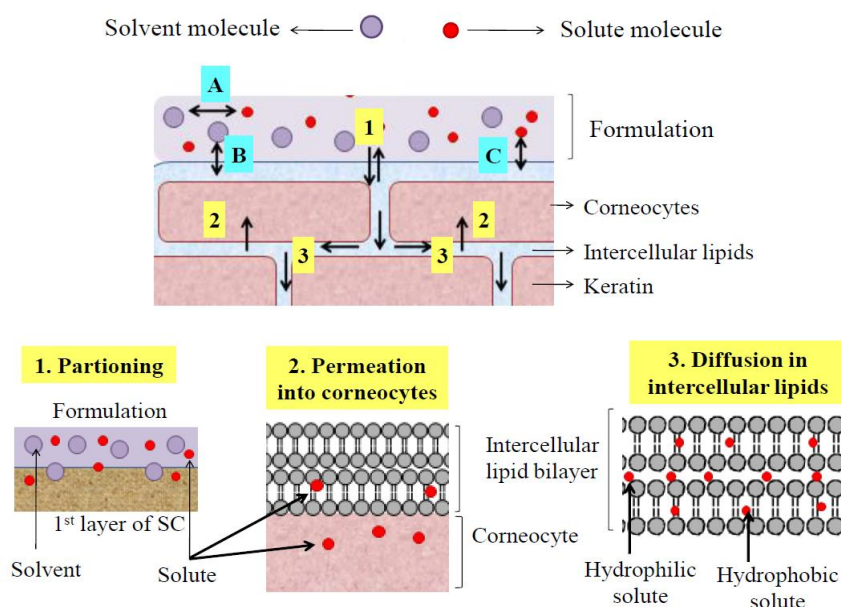


Figure 1.4 Partition and diffusion during percutaneous absorption of a solute through the SC (Roberts 2002).

Percutaneous absorption of the solute (API) involves a series of transport processes mainly determined by the solubility and diffusivity of the solute. A solute must first be in a solution to partition into the outermost lipid layer of SC and then diffuse through it. These processes are influenced by the interactions between solvent, solute and skin. The solution can also penetrate the corneocytes during this process. The next step involves several partition steps followed by diffusion in the viable epidermis and the papillary dermis (Hadgraft 2001). The solute is absorbed into the papillary dermis

by the capillary plexus, where it is then transferred into the systemic circulation. A small amount of the permeant may however diffuse back into the deeper tissue. Given that the intercellular route is the major pathway, hydrophilic molecules are thought to permeate through the polar head groups, and hydrophobic molecules permeate through the lipid chains of the intercellular route's bilayer regions (Hadgraft 2001).

Diffusion of a solute through the skin is primarily a passive process, and despite the numerous interactions that can occur between the solute and the tissue, the skin is modelled as homogeneous. Solutes move spontaneously from a high-concentration region, with the formulations on the skin surface, to a low-concentration region, the target skin layer or the systemic circulation. Continuous clearance of the solute from the tissue means the concentration is relatively low and a chemical potential gradient is maintained as such. Fick's first law of diffusion (Equation 1.1) can describe the passive diffusion process of a solute (Hadgraft 1989, Watkinson and Brain 2002, Mitragotri, Anissimov et al. 2011).

$$J = -D \left(\frac{\partial C}{\partial x} \right) \quad (1.1)$$

The rate of transfer or flux of the permeant is J . D is the diffusion coefficient, ΔC is the concentration gradient across the membrane and Δx is the membrane thickness. The minus sign is due to diffusion decreasing the concentration of active external to the SC. The membrane of the skin is assumed to be inert and homogenous, and the

barrier properties do not vary with time and position (Hadgraft 1989, Watkinson and Brain 2002, Mitragotri, Anissimov et al. 2011).

The equation can be rewritten to give the steady state flux through the skin for *in-vitro* permeation studies (Equation 1.2).

$$J_{ss} = \frac{AKD\Delta C}{h} \quad (1.2)$$

J_{ss} is the steady state flux of the solute, A is the diffusion area of the skin, K is the partition coefficient, D is the diffusion coefficient, ΔC is the concentration gradient across the membrane and h is the diffusion path length. The concentration of the solute in the solution is considered to be much greater than the concentration below the SC. Equation 1.2, however, only applies when steady-state diffusion is reached (Hadgraft 1989, Watkinson and Brain 2002, Mitragotri, Anissimov et al. 2011). The time required to establish steady-state diffusion is known as the lag time (t_{lag}) described in Equation 1.3.

$$t_{lag} = \frac{h^2}{6D} \quad (1.3)$$

Equation 1.2 may be simplified to equation 1.4 where C_{app} is the concentration of solute applied to the skin.

$$J_{ss} = Ak_p C_{app} \quad (1.4)$$

The coefficient of permeability, k_p , is used to characterize the diffusion of the solute through the skin in Equation 1.5 (Hadgraft 1989, Watkinson and Brain 2002, Mitragotri, Anissimov et al. 2011).

$$k_p = \frac{KD}{h} \quad (1.5)$$

This can be simply further to Equation 1.6 by combining Equation 1.4 and 1.5 to show that the steady-state flux (J_{ss}) value can be calculated from the permeability coefficient (k_p) and C_{app} the concentration of solute applied to the skin (Hadgraft 1989, Watkinson and Brain 2002, Mitragotri, Anissimov et al. 2011).

$$J_{ss} = k_p \times C_{app} \quad (1.6)$$

The ideal physicochemical properties required for topical drug delivery are generally considered to be balanced hydrophilic and lipophilic characteristics, low molecular weight, and low melting point. Equation 1.7 demonstrates the dependence of k_p on the partition coefficient ($K_{o/w}$), molecular weight (MW) and Melting Point (MP) (Hadgraft 2004).

$$\log k_p = -2.7 + 0.71 \log k_{o/w} - 0.0061MW$$

(1.7)

Ideally, a drug must be under 500 Da in MW and have a log $K_{o/w}$ value between 1 and 3 with an MP under 232°C to efficiently penetrate the skin barrier (Bos and Meinardi 2000).

The amphoteric properties of an API are essential pre-formulation information. Both the pH and degree of ionisation play a major role in topical drug delivery. Since the majority of drug compounds contain ionisable groups, their ionisation state will be affected by the pH of the formulation it finds itself in as well as the varying physiological pH range it encounters while travelling through the skin (Potts, Guy et al. 1992).

1.6 Passive enhancement strategies in topical delivery

An approach commonly used for promoting the delivery of actives into the skin is the incorporation of chemical penetration enhancers (CPEs) in a formulation. CPEs are pharmacologically inactive compounds that partition and diffuse into the skin by interacting with components in SC. The mechanisms of action of many penetration enhancers are associated with their ability to interact with skin lipids (Williams and Barry 2004, Williams and Barry 2012). The critical parameters for effective delivery into the skin are the solubility of the active in a vehicle and the residence time of that

vehicle in the skin. The relative solubility of an active in two phases determines its partition coefficient and therefore its ability to cross the SC barrier from a vehicle (Suhonen, Bouwstra et al. 1999). Compounds solubilised in a vehicle partition into the outmost lipids of the SC, then diffuse through the intracellular lipid bilayer before partitioning back out of the SC into the viable epidermis. This Diffusion-Partition-Solubility dynamic best describes how penetration enhancers function as drug delivery vehicles. Diffusion through the skin is mediated by those vehicles which intercalate with lipid bilayers and disrupt or fluidise them. Such effects are associated with vehicles that exist as discrete phases in the intercellular lipid regions (Williams and Barry 2004, Williams and Barry 2012).

CPEs can alter the partition parameter of the skin and interact with either the intracellular or intercellular regions of the SC. Combinations of CPEs are often desirable, particularly if they act via different mechanisms to increase the permeation of a drug across the SC. CPEs can increase the thermodynamic activity of delivery and also directly modify the skin barrier properties promoting the topical delivery of the API (Lane 2013). When identifying an optimal penetration enhancer, several criteria should be considered. The penetration enhancers should specifically promote the penetration of actives across the skin without damaging or exhibiting irreversible effects on its properties. Ideally, they should be pharmacologically inert, non-toxic,

non-irritating and non-allergenic. They should also be stable, aesthetically acceptable in a formulation, as well as relatively cheap and easy to source (Hadgraft and Walters 1994, Lane 2013).

1.7 Franz diffusion cell permeation and mass balance studies

In-vitro skin permeation experiments are by far the most common approach for evaluating and researching topical formulations. Permeation studies allow for the quantification of actives and excipients that cross the skin barrier. They are coupled with mass balance studies which provide information on both the amount of active on the skin surface but also the amount delivered inside the skin (Franz 1975, Tsai, Cappel et al. 1992)

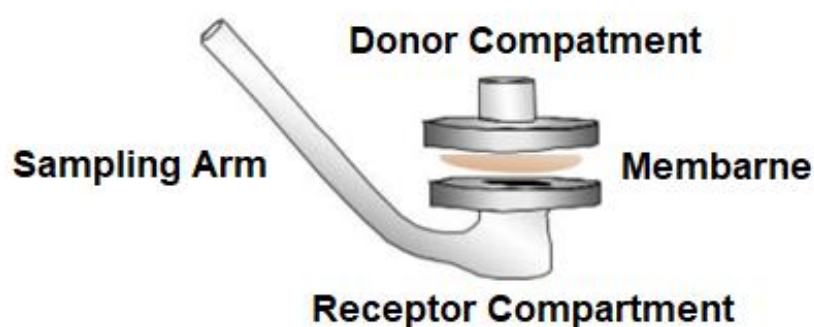


Figure 1.5 Schematic representation of the vertical Franz diffusion cell for *in-vitro* studies.

A Franz cell consists of both a donor and receptor compartment, with a membrane placed between them, forming a sandwich configuration. Topical formulations are

applied to the donor compartment while the receptor compartment is filled with an appropriate receptor fluid that aims to maintain sink conditions. The receptor solution is extracted via the sampling arm at fixed time points to determine the amount of active or excipient that permeated through the membrane as a function of time (Moser, Kriwet et al. 2001).

Selecting the right membrane to evaluate skin permeation is an extremely important experimental factor. Human skin is considered the most appropriate membrane for *in-vitro* permeation and mass balance studies. However, due to strict ethical regulations, limited availability and high costs, skin samples from various other animal species are widely used instead. Although skin from other species is cheaper and more readily available than human skin, there is a degree of biological variability associated with different membranes. Numerous animal models have been used in dermatological research with rats, guinea pigs and pigs being the most popular (Schmook, Meingassner et al. 2001, Frasch and Barbero 2009).

However, the animal model that most closely resembles human skin has been established to be porcine skin and is the ideal membrane when assessing the cutaneous absorption of APIs and excipients. Several studies have confirmed porcine ear skin to be the most reliable animal model in terms of API permeability. Both human and porcine skin have comparable SC and epidermal thicknesses, high

surface lipid contents and large amounts of elastic tissue in the dermis (Dick and Scott 1992, Herkenne, Naik et al. 2006).

Another important factor to be considered in the design of *in-vitro* permeation and mass balance studies is the dose being applied to the donor compartment. Depending on the amount of formulation applied to the skin, the study may be classified as being either infinite or finite (Franz, Lehman et al. 1993). Dose selection is primarily determined by a study's objective. If the amount of formulation applied to the skin is great enough to ensure it does not completely deplete, the dose is considered infinite as an excess amount of formulation on the skin surface would remain throughout the study. On the other hand, a dose is considered finite if the amount of formulation applied to the skin is small enough to ensure full depletion by the end of the study (Selzer, Abdel-Mottaleb et al. 2013).

Infinite dose studies are ideal for initially investigating APIs, vehicles and/or formulations that have not been extensively evaluated. However, the limitation of using an infinite dose is the fact this does not accurately represent an *in-vivo* situation. In contrast, finite dosing becomes more important when trying to mimic an *in-vivo* situation that could potentially extrapolate clinically relevant data (Selzer, Abdel-Mottaleb et al. 2013).

For *in-vitro* permeation studies to be effective, the chosen receptor solution must simulate, as closely as possible, what is observed *in-vivo* where the compound is constantly cleared from the skin via the bloodstream. The receptor solution must, therefore, maintain sink conditions throughout a study, so that absorption through the skin is not hindered in any way or able to reach saturation (Zsikó, Csányi et al. 2019). To achieve this, the thermodynamic activity of a compound in a receptor solution should not exceed 10% of the thermodynamic activity in the donor solution and should have the receptor solution constantly stirred to help maintain sink conditions allowing the compound to readily be solubilised. Additionally, the chosen receptor solution must not affect the stability of the compound or the integrity of the skin membrane (Frasch and Barbero 2018, Zsikó, Csányi et al. 2019).

The maintenance of sink conditions throughout a permeation study is closely related to sampling intervals and volumes. The sampling intervals should be frequent enough to establish an accurate compound absorption profile. If too many samples are collected in a relatively short period, the compound might be too diluted for effective quantification. On the other hand, if samples are not collected frequently enough, this may well lead to a loss of sink conditions because of compound accumulation in the receptor solution. Sampling volumes should always be large enough to allow for compound quantification and be replaced with an equivalent

volume of fresh receptor solution to ensure skin conditions (Friend 1992, Zsikó, Csányi et al. 2019). Very large sampling volumes may affect compound quantification through excessive dilution of the receptor solution while very small sampling volumes may result in the loss of sink conditions brought about by the accumulation of the compound in the receptor solution.

The duration of a permeation study is another important factor to be considered and is related to the rate of compound absorption. Typically experiments last between 24 to 72 h provided that the skin membrane integrity is maintained throughout (Friend 1992, Zsikó, Csányi et al. 2019). To perform a successful mass balance, the solvents used to solubilise the compound on the skin surface and membrane should be carefully selected. Solvents used for skin surface washing should be able to solubilise large amounts of a formulation containing the compound. Similarly, solvents used for skin extraction should not only solubilise considerable amounts of the compound but also be able to penetrate the skin membrane readily. The stability of the compound in the chosen solvent must also be assessed to ensure no significant reduction in concentration occurs during washings and extractions (Friend 1992, Zsikó, Csányi et al. 2019).

1.8 Tape-stripping for drug penetration and SC protein analysis

Tape-stripping is a minimally invasive procedure used to investigate the structure, properties, and function of the SC *in-vivo*. SC tape-stripping procedures involve the repeated application and removal of adhesive tape from the skin surface. Theoretically, a single tape strip can remove a layer of corneocytes, however, in practice, this is often not the case. The amount of SC removed by a single tape strip is not linearly proportional to the number of tapes being removed. The first tape strips often contain a complete layer of corneocytes and as the number of tape strips increases, the number of corneocytes removed by each tape strip typically decreases as the SC is gradually stripped away (Escobar-Chavez, Merino-Sanjuan et al. 2008).

The actual amount of SC removed by each tape strip will vary according to the depth of removal, the tape-stripping method used, as well as extrinsic and intrinsic factors directly influencing the SC. Consequently, the amount of formulation and SC removed by tape stripping must be determined using validated methods. As the rate-limiting step for percutaneous absorption, determining the concentration of a permeant in the SC can serve as a surrogate for the expected concentrations in the viable epidermis (Hughes, Tawfik et al. 2021)

Removal of the SC should be performed uniformly, and this requires the application site to be free from hair follicles and uneven areas of the skin, such as scars. If a site

with hair cannot be avoided, hairs should be carefully removed without damaging the skin. Shaving hair using a machine should be avoided as this may unintendedly remove superficial layers of the SC. The flexor forearm is an ideal application site due to the ease of access and the relatively small amount of hair in this area (Hughes, Tawfik et al. 2021).

Several types of adhesive tape strips are currently available on the market, however, when choosing a tape strip, it must guarantee a uniform distribution of adhesion over the area of examination. The flexibility, transparency and composition of the chosen tape strip should also be taken into consideration, as they could affect the volunteer of a study and/or the method of quantification. To ensure the safety of each volunteer in a study, the compatibility of the adhesive tape strip with each subject should be determined before the start of a study to ensure no adverse reactions arise (Escobar-Chavez, Merino-Sanjuan et al. 2008).

Before the application of an adhesive tape strip onto the skin, the areas that are under investigation should be marked to differentiate the site of interest from the rest of the skin. After the area of interest is marked, tape strips can be carefully placed on the area of interest avoiding any folds. The procedure becomes problematic when the intended tape strip differs in size from the area under investigation. When the area under investigation is substantially smaller than the chosen adhesive tape strip,

the initial marks on the skin should be redrawn after the removal of several tape strips to ensure the precise area is being investigated. If the skin area is larger than the adhesive tape strip, the initial marking on the skin is sufficient, as long as the borders on the skin remain visible (Escobar-Chavez, Merino-Sanjuan et al. 2008).

When applying adhesive tape strips to the skin, a uniform pressure should ideally be applied throughout to limit inconsistencies in the experimental procedure. A constant weight applicator is used to attain a complete uniform pressure distribution across the tape strip. The constant weight applicator presses the adhesive tape strip into the grooves of the skin which is vital in maintaining consistency. When removing adhesive tape strips, a constant rate of removal should also be maintained. Decelerating the removal of the tape strip could ultimately lead to higher amounts of SC adhered to the strip whereas an accelerated removal might result in a much lower amount of corneocyte adhesion (Escobar-Chavez, Merino-Sanjuan et al. 2008).

After the successful removal of the SC, quantifying the absolute amount of SC removed by each tape strip is critical. Quantifying the amount of SC removed is typically based on determining the corneocyte protein content as it is the main component of the SC. Using infrared densitometry (IRD), the protein content of each

tape strip can be measured at an absorbance of 850nm by equation 1.7 (Mohammed, Yang et al. 2012).

$$C_{Protein} (\mu g/cm^2) = 1.366 * Absortion (\%) - 1.557$$

(1.7)

Furthermore, protein content has been shown to relate to SC weight by equation 1.8 (Mohammed, Yang et al. 2012).

$$C_{Protein} (\mu g/cm^2) = 0.420 (\pm 0.009) * SC \text{ weight } (\mu g/cm^2)$$

(1.8)

A water gradient exists in the epidermis as the SC moisture content becomes substantially lower in the deeper layers of the dermis. Consequently, water from the inner layers passively diffuses through the SC out toward the skin surface. This loss of water process is referred to as Transepidermal Water Loss (TEWL) and has been found to have a flux of 0.5-1.0 mg/cm²/h (Mohamad, Msabbri et al. 2012). This gradient is tightly controlled and any damage to it would result in an impairment of the SC barrier function. Tape-stripping experiments cause damage to the skin by removing multiple layers of the SC. What is happening in effect is that the skin loses some of its ability to retain water within the SC and an increase in TEWL results due

to higher volumes of water evaporation (Mohamad, Msabbri et al. 2012). Therefore, TEWL can be quantified by measuring the density gradient of water evaporation from the skin surface. To do this, a closed chamber probe fitted with both a temperature and humidity sensor is a current method used to quantify TEWL measurements. Low TEWL values typically indicate that the skin barrier function is intact, while an increase in TEWL usually suggests a disruption to the skin barrier (Gioia and Celleno 2002, Hadgraft and Lane 2009).

1.9 Raman scattering and Confocal Raman Spectroscopy for non-invasive analysis

When photons of light interact with matter, part of the light is deflected from the direction of the incident referred to as scattering, which can either be elastic or inelastic. Elastic scattering, or Rayleigh scattering, involves no energy transfer in the scattering event and consequently, the scattering light has the same frequency as the incident light (Miles, Lempert et al. 2001). Inelastic, or Raman scattering, on the other hand, results in energy transfer in the scattering event and, as a result, the scattering light has a different frequency than the incident light. If the frequency of the scattered light is higher than that of the incident light it is referred to as Stokes Raman scattering. On the contrary, if the frequency of the scattering light is lower than the incident light it is referred to as anti-Stokes Raman scattering. Stokes-

Raman scattering is detected at longer wavelengths i.e. lower energy levels while anti-Stokes scattering is detected at much shorter wavelengths i.e. higher energy levels (Williams and Barry 2001).

All molecules have a unique combination of vibrational levels corresponding to a Raman spectrum which is highly specific and comparable to a molecular fingerprint.

A Raman spectrum is represented by a wave number shift from the incident light to scattered photons against the scattering intensity. All Raman scattering is a linear process, and the intensity of a Raman wave shift is proportional to the concentration of the respective compound. The position, relative intensities and shapes of the wave shifts in a Raman spectrum carry detailed quantitative information about the molecular composition of a sample and the molecular structures and interactions present (Petry, Schmitt et al. 2003).

The strongest wave shift in a Raman spectrum corresponds to non-polar functional groups or aromatic rings due to large changes in their polarizability associated with delocalized electron clouds. Most small compound drugs contain aromatic structures and therefore tend to be good scatterers and show strong distinct Raman bands, making them very easy to detect in small amounts (Lu, Li et al. 2004).

Biological membranes such as the skin are highly variable in composition resulting in very complex Raman band patterns. To be able to successfully utilise the Raman

effect to spectroscopically analyse biological membranes a high-powered laser, sensitive detector and sophisticated optical engineering are required (Fabian and Anzenbacher 1993). The evolution of technology has led to the rise of very sophisticated commercially available Raman instrumentations opening the door for multiple applications in skin research including analysing skin components in addition to drug and excipient tracking in the skin (Caspers, Lucassen et al. 1998).

A Raman spectrometer consists of a highly powered monochromatic light source, typically a laser and sample stage that can move and an advanced spectrometer. A CCD-based (Charge Coupled Device) system is currently the most effective technology available for filtering out unwanted elastic scatter to enhance Raman scatter detection. In a CCD-based spectrometer, the different wavelengths of the scattered light are dispersed by an optical grating and projected on a large array of detectors that enable simultaneous recording of a complete Raman spectrum in a single exposure (Caspers, Lucassen et al. 1998). In a sample stage for the skin measurements, the laser light is focused via a microscope objective in a small region in the skin. Scattered light that emerges from this irradiated volume is collected by the microscope objective and projected onto the core of an optical fibre. The core of the optical fibre acts as a pinhole and permits only light emerging from the region where the laser light is focused to enter the fibre, whereas light from out-of-focus

regions is blocked. The focus from the scattered light is detected and the focus irradiated by the laser coincides, hence the name confocal (Caspers, Lucassen et al. 1998).

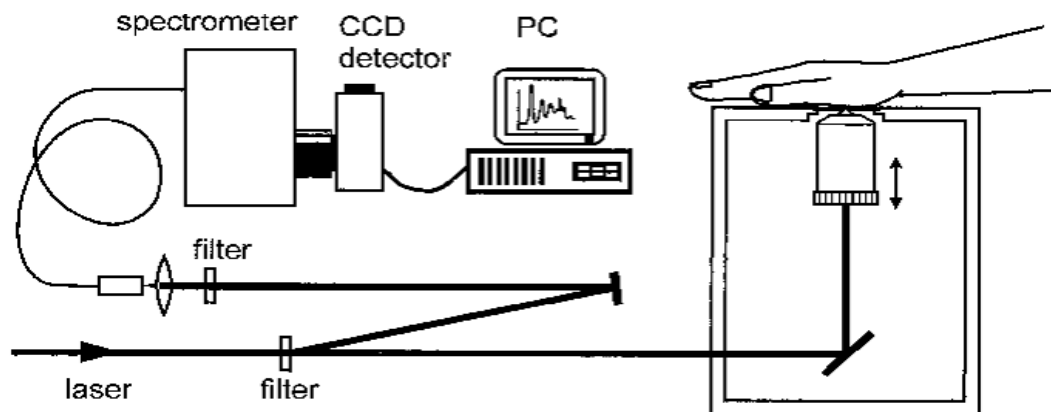


Figure 1.6 A complete Confocal Raman instrumentation set-up used for real-time in-vivo skin measurements (Caspers, Lucassen et al. 2001)

The use of CRS to measure water concentration across the skin has evolved into a powerful tool to help better understand the distribution and function of water within the epidermal layer. Due to the steep increase in water concentration from the outer to the inner side of the SC, it is possible to estimate the border between the SC and SG, therefore SC thickness, through CRS by collecting water concentration profiles across the SC and epidermis. The water content typically increases from approximately 30% at the skin surface to 70% at the inner SC. Natural moisturizing factor (NMF) content is another parameter used to define the SC border via CRS as it is only found within SC. The SC border is situated at the point where the increasing water concentration begins to level off and NMF content becomes constant

(Caspers, Lucassen et al. 2000). Using the water mass percentage, we can calculate the water concentration in the skin [$\text{mg}_{\text{water}}/\text{cm}^3$] with equation 1.10 by converting equation 1.11 into a water mass fraction (Lucassen, Caspers et al. 2000).

$$W_{\text{water}}(z) = \frac{m_{\text{water}}(z)}{m_{\text{water}}(z) + m_{\text{dry SC}}(z)} \quad (1.10)$$

This can be rearranged to equation 1.11

$$\frac{m_{\text{water}}(z)}{m_{\text{dry SC}}(z)} = \frac{w_{\text{water}}(z)}{1 - w_{\text{water}}(z)} \quad (1.11)$$

The water concentration as a function of depth in the skin can be defined by equation 1.12.

$$\gamma_{\text{water}}(z) = \frac{m_{\text{water}}(z)}{V(z)}$$

(1.12)

Where $V(z)$ is the measurement volume at a certain depth which can be calculated using equation 1.13 (Lucassen, Caspers et al. 2000).

$$V(z) = V_{\text{water}}(z) + V_{\text{dry SC}}(z) = \frac{m_{\text{water}}(z)}{\rho_{\text{water}}} + \frac{m_{\text{dry SC}}(z)}{\rho_{\text{dry SC}}} \quad (1.13)$$

In which ρ_{water} is the density of water ($1.0 \text{ g}/\text{cm}^3$) and $\rho_{\text{dry SC}}$ is the density of dry SC ($\sim 1.15 \text{ g}/\text{cm}^3$) assumed to both be constant.

By substituting equation 1.11 into equation 1.12 and using equation 1.13, we can express the water concentration as a function of distance to the skin surface using equation 1.14 (Lucassen, Caspers et al. 2000).

$$\gamma_{water}(z) = \frac{\rho_{dry\ SC} * \rho_{water} * w_{water}(z)}{\rho_{dry\ SC} * w_{water}(z) + \rho_{water} * (1 - w_{water}(z))} [mg_{water}/cm^3]$$

(1.14)

By integrating $\gamma_{water}(z)$ over the depth of the full SC thickness using equation 1.15, we can also calculate the total amount of water per unit area of the skin surface (Lucassen, Caspers et al. 2000).

$$M_{water} = \int_0^{SC\ Thickness} \gamma_{water}(z) * dz [\mu g/cm^2]$$

(1.15)

CRS has been used to obtain detailed semiquantitative information about the molecular composition of the skin as well as the molecular concentration gradients in the skin. Semiquantitative analysis of actives and excipients in the skin using CRS has evolved into a powerful quantitative technique based on spectral fitting of the skin Raman spectra with the Raman spectra of intrinsic skin constituents and the spectra of the desired analyte (Caspers, Lucassen et al. 2001).

For a material dissolved in a solvent, we can write equation 1.16.

$$\frac{R_{material}}{R_{Solvent}} = C_{material:solvent} * \frac{\gamma_{material}}{\gamma_{solvent}}$$

(1.16)

Where $R_{material}/R_{Solvent}$ is the Raman signal intensities ratio, $\gamma_{material}/\gamma_{solvent}$ the concentration ratio and $C_{material:solvent}$ the proportionality constant of the dissolved material (Caspers, Nico et al. 2019).

The material dissolved in the solvent shares the same measurement volume, therefore equation 1.16 turns into equation 1.17 when we substitute $m_{material}/m_{solvent}$ for $\gamma_{material}/\gamma_{solvent}$ (Caspers, Nico et al. 2019).

$$\frac{R_{material}}{R_{Solvent}} = C_{material:solvent} * \frac{m_{material}}{m_{solvent}} \quad (1.17)$$

$C_{material:solvent}$ is determined by plotting a range of Raman signal intensities ratios $R_{material}/R_{Solvent}$ against its corresponding mass ratios $m_{material}/m_{solvent}$ to form a calibration curve. By conducting this procedure for two materials A and B in the same solvent we get proportionality constants $C_{A:solvent}$ and $C_{B:solvent}$ then we can write equation 1.18 (Caspers, Nico et al. 2019).

$$C_{A:B} = C_{A:solvent} * C_{B:water}^{-1} \quad (1.18)$$

We, therefore, can write equation 1.19 by substituting equation 1.17 in equation 1.18.

$$\frac{m_A}{m_{protein}} = c_{protein:solvent} * c_{A:solvent}^{-1} * \frac{R_A}{R_{protein}} \quad (1.19)$$

By multiplying the mass ratio $m_A/m_{protein}$ with the protein concentration in the skin we can calculate the concentration of material A in the skin γ_A as a function of distance from the skin surface expressed by equation 1.20 where $\gamma_{Protein}$ is defined by equation 1.21 (Caspers, Nico et al. 2019).

$$\gamma_A(z) = \left(\frac{m_A}{m_{protein}}\right)_z * \gamma_{protein}(z) [mg/cm^3] \quad (1.20)$$

$$\gamma_{protein}(z) = m_{protein} * \left(\sum_i^n \frac{m_i}{p_i}\right)^{-1} = \left(\sum_i^n \frac{1}{p_i} * \frac{m_i}{m_{protein}}\right)^{-1} [mg/cm^3] \quad (1.21)$$

Where $m_{protein}$ is the mass of protein in a given volume, p_i is the density and m_i is the mass of material i in a mixture. By integrating $\gamma_A(z)$ over the entire penetration depth of the SC, we can calculate the total amount of material A M_A per skin surface area using equation 1.22 (Caspers, Nico et al. 2019).

$$M_A = \int_0^{skin\ thickness} \gamma_A(z) * dz \quad [\mu g/cm^2] \quad (1.22)$$

1.10 Aims and objectives.

- Characterise the physicochemical properties of the third-generation retinoid tazarotene in a range of chemical penetration enhancers (CPEs).

- Formulate topical delivery systems using combinations of CPE to promote the deposition of tazarotene into the skin.
- Conduct *in-vitro* infinite and finite dose Franz diffusion cell studies with the different topical tazarotene formulations to establish the best performing compared to the commercial Zorac gel formulation.
- Use Confocal Raman Spectroscopy (CRS) to quantify tazarotene deposited in the SC first *in-vitro* then *in-vivo* from the best performing formulations compared to the commercial Zorac gel formulation along with studying CPE effects.
- Conduct *in-vivo* tape stripping studies with the best performing formulations and compare them with CRS results to assess correlations between the techniques in analysing tazarotene deposition into the skin.

Chapter Two:

Physiochemical Characterisation and *in-vitro* HPLC Evaluation of Topical Tazarotene Formulations

Chapter Two

Physicochemical characterisation and *in-vitro* HPLC evaluation of topical tazarotene formulations

2.1 Introduction

Developing a topical formulation is a multifaceted process intended to deliver an API safely and efficiently to a specific area of the skin in a cost-effective manner. A rational formulation design approach is based upon a robust pre-formulation phase that involves selecting the optimal combination of excipients for a particular API and then assessing their physicochemical properties before *in-vitro* and *in-vivo* studies. This is because the physicochemical properties of an API and selected excipients greatly affect topical delivery to the skin in addition to how a formulation is prepared. This ultimately forms the basis for the rational design of a formulation (Lane, Hadgraft et al. 2012). Information on the physicochemical characteristics of some APIs and excipients, however, may not always be readily available in scientific literature. Therefore, they must be determined experimentally, which is often the case for compounds that either have not been widely studied or have been recently discovered or synthesised. Knowledge of the solubility of an API in a wide range of solvents is extremely important. Solvents being selected must be able to solubilise

an adequate amount of the API so that the desired concentration in the formulation can be achieved (Savjani, Gajjar et al. 2012). The assessment of API stability is another essential process for any topical formulation design. Drug-excipient and excipient-excipient interactions may affect the stability and tissue disposition of an API along with its efficacy and safety (Joseph, Satinder et al. 1978). It is therefore critical to evaluate the solubility, stability, and miscibility of an API during the pre-formulation phase to avoid any compatibility issues at a later stage of the formulation design (Machui and Brabec 2012). Once the physicochemical properties of the desired API and excipients have been determined, well-established *in-vitro* techniques, such as Franz diffusion cell permeation and mass balance studies, can be employed to evaluate the efficacy of the formulation (Hadgraft and Lane 2012). The strategy used to passively promote topical delivery of an API into the skin using CPEs has been described in section 1.6 followed by the principles and the various experimental parameters to be considered when designing Franz diffusion cell and mass balance studies in section 1.7. Glycols like PG can permeate through the SC well by altering the thermodynamic activity of a drug modifying the driving forces for diffusion, with PG partitioning into the tissue to facilitate the uptake of drug into the skin causing a minor disturbance to the intercellular lipid packing within the SC (Williams and Barry 2012). The interaction of PG with the SC was investigated using DSC and X-ray diffraction techniques with results suggesting that PG integrates into

the hydrophilic regions of the packed lipids as PG was observed to increase the distance in the lamellar phase (Brinkmann and Muller-Goymann 2005). The solubility and diffusivity of 4-cyanophenol in TC were investigated using attenuated total reflectance Fourier transform infra-red (ATR-FTIR). The ATR-FTIR data suggested that TC enhanced permeation of 4-cyanophenol through changes in solubility rather than diffusion in the membrane (Harrison, Watkinson et al. 1996). Symmetric and asymmetric models have been used to investigate the effects of IPM and IPA in human skin which showed IPM and IPA uptake correlated well with estradiol solubility in the SC (Liu, Cettina et al. 2009). DSC and X-ray diffraction studies of the SC revealed that by disturbing the intercellular lipid bilayer structure, IPA increases lipid fluidity thus enhancing drug permeation (Brinkmann and Muller-Goymann 2003). DSC studies of IPM showed a decrease in enthalpy and a negative phase transition shift indicating an integration with the lipid bilayer effecting lipid fluidity (Leopold and Lippold 1995). X-ray diffraction studies, however, also indicated that IPM marginally increases the short-distance orthorhombic lipids, whilst simultaneously decreasing the hexagonal lipids and maintaining a constant inter-lamellar distance (Brinkmann and Muller-Goymann 2003). In this chapter, the physicochemical properties of the third-generation retinoid tazarotene alone and in combination with various CPEs are examined before proceeding with *in-vitro* Franz

diffusion cell studies to evaluate the effectiveness of different formulations to deliver tazarotene into porcine skin.

2.2 Materials and methods

2.2.1 Materials

Tazarotene >98% was purchased from Insight Biotechnology, (UK).

Zorac[®] gel 0.1% was supplied by Allergan, (IRL).

Transcutol (TC), propylene glycol monocaprylate (PGMC), propylene glycol monolaurate (PGML), propylene glycol dicaprylocaprate (PGDC), medium chain triglycerides (MTC) were gifted by Gattefossé, (UK).

Isopropyl myristate (IPM), isopropyl alcohol (IPA), dipropylene glycol (DiPG), propylene glycol (PG), hexylene glycol (HG), HPLC grade water, HPLC grade acetonitrile (ACN), HPLC grade methanol (MeOH) were purchased from Fisher Scientific, (UK).

Dulbecco PBS (pH = 7.3 ± 0.2 at 25°C) was supplied by Oxoid (UK).

BrijO20[®], bovine serum albumin (BSA), Parafilm[™], Eppendorf centrifuge tubes, HPLC amber glass vials, 200ml vial inserts, HPLC column and guard column were purchased from Sigma Aldrich, (UK).

Franz diffusion cells were supplied by SES GmbH (UK).

Porcine ears were sourced from a local abattoir.

2.2.2 Molecular modelling

The Hildebrand and Hansen solubility parameter for tazarotene and each vehicle was determined using Molecular Modelling Pro V7.08 (Chemistry Software USA).

2.2.3 HPLC method development and validation for tazarotene analysis

For an initial UV absorbance spectrum measurement, tazarotene was dissolved in HPLC-grade MeOH. A concentration of 10 µg mL⁻¹ was measured using a Biomate 3 UV-VIS spectrophotometer (Thermo Spectronic, USA). Tazarotene had a specific absorption at 348 nm corresponding to the maximum absorption.

The following method was developed and validated:

Column	C ₈ 150mmX4.6 mm (Phenomenex, UK)
Mobile phase	70% Acetonitrile 30% Water HPLC grade
Temperature	25 °C
Flow rate	1.0 mL/min
Run time	7 min
Wavelength	348 nm
Injection volume	10 µL

Analysis was conducted at 25°C using a Phenomenex® C8 column with dimensions of 150 × 4.6 mm, a 2 µm stationary phase, fitted with a C8 4 × 3 mm, 5 µm guard cartridge and a 5 µm SecurityGuard™ ULTRA (Phenomenex, USA). Degassed mobile phases consisting of acetonitrile (ACN) and HPLC grade water were delivered by a binary pump at a total combined flow rate of 1 mL min⁻¹. The sample injection volume was 10 µL and samples were prepared in 1.5 mL amber glass vials containing 250 µL glass inserts and 8 mm screw caps with rubber septa. The method run time was 7 mins and the retention time of tazarotene was 4.6 mins. Chromatogram data were integrated using Agilent ChemStation for HPLC systems (Agilent Technologies, USA). Method reproducibility was evaluated, and validation is shown in this chapter. Stock standard solutions of tazarotene for calibration were prepared in methanol at a concentration of 1 mg/mL and stored at -20°C. Working standard solutions of tazarotene were prepared by dilution of stock solutions in MeOH and stored at -20°C. The working solutions of tazarotene for calibration curves were prepared at concentrations of 1.56, 3.12, 6.25, 12.50, 25 and 50 µg/mL by spiking blank methanol with the working standard to make up 100 µL. The samples were transferred to injection vials, and 10 µL were injected into an HPLC system for analysis. All experiments were conducted in triplicates except for precision done in twelve measurements for statistical analysis.

2.2.4 Solubility studies of tazarotene

To determine the solubility of tazarotene in the selected vehicles, a solubility study was conducted at $32 \pm 1^\circ\text{C}$. An excess amount of tazarotene was added to a 2 ml Eppendorf tubes tube containing 100 μl of the appropriate vehicle or receptor medium. Transcutol (TC), propylene glycol monocaprylate (PGMC), propylene glycol monolaurate (PGML), propylene glycol dicaprylocaprate (PGDC), medium chain triglycerides (MTC), dipropylene glycol (DiPG), propylene glycol (PG), hexylene glycol (HG) and isopropyl myristate (IPM) served as vehicles. Tazarotene in phosphate-buffered saline (PBS) alone or either with BrijO20[®] or bovine serum albumin (BSA) served as the receptor medium. Tubes were sealed with Parafilm[™] and placed in an orbital mini shaker (VWR, UK) at 8000 rpm for approximately 48 hours at $32 \pm 1^\circ\text{C}$. Tubes were checked periodically to ensure an excess of tazarotene was present. A suitable number of 200 μl pipette tips (VWR, International) were placed into an oven at $32 \pm 1^\circ\text{C}$ to avoid variation of the experimental temperature during use. After 24 h tubes were placed in a centrifuge (Eppendorf, Germany), pre-warmed to $32^\circ\text{C} \pm 1^\circ\text{C}$ then centrifuged at 13200 rpm for 15 min. The supernatant was then removed, and samples were centrifuged again at 13200 rpm for 15 min. A known volume of supernatant was diluted with methanol before tazarotene concentration was determined by HPLC.

2.2.5 Stability studies of tazarotene

The stability of tazarotene in the selected solvents and receptor fluid was investigated over 24 h at $32 \pm 1^\circ\text{C}$. A known concentration of tazarotene in each solvent was prepared and placed in 2 mL Eppendorf tubes. The tubes were sealed with Parafilm™ to avoid evaporation of the solvents, then placed in an orbital mini shaker (VWR, UK) at 8000 rpm for 24 h at $32 \pm 1^\circ\text{C}$ with samples being taken at 0, 1, 2, 4, 8, 12 and 24 h. Samples were then suitably diluted with menthol and the concentration of tazarotene was determined by HPLC. The percentage of drug recovered after 0, 1, 2, 4, 8, 12 and 24 hours was calculated as a function of the concentration and used as an indicator of tazarotene stability in the solvent. All experiments were conducted in triplicates for statistical analysis.

2.2.6 Miscibility studies of CPEs

To determine the miscibility of tazarotene in the selected vehicles, miscibility studies of PG and HG in binary were conducted at $32 \pm 1^\circ\text{C}$. Various ratios of each vehicle were placed in 2 mL clear Eppendorf Tubes® with known amounts of tazarotene. The tubes were vortexed for approximately 30 s and then placed in a tube stand to visually assess miscibility. In some cases, to distinguish the miscibility, Sudan III red (Fisher Scientific, UK) was added to help identify any immiscibility. All experiments were conducted in triplicates for statistical analysis.

2.2.7 Tazarotene formulation preparation

All formulations were made fresh as required. The appropriate mass of tazarotene was weighed in a 2 mL plastic Eppendorf with a locking lid. For binary and ternary formulations, a total of 1 mL of the required solution was pipetted into a 2 mL Eppendorf containing the pre-weighed amount of tazarotene to give a final concentration of 0.1% (w/w). Eppendorfs were then locked, wrapped in Parafilm™ and placed into an incubating orbital mini shaker (VWR, UK) at 800 RPM and 25 °C \pm 1°C for approximately 3 h to ensure complete solubilization of the tazarotene. Single solvents included propylene glycol (PG), hexylene glycol (HG), dipropylene glycol (DiPG), Transcutol (TC), propylene glycol monocaprylate (PGMC), propylene glycol monolaurate (PGML), propylene glycol dicaprylocaprate (PGDC), medium chain triglycerides (MTC), and isopropyl myristate (IPM). Binary vehicle included PG:TC (4:1), HG:TC (4:1), PG:MC (4:1). Ternary vehicles included HG: IPM: IPA (8:1:1), HG:PG:TC (2:2:1). The quaternary vehicle was composed of HG:PG:TC:IPM (2:2:1:1). All formulation constituents were weighed using an analytical balance (Mettler Toledo, UK). The concentration of tazarotene in all the solutions prepared was measured via HPLC.

2.2.8 Porcine skin preparation

Porcine tissue was selected as a suitable model because of the similarities shared with human skin. Porcine ear skin, in particular, is the closest anatomical site to human skin and was selected for use in this study (Dick and Scott 1992). Porcine tissue was obtained from healthy animals on the day of slaughter from a local abattoir. Ears were washed gently with distilled water to remove particulate contamination. Hairs were carefully trimmed, followed by a final rinse in distilled water. Using a scalpel, a continuous cut was made around the perimeter, about 5 mm from the edge on the back of the ear. The scalpel was then used to cut the skin away from the cartilage avoiding damage to the underside. The surgically removed full-thickness porcine skin was mounted on aluminium foil, placed in polyethylene bags, and stored at -20 °C until required. Frozen porcine skin was rapidly cut into discs using an 18 mm circular cork borer. Once thawed, the skin was blotted dry and clamped between the receptor and the donor compartments of a Franz cell.

2.2.9 Receptor fluid preparation

PBS tablets Dulbecco A, pH 7.3 ± 0.2 (Oxoid, UK), were dissolved in the appropriate volume of HPLC grade water with polyoxyethylene (20) oleyl ether (BrijO20®) to a concentration of 6% in a Duran bottle (Sigma Aldrich, UK). The receptor fluid was then degassed in an ultra-sonication bath (Thermolyne, USA) for 15 min. Until the

receptor fluid was required, it was placed in a Nova thermostatic water bath (Grant Instruments, UK) at $32\text{ }^{\circ}\text{C} \pm 1\text{ }^{\circ}\text{C}$.

2.2.10 Mass balance validation

To assess stability in methanol, a fixed amount of tazarotene was transferred to a 2ml microcentrifuge tube containing 100 μl of HPLC grade methanol $\geq 98\%$. The tubes were sealed with Parafilm[®] then placed in an incubating mini shaker (VWR, International) at $32 \pm 1^{\circ}\text{C}$, and 10,000 RPM for 24 h. Samples were withdrawn at set time points throughout the 24 h incubation period and then analysed via HPLC. The mass balance method was validated using a 0.1% w/w solution of tazarotene in MTC. Experiments were conducted using glass vertical Franz diffusion cells (Soham Scientific, UK) and porcine ear skin obtained from an abattoir. The Franz diffusion cells were assembled with the porcine skin in between the donor and receptor compartments and then clamped together. However, the receptor compartments were left empty. The cells were then placed in a SUB 28 (Grant Instruments UK) thermostatically controlled water bath. 50 μL of donor solution was then applied to the skin surface for 6 h. At the end of the 6 h period, the skin surface was washed 5 times with each wash consisting of 5 solvent rinses of methanol. The Franz diffusion cells were then disassembled, and the skin membranes were placed in microcentrifuge tubes and extracted with methanol using an incubating mini shaker

(VWR, International) at $32 \pm 1^\circ\text{C}$, and 10,000 RPM for 24 h. The tubes were centrifuged at 12000 rpm for 10 min and then the supernatant was taken for HPLC analysis. All experiments were conducted in triplicates for statistical analysis.

2.2.11 In-vitro infinite dose permeation studies of topical tazarotene formulations

Permeation studies were conducted using glass vertical Franz diffusion cells with porcine ear skin obtained from an abattoir. Franz cell donor and receptor compartments were matched according to size and the diameters of both compartments were measured. The compartment with the smaller diameter was used to calculate the diffusion area. Porcine ear skin was punched out into approximately 3 cm^2 circular pieces. The donor and receptor compartments were covered with a thin layer of high vacuum grease (Dow Corning, U.S.A.) before placing the porcine skin between the two compartments. To create a tight leak-proof seal around the porcine skin, the donor and receptor compartments were clamped together with a custom-made vice lock. Using a syringe, the receptor compartment was filled with approximately 2 mL of degassed receptor solution determined gravimetrically. A 5 mm polytetrafluoroethylene (PTFE) coated magnetic stir bar was inserted into the sampling arm of the receptor compartment sampling arm covered with Parafilm® to prevent evaporation of the receptor solution. Franz cells were placed in a temperature-controlled water bath (Grant Instruments, U.K.) containing a

submersible multi-plate magnetic stirrer (Variomag®-USA, U.S.A.). Using a Multipette® plus dispenser (Eppendorf, Germany), a 50 µL infinite dose of each formulation was evenly applied to the donor compartment. At designated time points, 200 µL aliquots of receptor fluid were sampled. Receptor fluid samples were withdrawn from the sampling arm using polyvinyl chloride tubing (Thermo Scientific, USA) mounted to a 200 µL pipette plastic tip. All samples were analysed for tazarotene content using HPLC and then normalised to diffusion area and receptor volume. All experiments were conducted in triplicates for statistical analysis.

2.2.12 Mass balance of topical tazarotene formulations

At the end of the permeation experiment, the receptor fluid was removed and then discarded. Using 100% HPLC grade methanol, the skin surface was washed five consecutive times in 1 mL volumes and then dried with a cotton swab. All washes and swabs were transferred into a 2 mL Eppendorf tube. Franz cells were disassembled, and porcine skin was removed from the receptor compartment and then placed into 2 mL Eppendorf tubes filled with 1 mL of HPLC-grade methanol to extract the remaining tazarotene from the skin. All tubes were sealed with Parafilm™ and placed into an orbital mini shaker (VWR, UK) at 8000 rpm for approximately 24 h at 25°C ± 1°C. All washes and extractions were centrifuged at 12000 rpm for 15 min

at 25°C ± 1°C then the supernatant was removed for HPLC analysis. All experiments were conducted in triplicates for statistical analysis.

2.2.13 Data collection and statistical analysis of *in-vitro* results

Chromatogram data were integrated using Agilent ChemStation® for HPLC systems (Agilent Technologies, USA). Microsoft® Excel Office 2018 (Microsoft, USA) was used to analyse and graph the data. Parametric statistical tests, ANOVA and t-tests were conducted to investigate statistical differences using GraphPad Prism® 6 (Dotmatics, USA). All results, unless stated otherwise, are presented as mean ± standard deviation (SD).

2.3 Results and discussion

2.3.1 Molecular modelling calculations

In 1936, Joel H. Hildebrand derived an equation that could quantify the miscibility behaviour of different solvents. This value is known as the Hildebrand solubility parameter defined as the square root of the cohesive energy density for a pure liquid (Hildebrand 1936).

$$\delta = \sqrt{\left[\frac{\Delta H_v - RT}{V_m} \right]} \quad (2.1)$$

$$1 \text{ Hildebrand} = 1 \text{ cal}^{1/2} \text{ cm}^{-3/2}$$

Where ΔH_v is the heat of vaporization, V_m molar volume and RT is the ideal gas constant.

In 1967, Charles M. Hansen proposed an extension to the Hildebrand parameter that would estimate the relative miscibility of polar and hydrogen bonding systems. Hansen split the Hildebrand parameter into three individual components: dispersion forces, polar forces and hydrogen bonding, thus encompassing a 3-dimensional solubility parameter (Hansen 1967).

$$\delta_{\text{total}} = \delta_{\text{d}}^2 + \delta_{\text{p}}^2 + \delta_{\text{h}}^2 \quad (2.2)$$

Where $\delta_{\text{d}}^2 + \delta_{\text{p}}^2 + \delta_{\text{h}}^2$ are the dispersion forces, polar electrostatic forces, and hydrogen bonding components of δ respectfully.

Using the original Hildebrand equation, one can easily determine δ for molecules whose ΔH_v can be measured or calculated (Bogdanic 2006).

In recent years, computer programs have been used to estimate the Hildebrand and Hansen solubility parameters of compounds. Choi and Kavasallis first estimated the Hildebrand solubility parameters of alkyl phenol ethoxylates using atomistic simulation and then later applied it to estimate the Hansen 3D solubility parameter (Choi, Kavassalis et al. 1992, Kavassalis, Choi et al. 1993). The accuracy of computational estimations depends on the ability to construct the correct chemical

structure and the molecular force field parameters used in the algorithm for the calculation (Bogdanic 2006). To help refine the search for optimum vehicles, the solubility parameter values of tazarotene and different vehicles were determined.

Table 2.1 Hildebrand and Hansen solubility parameters for tazarotene

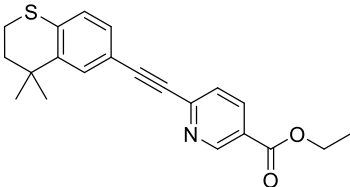
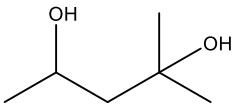
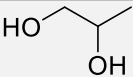
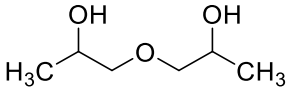
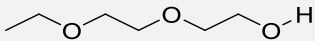
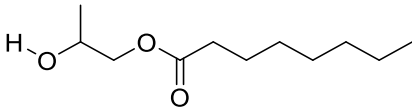
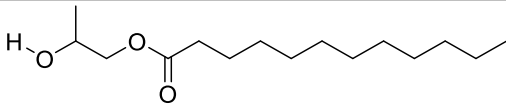
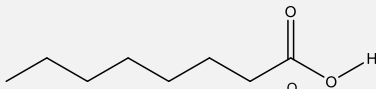
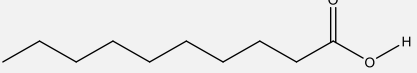
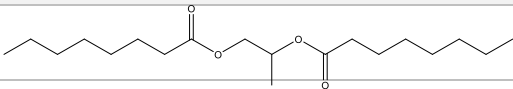
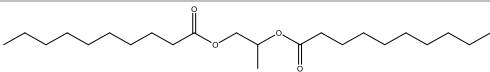
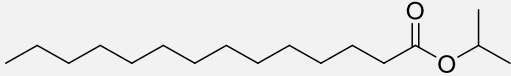
Drug	Molecular Information	Hildebrand Solubility parameter $/(cal\ cm^{-3})^{1/2}$	Hansen 3D solubility parameter/ (MPa ^{1/2}) ($\delta_d, \delta_p, \delta_h$)
Tazarotene	<chem>C21H21NO2S</chem> 	11.70	21.35, 6.60, 5.68

Table 2.2 Hildebrand and Hansen solubility parameters for a range of vehicles

Vehicle	Molecular Information	Hildebrand Solubility parameter / (cal cm ⁻³) ^{1/2}	Hansen solubility parameter/(MPa ^{1/2}) (δ _d , δ _p , δ _h)
Hexylene glycol	C ₆ H ₁₄ O ₂ 	25.72	16.09, 8.74, 17.62
Propylene glycol	C ₃ H ₈ O ₂ 	14.07	16.75, 9.33, 23.33
Dipropylene glycol	C ₆ H ₁₄ O ₃ 	12.19	15.79, 12.56, 16.83
Diethylene glycol monoethyl ether	C ₆ H ₁₄ O ₃ 	10.62	6.20, 9.22, 12.33
Propylene glycol monocaprylate	C ₁₁ H ₂₄ O ₃ 	9.84	16.46, 5.19, 12.22
Propylene glycol monolaurate	C ₁₅ H ₃₀ O ₃ 	9.44	15.47, 4.48, 10.68
Medium-chain triglycerides (Caprylic acid) (Capric acid)	C ₈ H ₁₆ O ₂  C ₁₀ H ₂₀ O ₂ 	9.44 9.19	15.17, 3.14, 8.23 5.55, 0, 7.50
Propylene glycol dicaprylocaprate	C ₁₉ H ₃₆ O ₄ 	8.72	13.95, 4.76, 13.18

(Propylene glycol dicaprylate) (Propylene glycol dicaprate)	$C_{23}H_{44}O_4$		8.62	15.65, 4.61, 13.25
Isopropyl myristate	$C_{17}H_{34}O_2$		8.21	15.52, 2.70, 2.92

The solubility parameters calculated may be used to predict the solubility of tazarotene in the selected vehicles by comparing the similarity between values. Using the Jouyban-Acree model and combining solubility parameters, Jouyban et al. were able to successfully predict the solubility of drugs in binary and ternary solvent mixtures (Jouyban, Shayanfar et al. 2011). Based on the results in tables 2.1 and 2.2 tazarotene is expected to be fully soluble in all the vehicles selected to varying extents and this will be confirmed by conducting solubility studies.

2.3.2 HPLC method development and validation

Although conducting a thorough method validation can be tedious, performing this incorrectly would result in wasted time, money as well as resources. During analytical method development, the chromatographic and the ideal experimental conditions are first established and then validated using the following parameters: linearity, precision, accuracy, robustness, the limit of detection (LOD), the limit of quantification (LOQ) and system suitability (Green 1996).

Linearity

Linearity is the ability of an analytical method to obtain results which are either directly proportional or proportional after mathematical transformation, to the concentration of the analyte within a given range. Generally, linearity is demonstrated by the preparation of standard solutions at five concentration levels,

from 50 to 150% of the target analyte concentration, with each concentration level being analysed at least three times. The five levels are necessary for the detection of curvature in the plotted data. One of the main indicators used to judge the acceptability of linearity data is the correlation coefficient (R^2) (Green 1996, Lam 2004).

Table 2.3 HPLC peak areas of tazarotene at different concentrations

Concentration ($\mu\text{g/ml}$)	Peak area
50	3087.30
25	1525.13
12.5	777.60
6.25	385.83
3.13	194.57
1.5625	95.8

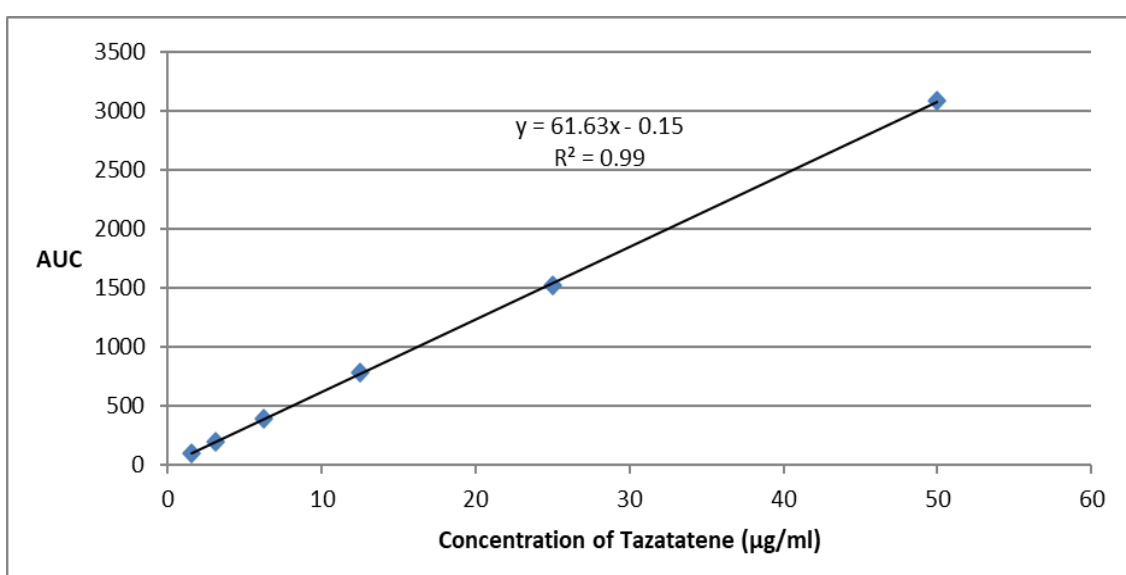


Figure 2.1 HPLC Linear calibration curve of tazarotene, $n = 3 \pm \text{SD}$

As shown in Figure 2.1, the representative linear equation was $y=61.63x - 0.15$. In this equation, 61.63 represents the slope and 0.15 the intercept. If the correlation coefficient (R^2) is ≥ 0.99 , the method has excellent linearity (Lam 2004). An R^2 value of 0.99 was obtained indeed demonstrating excellent linearity for the calibration curve of the selected method.

Accuracy

Accuracy is a measure of the deviation of test results obtained against its true expected value. A recovery study is a widely used method to determine accuracy. The recovery study is performed by spiking the analyte in blank matrices where spiked samples are prepared in triplicates at three levels, over a range of 100 to 15% of the target concentration. Accuracy is usually reported as the percentage recovery of a given amount of analyte added to the sample (Green 1996, Lam 2004).

$$\%Accuracy = \frac{\text{Mean observed concentration}}{\text{Expected concentration}} \times 100 \quad (2.3)$$

For tazarotene, accuracy was assessed in triplicates from three solutions of different concentrations in MeOH (50, 25 and 1.56 $\mu\text{g/ml}$).

Table 2.4 HPLC accuracy results for tazarotene

Theoretical concentration (µg/ml)	Measured concentration (µg/ml)*	Recovery (%)	RSD (%)
50	49.86 ± 0.02	99.71	0.04
25	24.79 ± 0.02	99.18	0.14
1.56	1.58 ± 0.004	101.35	0.26
		mean 100.08	mean 0.13

*mean ± SD (n=3)

Table 2.4 shows the recovery values for the three different concentrations which were 99.71 ± 0.04 , 99.18 ± 0.14 and $101.35\% \pm 0.26\%$ with a mean value of $100.08\% \pm 0.13\%$. The expected accuracy of the recovery of drug substances in a mixture should be between 95% to 105% (Lam 2004). The recovery values for the three selected concentrations and the mean values were successfully in the range of 95% to 105% and therefore deemed satisfactory.

Repeatability & Precision

The precision of an analytical method is the degree of agreement among individual test results obtained when the method is subjected to multiple samplings. Precision is usually verified by applying the method to test a sample enough times to obtain valid results. The procedure to assess the precision of a method includes the determination of repeatability (intra-day) and intermediate precision (inter-day). Repeatability is assessed by carrying out twelve repeated analyses of the same

working solution under the same experimental conditions on the same day, and intermediate precision (inter-day) is determined by performing the analysis on three different days by another analyst in the same laboratory (Green 1996).

The precision is expressed as the relative standard deviation (RSD).

The precision of the tazarotene method was verified through repeatability and intermediate precision using three different solutions at low, medium, and high concentrations, which were 1.56, 25 and 50 µg/ml.

Theoretical concentration (µg/ml)	Inter-day measured concentration(µg/ml)*					
	day 1		day 2		day 3	
	Mean ± SD	% RSD	Mean ± SD	% RSD	Mean ± SD	% RSD
50	50.04 ± 0.07	0.14	49.58 ± 0.06	0.11	49.93 ± 0.05	0.10
25	24.77 ± 0.02	0.07	24.63 ± 0.02	0.09	24.72 ± 0.03	0.14
1.56	1.54 ± 0.005	0.30	1.60 ± 0.004	0.28	1.54 ± 0.004	0.23

Table 2.5HPLC Inter-day variability results for tazarotene

*mean ± SD (n=3); Inter-day precision was determined from three different runs over 1 week

Table 2.6 HPLC Intra-day variability results for tazarotene

Theoretical concentration (µg/ml)	Intra-day measured concentrations(µg/ml)*	
	Mean ± SD	%RSD
50	50.01 ± 0.08	0.17
25	24.70 ± 0.01	0.06
1.56	1.59 ± 0.002	0.15

*mean ± SD (n=12)

For both intra-day and inter-day studies, the variation of all quantitative results should not be beyond the range of ± 2%(Green 1996). As can be seen in tables 2.5 and 2.6, the %RSD values of the measurements ranged from 0.07 to 0.30% for inter-day variability studies, while the results obtained from intra-day variability studies ranged from 0.06 to 0.17% which were both satisfactory.

Robustness

The robustness of an analytical method is defined as its capability to remain unaffected by small changes under normal test conditions, such as different analysts, laboratories, instruments, percentage of organic content and pH of the mobile phase, buffer concentration, temperature, and injection volume. These parameters may be evaluated one factor at a time or simultaneously as part of a factorial experiment (Green 1996). The robustness of the proposed HPLC method was determined by analysing tazarotene under a variety of experimental conditions.

Method	Wavelength (nm)	Injection volume (μl)	Temperature (°C)	Mobile phase water: ACN (v/v)	R ²	Recovery (%)
1	348	10	30	30:70	0.99	100.67
2	348	15	30	30:70	0.99	100.71
3	350	15	30	30:70	0.99	100.53
4	348	10	25	35:65	0.99	99.23
5	348	15	30	35:65	0.99	99.36

Table 2.7 Robustness results for varied HPLC conditions

Table 2.7 presents the results and chromatographic conditions selected as variables in each experiment. There were no obvious differences in the chromatograms when specific modifications were made in the given experiments. The correlation coefficients (R²) of the calibration curves were all ≥ 0.99 and the recovery ranged between 99.23 and 100.71%. The results obtained show that the HPLC method is robust enough to analyse tazarotene.

Limit of Detection (LOD) & Limit of Quantification (LOQ)

There are three methods for determining the detection and quantification limits of an analytical method, namely visual determination, signal-to-noise determination, and standard deviation and slope determination (Green 1996).

In this validation method, the standard deviation and slope determination methods were employed. The limit of detection (LOD) may be expressed as:

$$\mathbf{LOD} = \frac{3.3 \sigma}{S} \quad (2.4)$$

Where σ is the standard deviation of the response, and S is the slope of the calibration curve.

The slope S may be estimated from the calibration curve of the analyte. The estimate of σ may be carried out based on the standard deviation of the blank or based on the calibration curve. In the latter method, a specific calibration curve should be studied using samples containing an analyte in the range of the LOD. The residual standard deviation of a regression line or the standard deviation of the y-intercepts of regression lines may be utilized as the standard deviation (Green 1996).

Similarly, to the LOD, the limit of quantification (LOQ) may be expressed as

$$\mathbf{LOQ} = \frac{10 \sigma}{S} \quad (2.5)$$

Where σ is the standard deviation of the response, and S is the slope of the calibration curve.

Based on the standard deviation and slope determination, the LOD and LOQ of this HPLC method were determined to be 0.0065 and 0.02 $\mu\text{g/mL}$ respectively, showing excellent sensitivity.

System suitability

A system suitability test is used after a method has been validated fully, and when the validated method is being routinely used to analyse actual samples. A system suitability sample is run on any day that samples are being analysed, always before and after the actual batch of samples, and often within that run of batches, to demonstrate that the instrumental system is performing properly (Green 1996).

For the proposed method, the system suitability was determined by performing six replicate injections sampled from freshly prepared standard solutions of tazarotene at a concentration of 50 µg/ml and a comparison of the chromatogram parameters with a standard trace was performed to allow a comparison of the peak shape, peak width, and baseline resolution.

Table 2.8 HPLC System suitability results for tazarotene

	Mean ± SD*	%R.S.D
peak area	3092.60 ± 0.96	0.25
retention time(min)	5.07 ± 0.02	0.32
Symmetry	0.960 ± 0.04	0.58

*n=6

Table 2.8 shows the excellent resolution of the tazarotene peak with a high degree of symmetry confirming the analytical system is suitable to measure tazarotene.

2.3.3 Saturation solubility of tazarotene

The ability of a substance to form a solution with another substance is known as solubility. Solubility is a routinely investigated pre-formulation parameter essential for any formulation development programme. Solubility is the ability of a solute to dissolve in a solvent vehicle to produce a homogeneous solution. The solubility of an API in a solvent is related to similarities in their respective solubility parameters in addition to the temperature and pressure of the system being studied (Savjani, Gajjar et al. 2012). The extent of the solubility is measured as the saturation concentration where adding more API would not increase its concentration in the solution. Solubility occurs under a dynamic equilibrium resulting from the dissolution of a solute into the chosen medium. Under certain conditions, equilibrium solubility may be exceeded to produce a supersaturated solution (Brouwers, Brewster et al. 2009).

The solubility of an API in a vehicle can be expressed by equation 2.8.

$$-\ln X_2 = \frac{\Delta H_f}{RT} \left(\frac{T_0 - T}{T_0} \right) + \frac{V_2 \Phi_1^2}{RT} (\delta_1 - \delta_2)^2 \quad (2.6)$$

Where X_2 = molar fraction; Φ_1 = volume fraction of vehicle t ; V_2 = molar volume of API; R = universal gas constant; T = temperature in degrees Kelvin; T_0 = melting point of API; ΔH_f = molar heat of fusion; δ_1 = the solubility parameter of the vehicle;

and δ_2 = the solubility parameter of the API. At a particular temperature, the first term of the equation is constant, therefore, the solubility of an API would be expected to increase as the difference between δ_1 and δ_2 decreases (Dias, Hadgraft et al. 2007).

To select suitable vehicles for *in-vitro* permeation studies, the solubility of several solvents was evaluated.

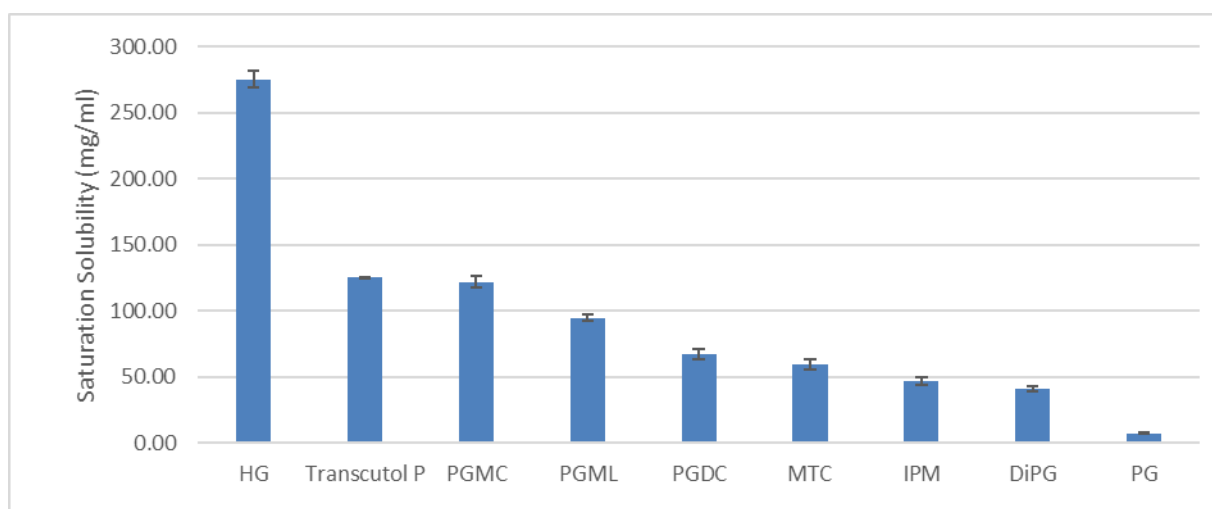


Figure 2.2 Saturation solubility of tazarotene in a range of vehicles, n=3, mean \pm SD

Figure 2.2 illustrates the saturation solubility of tazarotene in a broad range of vehicles that were investigated. Tazarotene was soluble in all the vehicles selected to varying extents with HG by far solubilising tazarotene the greatest (275.45 ± 6.39 mg/ml), followed by TC (125.30 ± 0.55 mg/ml), PGMC (121.91 ± 4.34 mg/ml), PGML (94.56 ± 2.57 mg/ml), PGDC (67.03 ± 3.75 mg/ml), MTC (59.42 ± 3.98 mg/ml), IPM (46.42 ± 2.94 mg/ml), DiPG (41.28 ± 1.91 mg/ml), and with PG being the least soluble vehicle (7.24 ± 0.29 mg/ml).

Selecting the correct receptor medium is critical for any *in-vitro* permeation study and therefore establishing the saturation solubility of a chosen API becomes essential in the selection process. The ideal receptor medium provides an accurate simulation of the *in-vivo* permeation conditions by maintaining the sink conditions of a test API. Generally, the concentration of the active in the receptor medium should not be allowed to exceed approximately 10% of the active's saturation solubility (Makino, Ohshima et al. 1992). Excessive receptor medium concentration of the API can lead to a decrease in the rate of absorption, which may result in an underestimation of skin uptake of the active.

The most used receptor medium is phosphate-buffered saline (PBS) pH7.4, however, this is not always the most appropriate medium. If an API has a water solubility of less than 10µg/ml, which is the case for tazarotene, then a wholly aqueous receptor medium is unsuitable and the addition of an appropriate solubiliser becomes necessary (Ng, Rouse et al. 2010). BSA and polyoxyethylene (20) oleyl ether (BrijO20[®]) were both investigated as solubilisers of tazarotene in PBS.

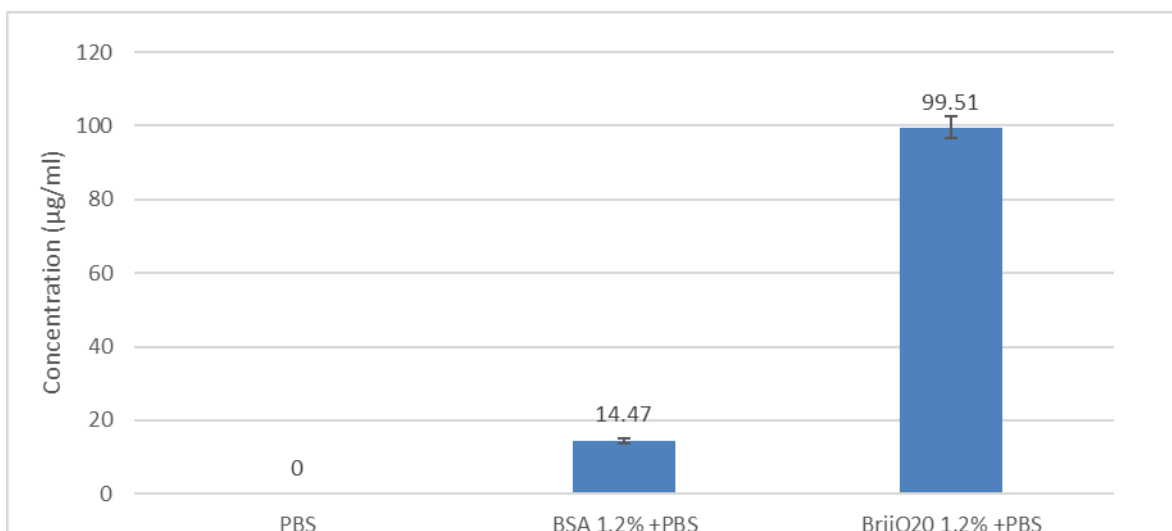


Figure 2.3 Saturation solubility of tazarotene in PBS, BSA + PBS and BrijO20® + PBS, n=3, mean +SD

Figure 2.3 illustrates the saturation solubility of tazarotene in PBS alone and with BSA and BrijO20®. The solubility of tazarotene in the PBS solution alone was lower than the limit of detection but could be detected but could be quantified with the addition of 1.2% BSA with saturation solubility at $14.47 \pm 0.7 \mu\text{g/ml}$ and for 1.2% BrijO20® the corresponding value was $99.51 \pm 2.94 \mu\text{g/ml}$. Tazarotene was solubilised in PBS significantly more ($p < 0.05$) in the presence of BrijO20® than in the presence of BSA solubilising $85.04 \mu\text{g/ml}$ more tazarotene at the same concentration.

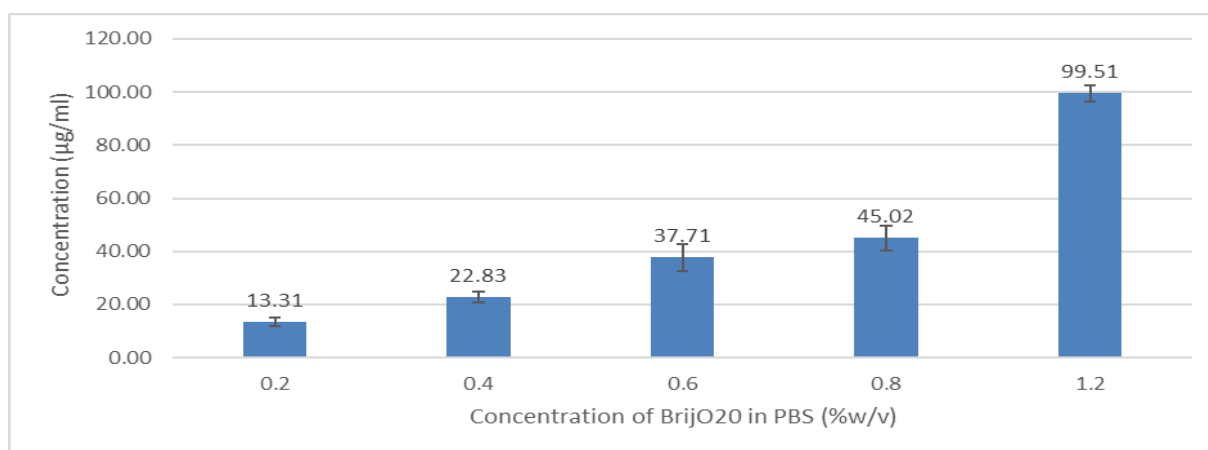


Figure 2.4 Saturation solubility of tazarotene in BrijO20® +PBS at increasing concentrations

Figure 2.4 illustrates the saturation solubility of tazarotene in PBS with the addition of increasing amounts of BrijO20[®]. At 0.2% of BrijO20[®] saturation solubility was 13.31 ± 1.63 µg/ml, for 0.4% of BrijO20[®] the value was 22.83 ± 2.18 µg/ml, for 0.6% of BrijO20[®] the value was 37.71 83 ± 5.19 µg/ml, for 0.8% of BrijO20[®] the value was 45.02 ± 4.71 µg/ml and for 1.2% of BrijO20[®] the value was 99.51 ± 2.94 µg/ml. As the concentration of BrijO20[®] increased, the saturation solubility of tazarotene also significantly increased (p<0.05) and BrijO20[®], therefore, was confirmed to be a suitable receptor medium additive to solubilise tazarotene.

2.3.4 Stability of tazarotene

Stability studies should include testing the properties of an API that are susceptible to change and are likely to influence its quality. Any evaluation should consider not only the API in question but also any degradation products (Joseph, Satinder et al. 1978). Stability studies have shown that retinoids overall are photosensitive with their degradation following first-order kinetics, and thus may require proper stabilization of their final formulations (Rakusa, Skufca et al. 2021). The stability of tazarotene in the selected vehicles was previously unreported and therefore had to be assessed before conducting *in-vitro* skin permeation studies.

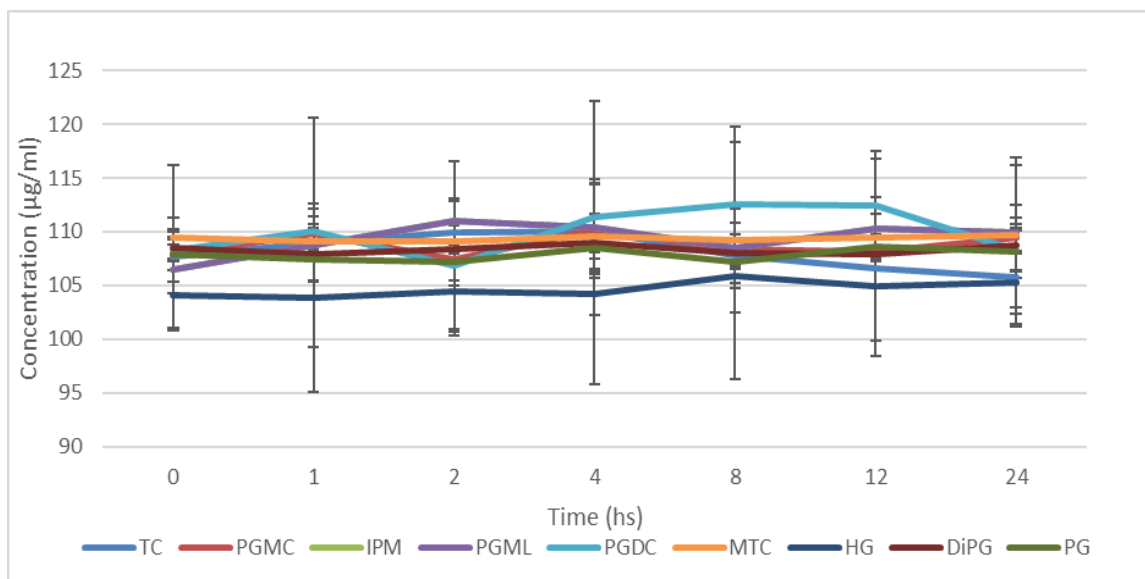


Figure 2.5 Stability of tazarotene in a range of vehicles over 24h, n=3, mean +SD

Figure 2.5 illustrates the chemical stability of tazarotene in several solvents over 24 h. HPLC peaks did not shift nor decrease in intensity during the entire analysis period, confirming that the concentration of tazarotene remained constant over the 24 h for all vehicles examined. Samples were also analysed for tazarotene's major metabolite tazarotenic acid, however again no traces of it were detected over the entire examination period. Tazarotene, therefore, was deemed stable enough to be further investigated in all selected vehicles without the need to stabilise the formulation.

2.3.5 Miscibility of CPE

Miscibility can be defined as the ability of two or more liquids to form a homogeneous mixture when added together. Miscibility is usually defined by thermodynamic

parameters where the Gibbs free mixing enthalpy ΔG_m is decisive for the compatibility of phases. ΔG_m can be determined according to changes in enthalpy (ΔH_m) and entropy of mixing the components (ΔS_m). According to equation 2.9, the change in enthalpy is the decisive parameter for thermodynamic miscibility (Stefanescu 2015).

$$\Delta G_m = \Delta H_m - T \Delta S_m \quad (2.7)$$

If ΔG_m is positive, components are not miscible. If ΔG_m is negative and the second derivative is positive, components are miscible. Independent of composition, a homogeneous blend is thus formed. If ΔG_m is negative and the second derivative is negative as well, the components are partially miscible. Phases with different compositions are formed consisting of all the components. ΔH_m is directly proportional to the number of interactions between components and becomes negative for strong interactions such as ion, acid-base, hydrogen bonds or dipole-dipole interactions (Robeson 2007, Stefanescu 2015). The miscibility of lipophilic drugs with hydroxypropyl methylcellulose acetate succinate (HPMCAS) grades was investigated and revealed that interactions between the drugs and polymeric grades are crucial in determining the drug precipitation (Jha, Shah et al. 2021).

Table 2.9 Miscibility of PG with TC, PGMC, PGML, PGDC, MTC, IPM, DiPG at room temperature. IM = immiscible; M = miscible

PG	TC		PGMC		PGML		PGDC		MTC		IPM		DiPG	
(% v/v)	(% v/v)	Mis.	(% v/v)	Mis.	(% v/v)	Mis.	(% v/v)	Mis.	(% v/v)	Mis.	(% v/v)	Mis.	(% v/v)	Mis.
10	90	M	90	M	90	M	90	IM	90	IM	90	M	90	M
20	80	M	80	M	80	M	80	IM	80	IM	80	M	80	M
30	70	M	70	M	70	M	70	IM	70	IM	70	M	70	M
40	60	M	60	M	60	M	60	IM	60	IM	60	M	60	M
50	50	M	50	M	50	M	50	IM	50	IM	50	M	50	M
60	40	M	40	M	40	M	40	IM	40	IM	40	M	40	M
70	30	M	30	M	30	M	30	IM	30	IM	30	M	30	M
80	20	M	20	M	20	M	20	IM	20	IM	20	M	20	M
90	10	M	10	M	10	M	10	IM	10	IM	10	M	10	M

Table 2.10 Miscibility of HG with TC, PGMC, PGML, PGDC, MTC, IPM, DiPG at room temperature. IM = immiscible; M = miscible

HG	TC		PGMC		PGML		PGDC		MTC		IPM		DiPG	
(% v/v)	(% v/v)	Mis.	(% v/v)	Mis.	(% v/v)	Mis.	(% v/v)	Mis.	(% v/v)	Mis.	(% v/v)	Mis.	(% v/v)	Mis.
10	90	M	90	M	90	M	90	M	90	IM	90	M	90	M
20	80	M	80	M	80	M	80	M	80	IM	80	M	80	M
30	70	M	70	M	70	M	70	M	70	IM	70	M	70	M
40	60	M	60	M	60	M	60	M	60	IM	60	M	60	M
50	50	M	50	M	50	M	50	M	50	IM	50	M	50	M
60	40	M	40	M	40	M	40	M	40	IM	40	M	40	M
70	30	M	30	M	30	M	30	M	30	IM	30	M	30	M
80	20	M	20	M	20	M	20	M	20	IM	20	M	20	M
90	10	M	10	M	10	M	10	M	10	IM	10	M	10	M

The miscibility tables 2.9 and 2.10 showed that PG and HG were fully miscible with TC, PGMC, PGML, IPM, DiPG, and only HG was miscible with PGDC at all ratios in the absence of tazarotene. PG and HG were however completely immiscible in MTC, and PG was also immiscible with PGDC at all ratios. The miscibility of the CPEs selected was adequate to begin developing combinations of CPEs formulations with tazarotene.

2.3.6 Mass balance development and validation

To perform a successful mass balance study, the solvents used to wash the skin surface and extract the API from the skin membrane must be carefully selected. For skin surface washing, a solvent should be able to dissolve all vehicles in a formulation and large amounts of the API. The solvent should also easily penetrate the skin to extract the API efficiently. The stability of the API in the solvent used for the skin washing and extraction procedures should maintain the API's stability throughout the mass balance process (Bucks, Guy et al. 2008).

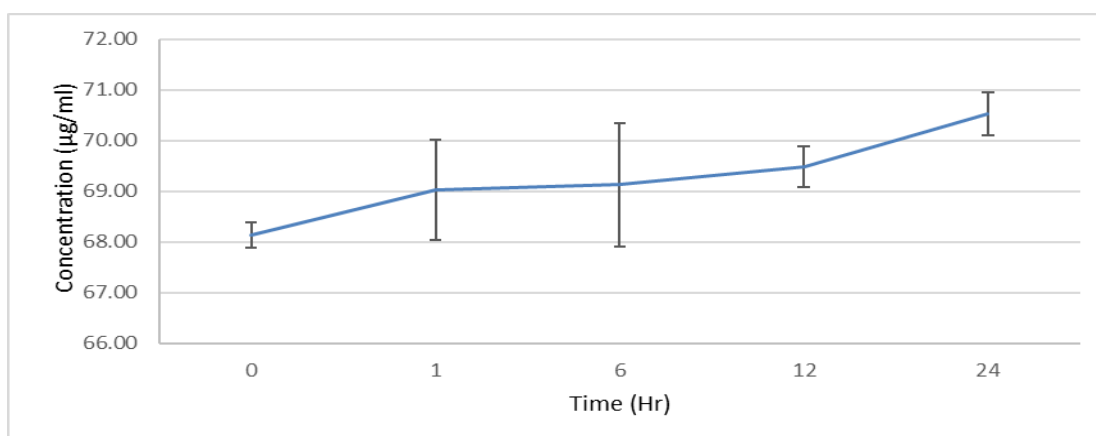


Figure 2.6 Stability of tazarotene in methanol over 24 h, n=3, mean +SD

Figure 2.6 illustrates the chemical stability of tazarotene in HPLC-grade methanol over 24 h. The concentration of tazarotene in the methanol solution remained constant for over 24 h. No traces of tazarotenic acid, tazarotene's major metabolite, were detected over the entire examination period. MeOH has therefore been deemed a suitable solvent for skin surface washing and extraction for mass balance studies of tazarotene.



Figure 2.7 Mass balance validation of tazarotene n=3, mean +SD

Figure 2.7 illustrates the amount of tazarotene found on the skin surface and inside the skin compared to the total applied amount. Tazarotene was only detected on the skin surface and not inside the skin. The total amount of tazarotene recovered, 98.42 \pm 4.48 %, was equal to the amount found on the skin surface. The mass balance

method developed was therefore deemed satisfactory to analyse tazarotene for *in-vitro* permeation studies.

2.3.7 Mass balance of topical tazarotene formulations

The most common methods for evaluating *in-vitro* skin permeation use diffusion cells. The major advantage of *in-vitro* investigations is that the experimental conditions can be controlled precisely such that the only variables are the skin, test material and the individual conducting the study. *In-vitro* systems are used to evaluate skin permeation and range in complexity from a simple two-compartment static diffusion cell to jacketed flow-through cells. Static diffusion cells are usually of the upright Franz type, with receptor chamber volumes between 2-10 ml and surface areas of exposed membranes between 0.2-2cm². Cell dimensions should be accurately measured, and precise values used in subsequent calculations, with due attention to the dilutions resulting from sampling and replenishment of the receptor phase (Friend 1992, Barbero and Frasch 2009).

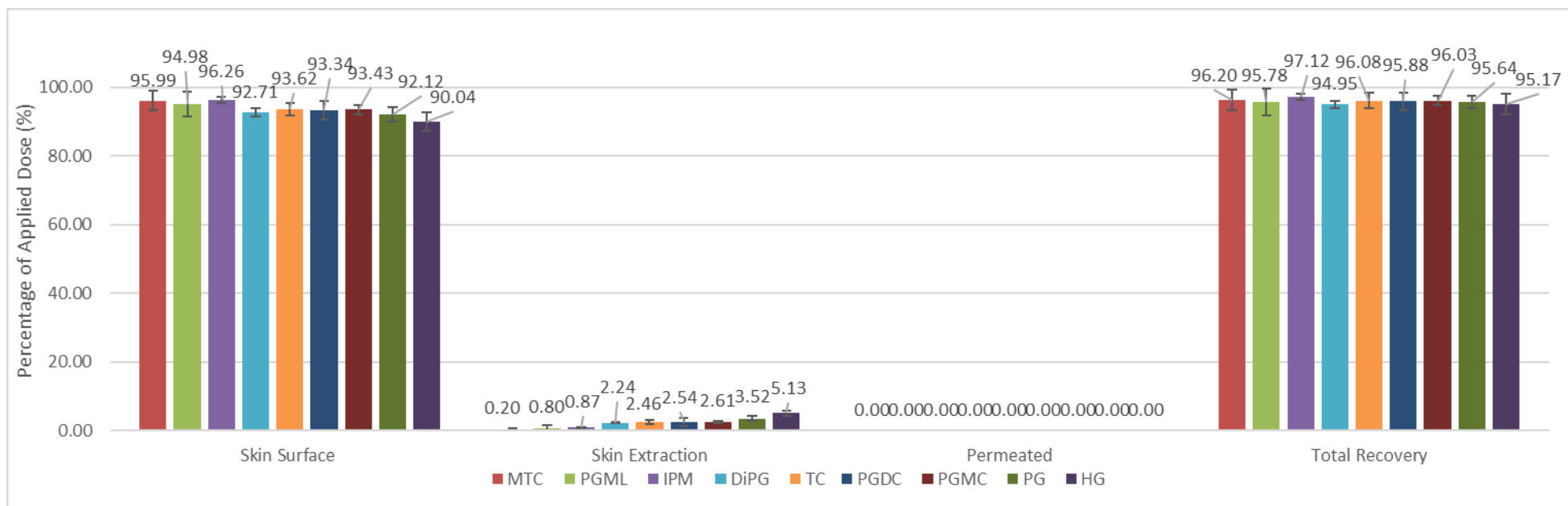


Figure 2.8 Infinite dose mass balance study of single solvents containing tazarotene applied to porcine skin after 24 h, mean \pm SD, n=5

Figure 2.8 illustrates the infinite dose mass balance study over 24 h of tazarotene in HG, PG, PGMC, PGDC, TC, DiPG, PGML and MTC applied to porcine skin. The mass balance studies showed that approximately 90% - 96% of the applied dose remained on the surface of the skin and approximately 0.2% - 5% penetrated the skin. No tazarotene was detected in the receptor medium throughout the entire period of any permeation study and the overall total recovery ranged between 94% - 97%.

HG was able to deliver the highest amount of tazarotene into the skin (5.13 ± 0.81 %) followed by PG (3.52 ± 0.79 %), PGMC (2.61 ± 0.32 %), PGDC (2.54 ± 1.18 %), TC (2.46 ± 0.54 %), DiPG (2.24 ± 0.13 %), IPM (0.87 ± 0.09 %), PGML (0.80 ± 0.66 %) and MTC with the least amount found in the skin (0.2 ± 0.46 %). Significant variance ($p < 0.01$) between vehicles was observed with HG and PG delivering significantly more ($p < 0.05$) tazarotene into the skin compared to the other CPEs examined.

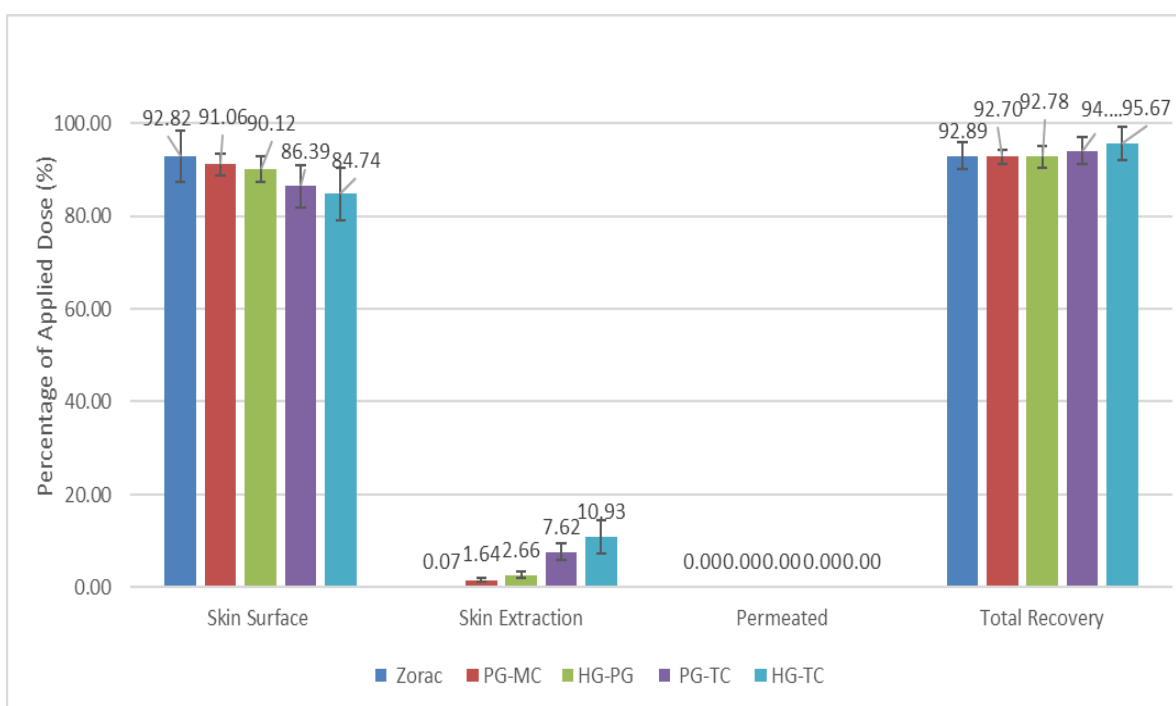


Figure 2.9 Infinite dose mass balance study of commercial Zorac[®] gel formulation and binary solvent systems containing tazarotene applied to porcine skin after 24 h, mean \pm SD, n=5

Figure 2.9 illustrates the infinite dose mass balance study of tazarotene in the commercial Zorac[®] gel, HG:TC, PG:TC, HG:PG and PG:MC over 24 h applied to porcine skin. The mass balance studies showed that approximately 85% - 92% of

the applied dose remained on the surface of the skin and approximately 0.07% - 11% penetrated the skin. No tazarotene was detected in the receptor medium throughout the entire period of any permeation study and the overall total recovery ranged between 93% - 95%. HG:TC delivered the highest amount of tazarotene into the skin (10.93 ± 3.67 %) followed by PG:TC (7.62 ± 1.81 %), HG:PG (2.66 ± 0.64 %), PG:MC (1.64 ± 0.49 %), and Zorac[®] gel with the least amount found in the skin (0.06 ± 0.14 %). Significant variance (p<0.01) between penetration groups was observed, with all binary solvent systems delivering significantly more (p<0.05) tazarotene into the skin compared to Zorac[®] gel, and HG:TC and PG:TC delivering the most active into the skin from the binary solvent systems.

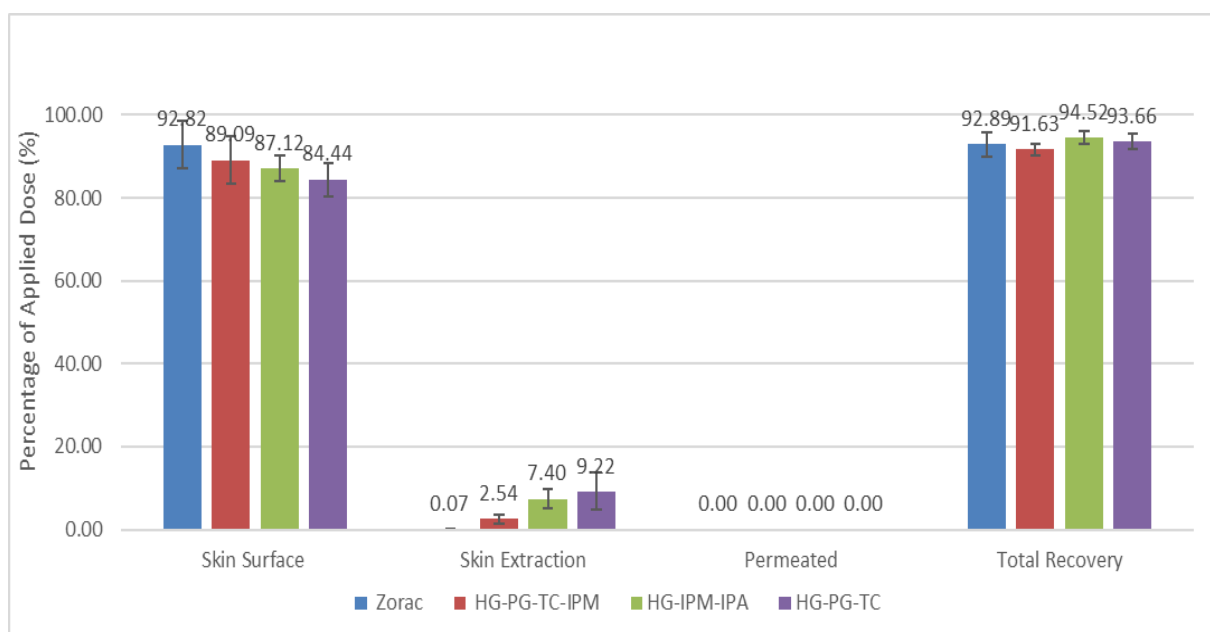


Figure 2.10 Infinite dose mass balance study of commercial Zorac[®] gel formulation, ternary and quaternary solvent systems containing tazarotene applied to porcine skin after 24 h, mean ± SD, n=5

Figure 2.10 illustrates the infinite dose mass balance study of tazarotene in the commercial Zorac[®] gel and HG:PG:TC, HG:IPM:IPA and HG:PG:TC:IPM over 24 hours applied to porcine skin. The mass balance studies showed that approximately 84% - 93% of the applied dose remained on the surface of the skin and approximately 0.07% - 9% penetrated the skin. No tazarotene was detected in the receptor medium throughout the entire period of any permeation study and the overall total recovery ranged between 92% - 94 %. HG:PG:TC delivered the highest amount of tazarotene into the skin (10.93 ± 4.51 %) followed by HG:IPM:IPA (7.40 ± 2.22 %), HG:PG:TC:IPM (2.54 ± 1.15 %), and Zorac[®] gel again with the least amount found in the skin (0.07 ± 0.14 %). Significant variance ($p < 0.01$) between penetration groups was observed with all ternary solvent systems delivering significantly more ($p < 0.05$) tazarotene into the skin compared to Zorac[®] gel while HG-PG-TC and HG-IPM-IPA delivered the most into the skin from the ternary and quaternary solvent systems examined.

2.4 Conclusions

The development of tazarotene, a third-generation selective retinoid, has improved clinical outcomes and reduced the occurrence of unwanted side effects typically associated with retinoid therapy. However, due to tazarotene's physicochemical properties, effective penetration into the skin remains a major challenge for formulation scientists. This chapter has set out the basis of a rational formulation design to enhance and optimise the delivery of tazarotene into the skin. The first stage of the work involved molecular modelling of tazarotene and selected CPEs to calculate their respective Hildebrand and Hansen solubility parameters. A satisfactory HPLC method was then developed and validated to analyse tazarotene before the solubility and stability of tazarotene were examined in the selected CPEs. Solubility parameter calculations related well with the actual experimental saturation solubility of tazarotene in the vehicles selected as all were able to solubilise tazarotene readily. Unlike other retinoids, tazarotene did not show any stability issues in the selected vehicles, receptor medium or solubilising solvent used to perform a mass balance. PG and HG were completely miscible, with most of the other penetration enhancers examined in binary systems, except for PGDC and MTC. Franz diffusion cell and mass balance studies showed penetration of tazarotene into porcine skin was achieved with all the single solvents selected as

well as with the more complex binary and ternary solvent systems to various extents ranging between 0.8% to 11% in the skin and between 85% to 96% on the skin, with the total recovery of all experiments not falling below 90%. The worst performing single solvent was by far MTC and PGML while the worst performing binary and quaternary solvent systems were PG:MC and HG:PG:TC:IPM. The best performing single solvent was HG while the best performing binary and ternary solvent systems were HG:TC and HG:PG:TC respectively which indicates HG and TC add the most value to the delivery of tazarotene into the skin. HG, PG and TC were all able to solubilise tazarotene extremely well to different degrees to exploit thermodynamic changes. HG and PG both being glycol are thought to have modified the diffusion of tazarotene through the SC by partitioning and then integrating into the hydrophilic regions between packed intercellular lipids increasing the lamellar phase distance to allow more of the drug through. TC on the other hand is thought to have altered the solubility parameter of the intercellular lipid domains providing a more favourable environment for tazarotene to diffuse through. Results in this chapter suggest that combinations of HG, PG, TC, IPM and IPA have the greatest potential to significantly enhance the penetration of tazarotene into human skin over the commercially available Zorac® gel.

Chapter Three:

In-vitro Confocal Raman Spectroscopy Evaluation of Topical Tazarotene Formulations

Chapter Three

In-vitro Confocal Raman Spectroscopy evaluation of topical tazarotene formulations

3.1 Introduction

The structure and composition of the SC lipids are recognized as playing a dominant role in the barrier function of the skin. Considerable effort has been undertaken to elucidate the mechanisms involved in this barrier function, using X-ray diffraction, electron microscopy, Infrared and Raman spectroscopy (Warner, Myers et al. 1988, Goldsmith 1991, Vonzglinicki, Lindberg et al. 1993, Anigbogu, Williams et al. 1995). Raman spectroscopy, however, has certain advantages, such as its relative insensitivity to water, which justifies its increasing popularity for skin characterisation. Raman spectroscopy is a non-destructive technique with a wide range of possible applications in the field of biomedical research. As the technique can be used non-invasively, it is of great interest to skin researchers, particularly in the field of skin permeation. Puppels et al. first used CRS to take confocal spectral measurements of the skin at specified depths. The CRS setup isolated Raman scattering within a small pinhole of 100 μm which was able to produce a depth resolution of 1.3 μm . With this arrangement, confocal spectral measurements of the skin at specified depths were possible (Puppels, Huizinga et al. 1990). The combined use of Raman scans taken

in the fingerprint and the high wavenumber regions allow for detailed information about the skin to be gathered in the form of depth profiles. *In-vivo* CRS spectra of the SC have highlighted the differences between several body sites in addition to identifying the spectra of the major amino acid components of the natural moisturizing factor (NMF) and sweat constituents, such as lactate and urea (Lucassen, Caspers et al. 1998, Caspers, Lucassen et al. 1999, Caspers, Lucassen et al. 2001). Substantial work has been performed on the hydration state of the skin using spectral CRS measurements in the high wavenumber region allowing for the water concentration to be determined for SC thickness calculations (Caspers, Lucassen et al. 2000, Lucassen, Caspers et al. 2000). Carotenoid distribution in the skin has been profiled in the palm, forehead, and volar forearm of human volunteers using CRS to compare the skin from different body sites which showed that the SC was thinnest on the forehead and thickest in the palms of the hands (Darvin, Fluhr et al. 2009). The *in-vivo* deposition of ibuprofen into the skin has also been investigated using CRS which was then compared with conventional *in-vitro* Franz cell permeation data showing a strong correlation between *in-vivo* and *in-vitro* results (Mateus, Abdalghafor et al. 2013, Mohammed, Matts et al. 2014). CRS is desirable when studying skin permeation as it allows for repeat analysis of the same site of application without disturbing the integrity of the skin under investigation. Another attractive feature of CRS is its ability to conduct real-time measurement providing a

more accurate depiction of permeation into the skin. Stamatias et al. were able to measure *in-vivo* spectra of vegetable oils and paraffin in the stratum corneum using a CRS technique only in the high wavenumber region. They concluded that there was no difference in the occlusive effect of oils they tested based solely on the CRS results (Stamatias, de Sterke et al. 2008). Raman spectroscopy was previously assessed as a simple and non-invasive method for SC thickness measurements showing good comparability of NIR densitometric and microscopic analysis with Raman spectroscopy presenting a useful and rapid alternative SC thickness measurement technique (Mahrhauser, Nagelreiter et al. 2015). Franzen et al. were able to conduct a systematic validation study utilising CRS for quantitative depth profiling *in vitro* of caffeine in human skin. They established an experimental procedure correlating the Raman signal with drug concentration in the skin establishing a proof-of-concept (Franzen, Anderski et al. 2015). Kis et al. demonstrated with Raman mapping that BG and PG could significantly enhance permeation by increasing the mobility of both lipids and amino acids in the SC. They also concluded that glycols have a non-monotonic response to permeation enhancement showing that higher concentrations did not give the highest permeation (Kis, Gunnarsson et al. 2022). Pudney et al used CRS to monitor the *in-vivo* effects chemical penetration enhancers have on trans-retinol delivery into human skin. Remarkable differences in the delivery of trans-retinol were observed

between formulations. Penetration into the skin was strongly correlated with the penetration depth of PG and oleic acid (Pudney, Melot et al. 2007, Melot, Pudney et al. 2009). In this chapter, a CRS method was developed to quantify the amount of tazarotene in the skin at different depths giving particular focus to the SC. SC thickness measurements were performed by analysing the water content throughout the SC and viable epidermis. CRS measurements were conducted *in-vitro* on porcine skin from Franz diffusion cells after the application of tazarotene-containing formulations. The correlation between CPEs and tazarotene depth were also examined.

3.2 Materials and methods

3.2.1 Materials

Zorac[®] gel 0.1% was supplied by Allergan pharmaceuticals (IRL).

Tazarotene was supplied by Insight Biotechnology (UK).

HG, PG, IPA and HPLC grade water, HPLC grade methanol, and HPLC grade ethanol were supplied by Fisher Scientific (UK).

TC was gifted by Gattefossé (UK).

IPM and BrijO20[®] were supplied by Sigma-Aldrich (UK).

Dulbecco PBS (pH = 7.3 ± 0.2 at 25°C) was supplied by Oxoid (UK).

Franz diffusion cells were supplied by SES GmbH (UK).

Porcine ears were sourced from a local abattoir.

3.2.2 CRS instrument

In-vitro experiments were conducted using the Model 3510 SCA Skin Composition Analyser (River Diagnostics, Rotterdam) class 2M laser device, offering an axial spatial resolution of 5 µm and a spectral resolution of 4 cm⁻¹ throughout the entire optical spectral range. This instrument consists of two near infra-red (NIR) lasers

each emitting monochromatic light, one at 785 nm used to capture fingerprint region spectra between 400 – 2400 cm^{-1} and the other at 671 nm used to capture high wavenumber region spectra between 2400 – 4000 cm^{-1} .

The instrument has an inverted microscope objective sample stage with an oil immersion lens used to focus the incident laser light to acquire skin scatter data. Scattered light from the skin bounces back through the microscope objective pinhole and is detected by a charge-coupled device (CCD) cooled to -70°C to reduce thermal noise. The instrument is fitted with an internal video camera that allows for the skin surface to be inspected to choose an ideal point of skin contact for analysis.

To allow for the instrument to adequately stabilise, it is switched on about 30 – 60 min before it is used. Laser power is verified by a Juno PD300-TP and StarLab V2.0 device (Ophir Photonics, Israel) to ensure the 785 nm laser is between 20 – 30 mW and the 671 nm laser is between 10 – 20 mW before calibration. To calibrate the instrument, a relative intensity correction standard calibration glass (NIST, USA) was used by placing it over the microscope objective lens and then, a pre-set calibration sequence was run. To achieve a successful calibration the signal-to-noise ratio was always confirmed 30 before use to ensure results were reliable.

3.2.3 Raman reference spectra collection and calibration

A Raman reference spectrum for all excipients used, HG, PG, TC, IPM, IPA, and EtOH, were collected in the fingerprint region with the 785 nm laser. The sample window was set to 0 mm displacement in Raman experiment mode. The microscope objective was set to a focus at 100 μm to ensure all spectra obtained were solely from the 20 μL sample placed on the objective window. A thirty-second exposure time was selected for HG, PG, TC and IPM and five seconds for IPA and EtOH as this produced a high-intensity spectrum with a low background noise without saturating the CCD camera. All reference spectra were collected using an average of ten frames per exposure time. For the Raman reference spectrum of tazarotene, tazarotene was dissolved in EtOH to produce five concentrations, 0.1%, 0.3%, 0.5%, 0.8% and 1% w/v. EtOH was used as tazarotene is highly soluble in it, enabling a good-quality reference spectrum to be obtained. A five-second exposure time was selected with an average of five frames per exposure time. All other measurement parameters remained the same as the neat solvents. To separate the Raman spectrum of tazarotene from EtOH in all five solutions, spectra were deducted from each other using SkinTools V2.0. After isolating the Raman spectrum of tazarotene, the spectra were uploaded into SkinTools V3.0 to calculate a linear regression using

the five mass ratios, Raman ratios and proportionally constant described in equation

3.1.

$$\frac{m_{Tazarotene}}{m_{Protein}} = C_{BSA:protein}^{-1} * C_{BSA:water} * C_{ethanol:water}^{-1} * C_{Tazarotene:ethanol}^{-1} * \frac{R_{Tazarotene}}{R_{Protein}} \quad (3.1)$$

3.2.4 Tazarotene formulation preparation

All formulations were made fresh as required. The appropriate mass of tazarotene was weighed in a 2 mL plastic Eppendorf with a locking lid. For binary and ternary formulations, a total of 1 mL of the required solution was pipetted into a 2 mL Eppendorf containing the pre-weighed amount of tazarotene to give a final concentration of 0.1% (w/w). Eppendorfs were then locked, wrapped in Parafilm® and placed into an incubating orbital mini shaker (VWR, UK) at 800 RPM and 25 °C ± 1°C for approximately 3 h to ensure complete solubilization of the tazarotene. Solvent systems examined include HG:TC (80:20), PG:TC (80:20), HG:PG (50:50), HG:PG:TC (40:40:20) and HG:IPM:IPA (80:10:10). All formulation constituents were weighed using an analytical balance (Mettler Toledo, UK). The concentration of tazarotene in all the solutions prepared was measured via HPLC.

3.2.5 Porcine skin preparation

Porcine ears used were prepared on the same day of slaughter. The ears were gently cleansed with deionised water and then dried before cutting all excess hair

short with scissors. The full thickness of the outer ear portion was delicately removed from the cartilage underneath it, using a scalpel to avoid damaging the SC. Once removed, the full-thickness porcine skin was rinsed with cold deionised water, blotted dry using filter paper then flat wrapped and packed in aluminium foil before being stored at $-20^{\circ}\text{C} \pm 1^{\circ}\text{C}$ before use.

3.2.6 *In-vitro infinite dose permeation* studies of topical tazarotene formulations

All the permeation studies were conducted using glass vertical Franz diffusion cells and porcine ear skin. Porcine ear skin was punched out into approximately 3 cm² circular pieces. The donor and receptor compartments were covered with a thin layer of high vacuum grease (Dow Corning, U.S.A.) before placing the porcine skin between them to create a tight leakproof seal around the skin. The donor and receptor compartments were clamped together with a custom-made vice lock. A receptor solution was prepared by dissolving 5 g of BRIJO20[®] in 100 ml of PBS (pH = 7.4 ± 0.2 at 25°C) in a glass beaker using a magnetic stirrer plate (Bibby Sterlin, UK). The receptor solution was degassed for approximately 30 min in an ultrasonication bath at a temperature of 25°C. Using a syringe, the receptor compartment was filled with approximately 2 mL of degassed receptor solution determined gravimetrically. A mini magnetic stirrer bar was inserted into the receptor compartment and the sampling arm was covered with Parafilm[®] to prevent

evaporation of the receptor solution. Franz cells were placed in a temperature-controlled water bath (Grant Instruments, U.K.) containing a submersible multi-plate magnetic stirrer (Variomag, USA). Using a Multipette® plus dispenser (Eppendorf, Germany), a 50 µL infinite dose of each formulation was applied to the donor compartment. Following a 6-hour application, porcine skin was removed from the Franz diffusion cell to be examined by CRS. All experiments were conducted in triplicates for statistical analysis.

3.2.7 Data collection and statistical analysis of *in-vitro* results

CRS depth profile spectra were obtained at a step size of 2 µm with an exposure time of ten-second per depth in one frame using the 785 nm laser collecting data in the fingerprint region (400–2000 cm⁻¹). Raman water profile spectra were obtained at a step size of 2µm with an exposure time of ten-second per depth in one frame, using the 671 nm laser in the high wavenumber region (2400 – 4000 cm⁻¹). All CRS data were acquired using RiverIcon® v.3.0013 and analyzed with Skin Tools® v.3.0 programs (River Diagnostics, The Netherlands). Microsoft® Excel Office 2018 (Microsoft, USA) was used to analyse and graph the data. Parametric statistical tests, ANOVA and t-tests were conducted to investigate statistical differences using GraphPad Prism® 6 (Dotmatics, USA). All results, unless stated otherwise, are presented as mean ± standard deviation (SD).

3.3 Results and discussion

3.3.1 Raman reference spectra and calibration

To track the deposition of compounds into the skin via CRS, a reference spectrum needed to first be collected. These reference spectra form the basis for future experimental analysis using the SkinTools[®] program (River Diagnostics, Netherlands).

As mentioned previously in chapter 1, the skin is a highly complex heterogeneous system made up of different lipids and proteins. This complexity becomes very much apparent when assessed through Raman spectroscopy, as several high-intensity bands primarily from the keratin protein are seen in the fingerprint region. This includes the phenylalanine at 1004 cm^{-1} , the amide III at 1298 cm^{-1} the CH_2 at 1440 cm^{-1} and the amide I at 1650 cm^{-1} illustrated in figure 3.1 (Barry, Edwards et al. 1992).

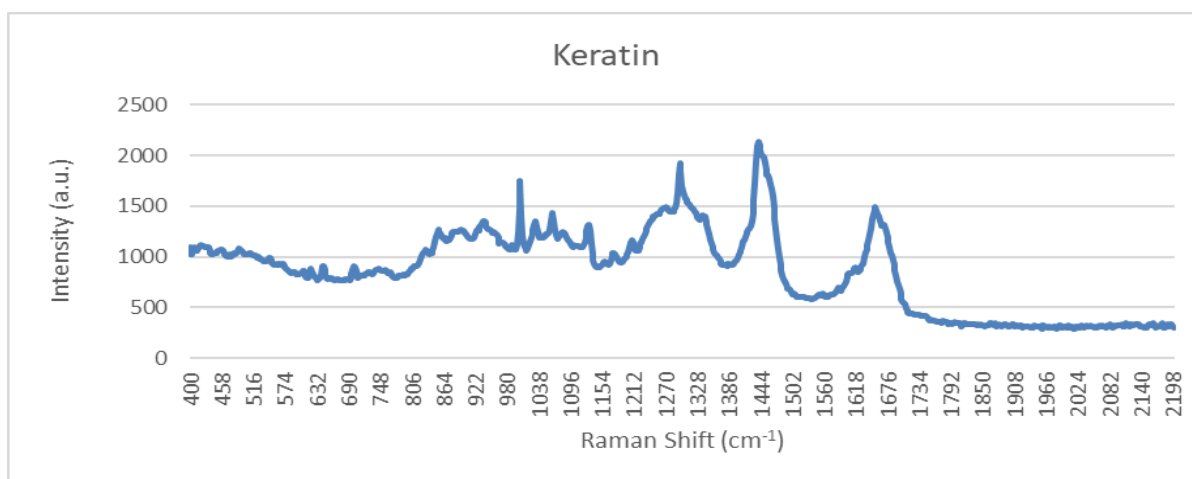


Figure 3.1 Raman fingerprint region spectra of keratin protein in porcine skin.

The Raman spectra of a compound, therefore, should ideally contain at least one unique highly intense band to differentiate it from the complex skin spectra background.

The reference spectra for all solvents used in this study are reported in figure 3.2.

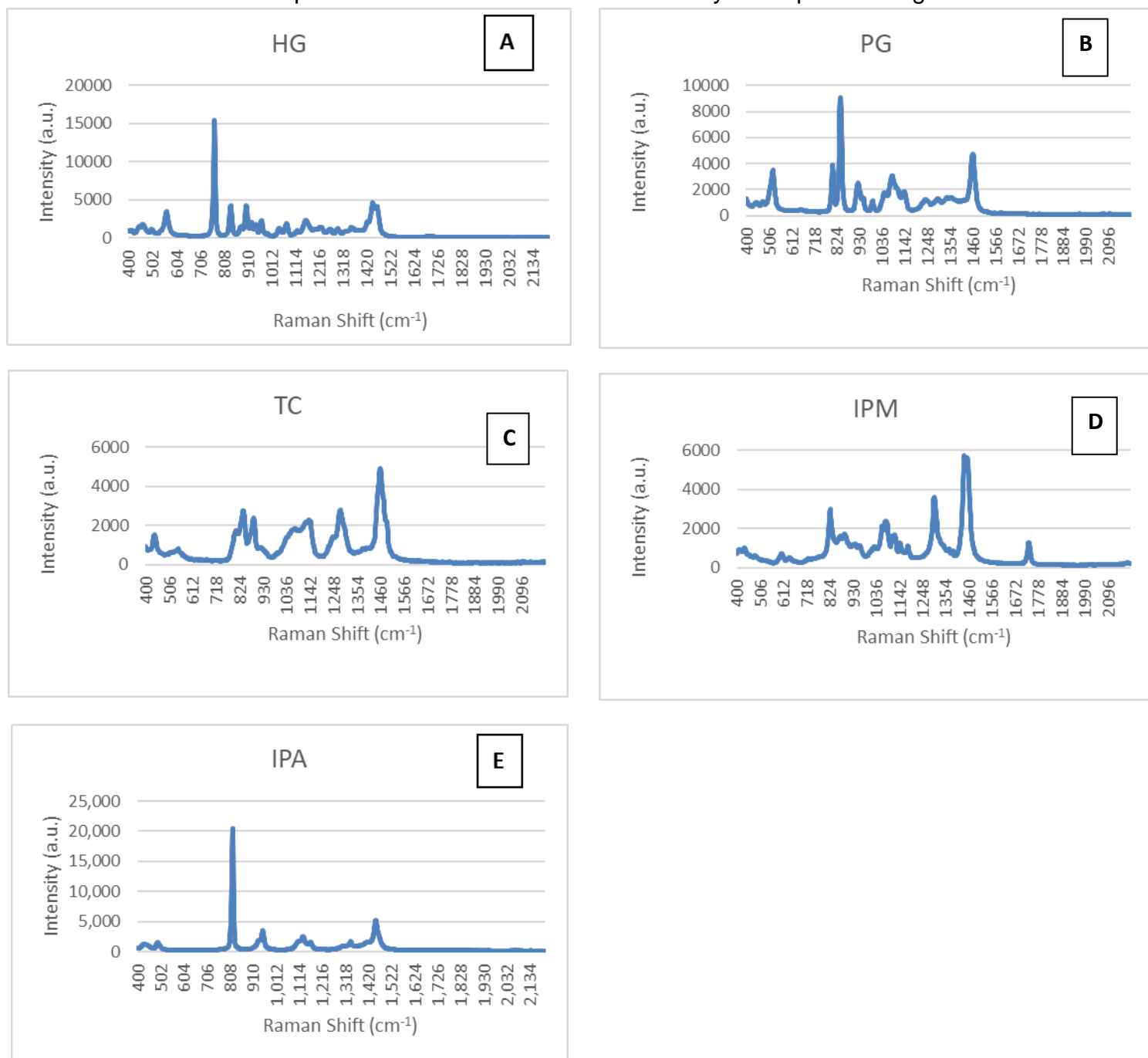


Figure 3.2 Raman fingerprint region spectra of solvents HG (A), PG (B), TC (C), IPM (D), and IPA (E)

HG, IPA, PG, IPM and TC have their most intense peaks at 768 cm^{-1} , 820 cm^{-1} , 840 cm^{-1} , 1440 cm^{-1} and 1460 cm^{-1} respectively. To plot a calibration curve for quantificational analysis of tazarotene, the reference spectra of tazarotene in EtOH at five concentrations, 1%, 0.8%, 0.5%, 0.3% and 0.1%, were generated. The Raman spectra of the five Tazarotene concentrations are reported in figure 3.3.

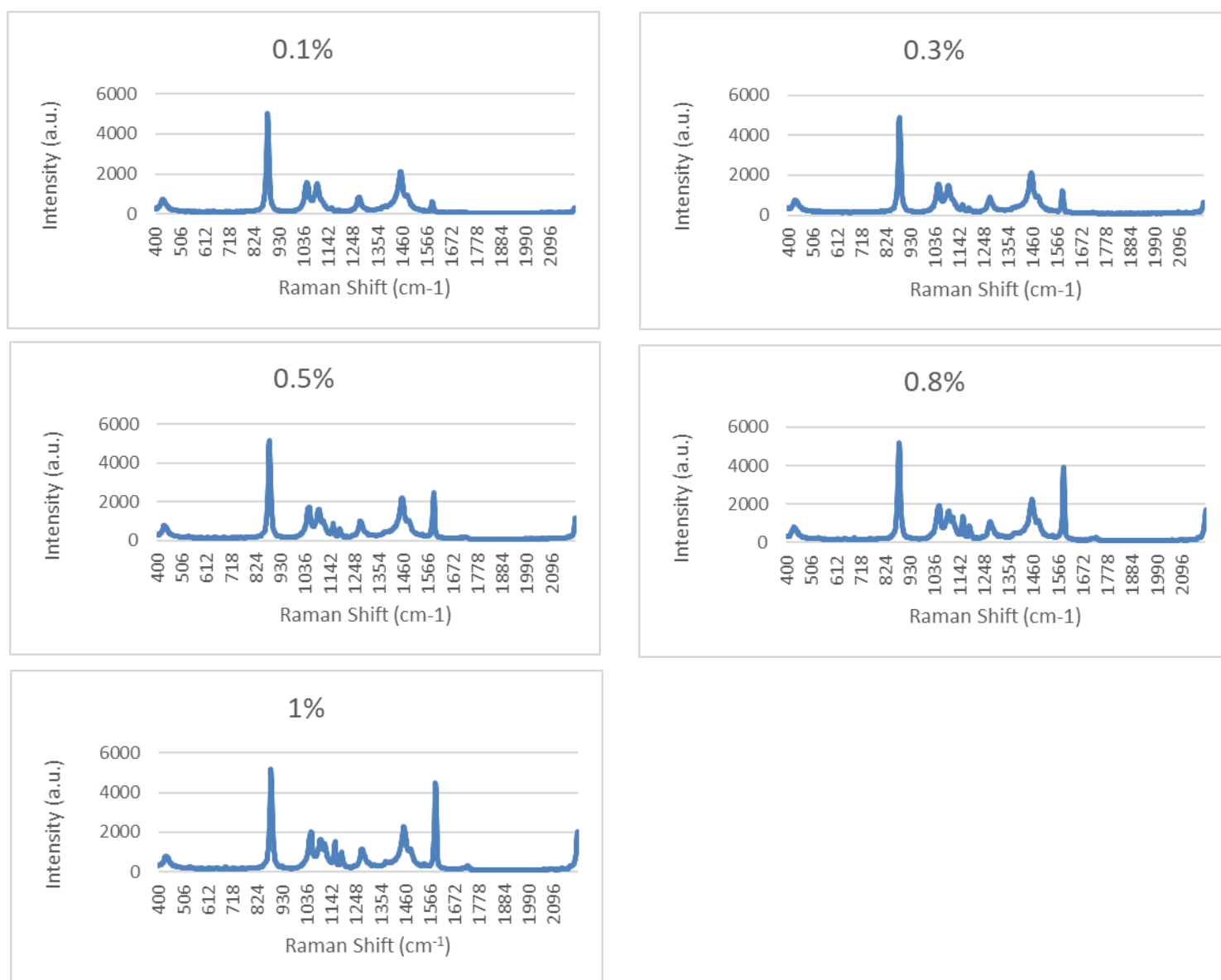


Figure 3.3 Raman fingerprint region spectra of tazarotene in ethanol at 0.1%, 0.3%, 0.5%, 0.8% and 1%

The most intense peak for tazarotene and EtOH is at 1590 cm⁻¹ and 884 cm⁻¹ respectively. All the Raman spectra were uploaded to the SkinTools[®] model spectra library for integration and to enable spectral fitting. The model library contains several integrated spectra that include the instruments' optical material, endogenous skin components such as keratin, NMF, ceramide and cholesterol, as well as a range of standard pre-set compounds that include the BSA protein.

Using SkinTools[®] the proportionality constants for tazarotene in ethanol $c_{Tazarotene:ethanol}^{-1}$ were calculated and then integrated into the software alongside pre-determined proportionality constants $c_{BSA:protein}^{-1}$, $c_{BSA:water}^{-1}$, $c_{ethanol:water}^{-1}$ used to determine the mass ratios $\frac{m_{tazarotene}}{m_{protein}}$ from the Raman intensity ratios $\frac{R_{tazarotene}}{R_{protein}}$ to plot a calibration curve for the quantification of tazarotene in the skin using equation 3.2 (Caspers, Nico et al. 2019).

$$\frac{m_{tazarotene}}{m_{protein}} = c_{BSA:protein}^{-1} * c_{BSA:water}^{-1} * c_{ethanol:water}^{-1} * c_{tazarotene:ethanol}^{-1} * \frac{R_{tazarotene}}{R_{protein}} \quad (3.1)$$

$$\frac{m_{tazarotene}}{m_{protein}} = c_{tazarotene:protein}^{-1} * \frac{R_{tazarotene}}{R_{protein}} \quad (3.2)$$

Tazarotene was normalized to the fit coefficient of keratin due to its abundance and relatively constant protein content throughout the SC. The Raman signal intensities for all compounds were determined by a multiple least square fit of the intensity

normalised reference spectra. After calculating the Raman intensity ratios between tazarotene and ethanol from their spectra, they were plotted against their corresponding mass ratio (Caspers, Nico et al. 2019).

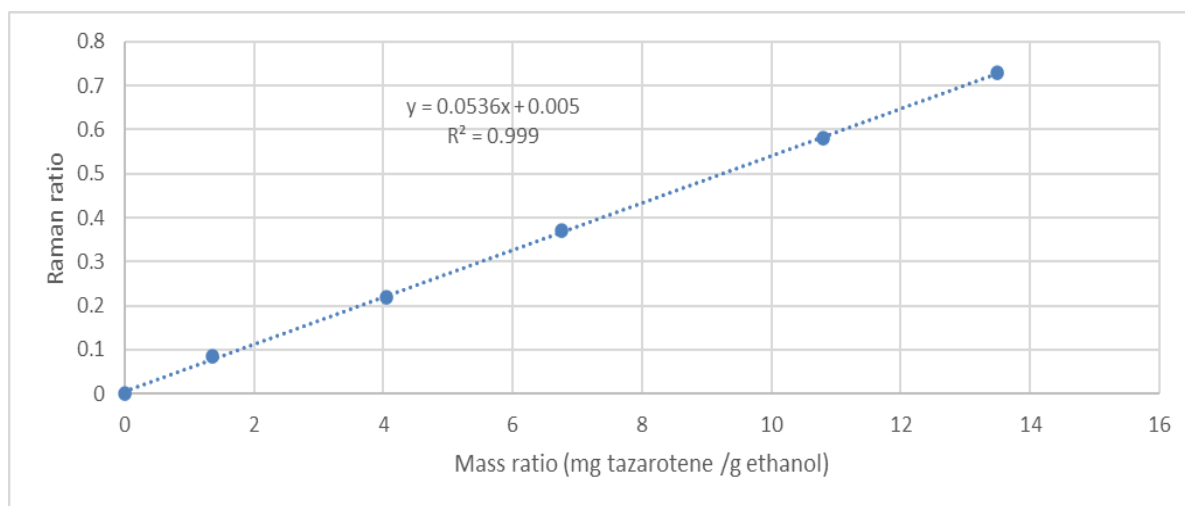


Figure 3.4 Raman ratio vs mass ratio of tazarotene calibration curve, mean \pm SD, n=3

Figure 3.4 illustrates the slope of the linear regression and represents the proportionality constant $c_{tazarotene:protein}^{-1}$ between the mass ratio and the Raman ratio. The correlation coefficient R^2 is > 0.99 indicating excellent linearity that ensures accurate quantificational analysis.

3.3.2 Water content measurements and SC thickness

Using a laser emitting radiation at 671 nm allows for Raman analysis in the high wavelength region between 2500 cm^{-1} and 3800 cm^{-1} . The ratio intensities of the Raman bands at 2935 cm^{-1} and 3390 cm^{-1} illustrated in figure 3.5 were used to

determine the water-to-protein ratio at different depths in skin tissue (Caspers, Lucassen et al. 2000, Caspers, Lucassen et al. 2001).

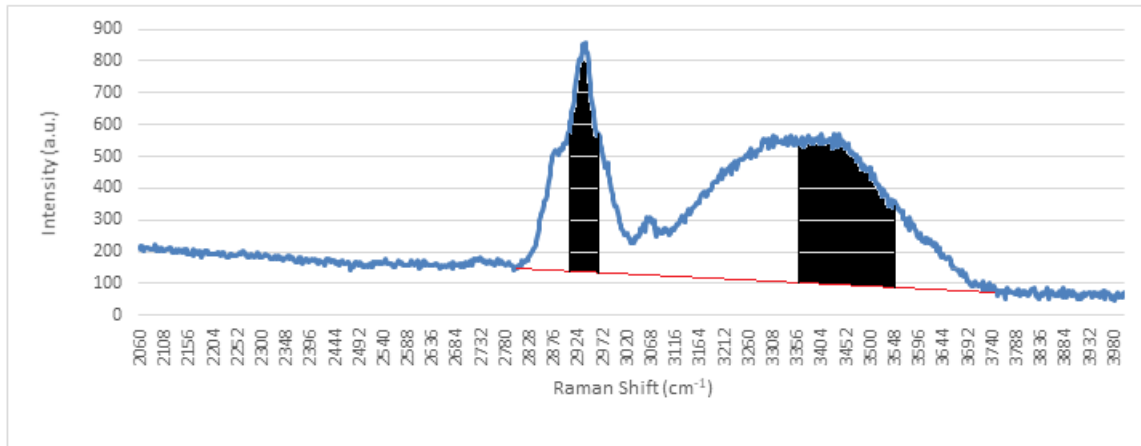


Figure 3.5 In vitro Raman high wavelength spectrum of the stratum corneum obtained from porcine skin. The water/protein ratio is calculated as the ratio between the integrated signal intensities areas between 2910-2965⁻¹ and 3350-3550 cm⁻¹ above the baseline. Experimental conditions: signal collection time 3s, laser power 100mW,

Equation 3.3 was used to calculate the water mass percentage in the skin from the Raman ratio between the integrated signal intensities of the CH₃ stretching vibrations of protein between 2910 to 2965 cm⁻¹ and OH stretching vibrations of water between 3350 – 3550 cm⁻¹. These spectral band ranges were chosen to maximize signal-to-noise and to avoid overlap between the N-H bond stretching vibration of protein at 3329 cm⁻¹ and the water Raman signal (Caspers, Lucassen et al. 2000, Caspers, Lucassen et al. 2001).

$$\text{Water mass \%} = 100\% * \frac{W/P}{W/P+R} \quad (3.3)$$

In equation 3.3 water mass percentage is expressed in grams of water per 100 grams of wet skin where W is the water band, P is the protein band and R is a

previously determined calibration constant equal to 2 (Caspers, Lucassen et al. 2000, Caspers, Lucassen et al. 2001)

By measuring the water-protein band ratio at sequential depth increments via CRS, it was possible to determine a water concentration profile of the porcine skin as water content by mass percentage.

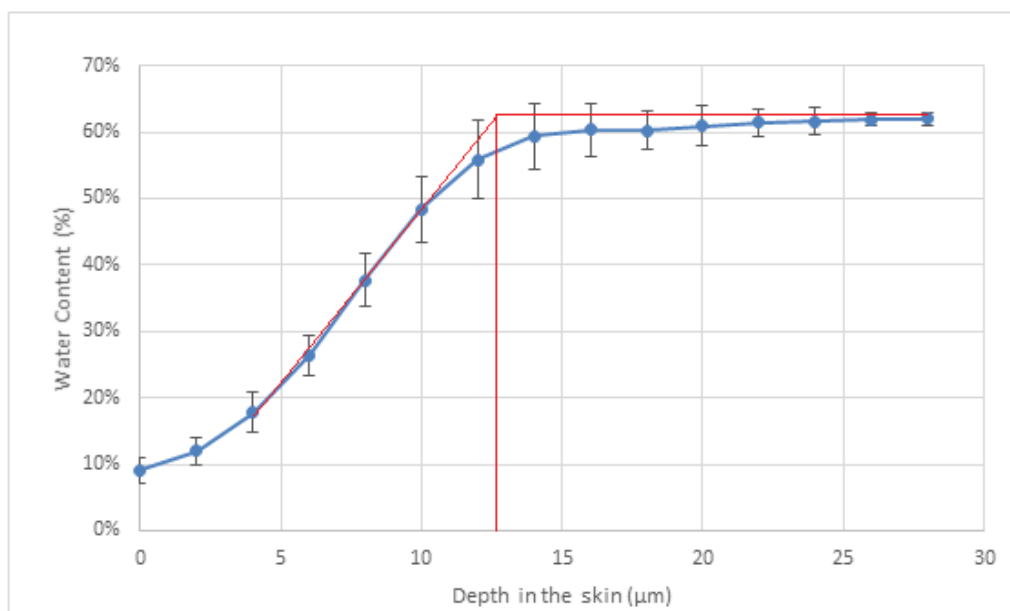


Figure 3.6 Water content profile of porcine skin with model fitting to calculate SC thickness, mean \pm SD n=5

Figure 3.6 illustrates the sigmoidal shape of the water concentration profile seen in the porcine skin examined. The graph shows the fit of two separate straight red lines. The first line is situated in the SC and the second line is in the viable epidermis. The intersection between these two lines indicates the lower boundary of the SC when a linear process of diffusion is imposed using the skin tools software. The slope of the

line fitting in the SC was determined from the corresponding SC water gradients (Caspers, Lucassen et al. 2000).

The steep red line indicates a steady increase in water concentration within the SC while the flattened red line indicates a constant uniform water concentration within the deeper epidermal layer of the skin below the SC. The intersection point of the two water gradients represents the SC thickness shown by the vertical red line (Caspers, Lucassen et al. 2000). Water concentration profiles were taken before and after formulation application to ascertain any changes in SC thickness. Results showed that there was no significant difference ($p < 0.05$) in SC thickness before and after formulation application. SC thickness values measured after formulation application were used to normalise all depth profiles. The average SC thickness of the porcine skin used in this study was calculated to be $12.8 \mu\text{m} \pm 0.2 \mu\text{m}$.

3.3.3 CRS studies of topical tazarotene formulations

Tazarotene in the stratum corneum

Tazarotene in the SC was measured 6 hours after the application of each formulation to the porcine skin. To highlight the difference between individual formulations, the sample donor was used throughout this study to reduce the variability between skin samples.

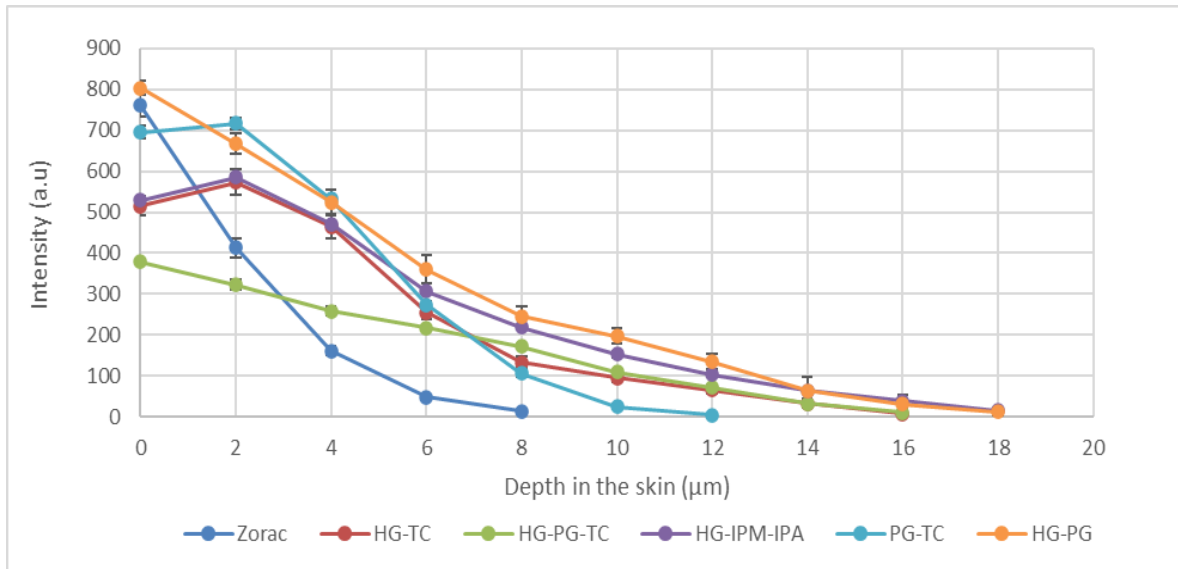


Figure 3.7 Semi-quantitative depth profiles of tazarotene in the commercial Zorac® gel formulation, HG:TC, PG:TC, HG:PG, HG:PG:TC and HG:IPM:IPA, mean \pm SD, n=5

Figure 3.7 illustrates the semi-quantitative depth profiles of tazarotene in HG:TC, HG:PG, PG:TC, HG:PG:TC, HG:IPM:IPA and the commercial Zorac® gel formulation. CRS data revealed that Zorac® gel was the least effective in delivering tazarotene into the skin as it was unable to be detected below a depth of 8 μm . On the contrary, tazarotene in the PG:TC solution could be detected below a depth of 12 μm while tazarotene in HG:TC, HG:PG, HG:PG:TC and HG: IPM:IPA could be detected below 16 μm .

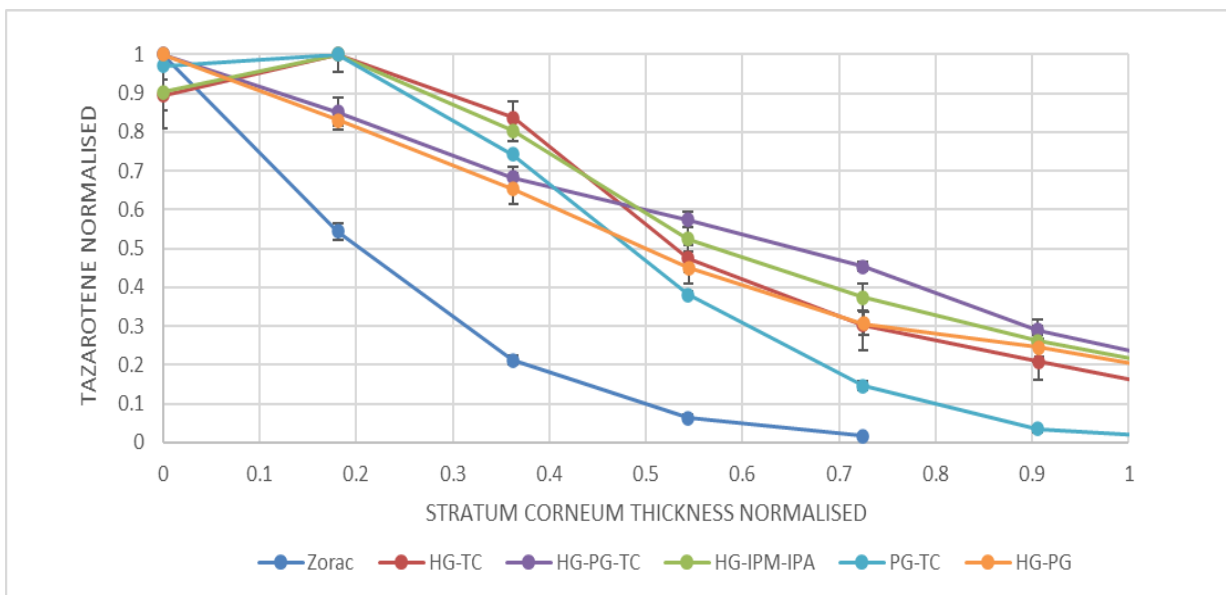


Figure 3.8 Normalised SC depth profiles of tazarotene in the commercial Zorac® gel formulation, HG:TC, PG:TC, HG:PG, HG:PG:TC and HG:IPM:IPA, mean \pm SD, n=5

By normalising the Raman intensity of tazarotene and SC thickness illustrated in figure 3.8, it was possible to evaluate whether the formulations being studied were successful in bypassing the SC barrier layer to deliver tazarotene into the viable epidermis. It is clear from figure 3.8 that Zorac[®] gel was not able to penetrate the SC and can only be faintly detected just over halfway through the SC. On the contrary, tazarotene in all the solutions examined managed to bypass the SC and could be detected in the viable epidermis.

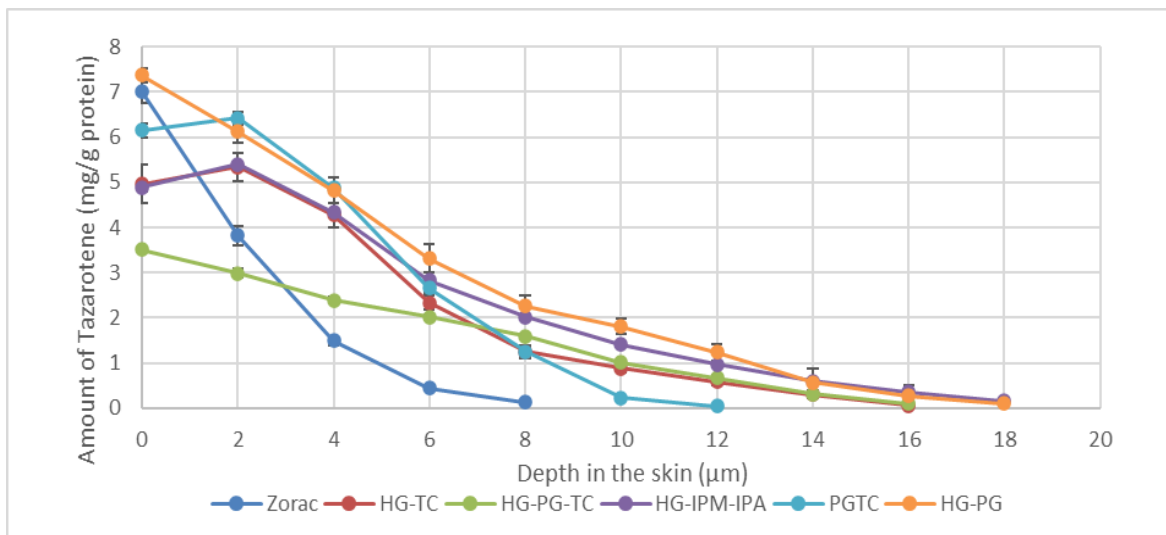


Figure 3.9 Quantitative mass ratio depth profiles of tazarotene in the commercial Zorac[®] gel formulation, HG:TC, PG:TC, HG-PG, HG-PG:TC and HG-IPM:IPA, mean \pm SD, n=5

By using equation 3.4, we can convert figure 3.7 from a Raman intensity (a.u.) into figure 3.9, a quantitative mass ratio $m_{\text{tazarotene}}/m_{\text{protein}}$ (mg/g protein) depth profile from the previously determined proportionality constant $c_{\text{tazarotene:protein}}^{-1}$ and Raman ratio

$\frac{R_{\text{tazarotene}}}{R_{\text{protein}}}$ of each semi-quantitative depth (z) point (Caspers, Nico et al. 2019).

$$\frac{m_{\text{tazarotene}}}{m_{\text{protein}}}(z) = c_{\text{tazarotene:protein}}^{-1} * \frac{R_{\text{tazarotene}}}{R_{\text{protein}}}(z) \quad (3.4)$$

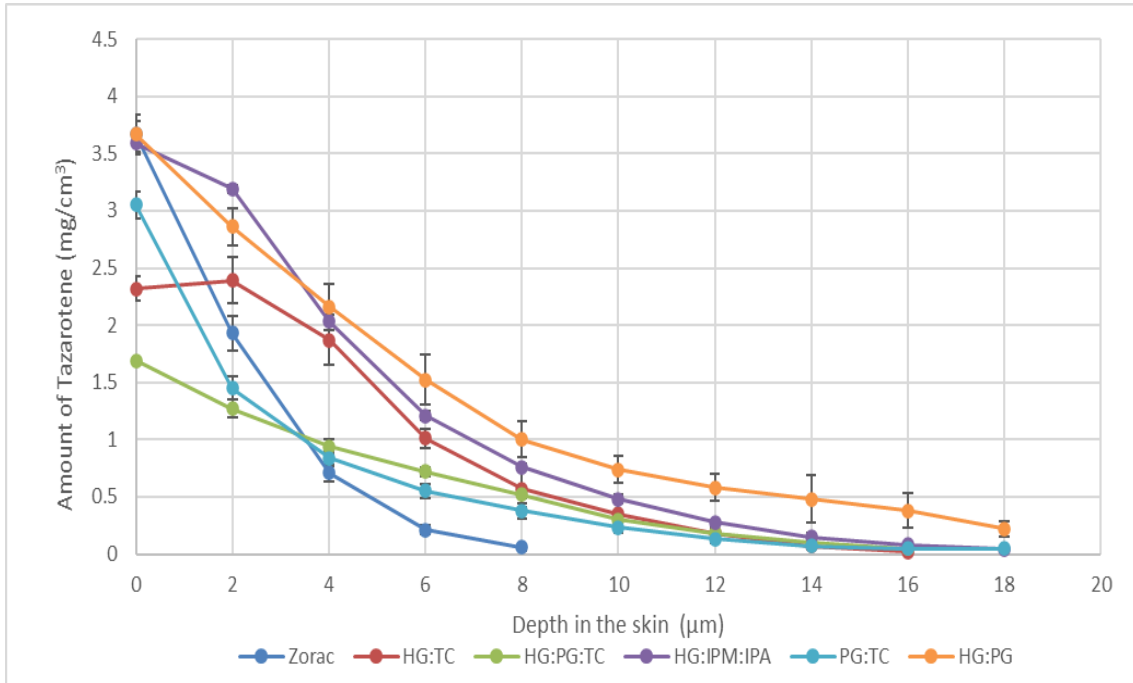


Figure 3.10 Concentration depth profiles of tazarotene in the commercial Zorac® gel formulation, HG:TC, PG:TC, HG:PG, HG:PG:TC and HG:IPM:IPA, mean ± SD, n=5

Using equations 3.5 and 3.6 and multiplying the mass ratio $m_{\text{tazarotene}}/m_{\text{protein}}$ in figure 3.9 at every depth (z) with the protein concentration in the skin, we can calculate the concentration (mg/cm³) of tazarotene in the skin $\gamma_{\text{tazarotene}}$ as a function of distance from the skin surface illustrated in figure 3.10.

$$\gamma_{\text{tazarotene}}(z) = \frac{m_{\text{tazarotene}}}{m_{\text{protein}}}(z) * \gamma_{\text{protein}}(z) \quad (3.5)$$

$$\gamma_{\text{protein}}(z) = \left(\frac{1}{\rho_{\text{dry SC}}} * \frac{m_{\text{dry SC}}}{m_{\text{protein}}} * \frac{1}{\rho_{\text{water}}} * \frac{m_{\text{water}}(z)}{m_{\text{protein}}(z)} \right) \quad (3.6)$$

The protein concentration in equation 3.6 was calculated from the dry SC mass fraction, the protein fraction of the dry SC mass and the dry SC density. As the dry SC mass consists of 15% lipids and between 20 – 30 % NMF, the mass ratio $m_{\text{protein}}/m_{\text{dry sc}}$ was calculated to be 60%. The mass ratio $m_{\text{water}}/m_{\text{protein}}$ was determined from the water concentration profile by multiplying the $m_{\text{water}}/m_{\text{protein}}$, and $m_{\text{water}}/m_{\text{dry sc}}$. The density of dry SC and water used in equation 3.6 were 1.15 g/cm^3 and 1.0 g/cm^3 respectively (Caspers, Nico et al. 2019).

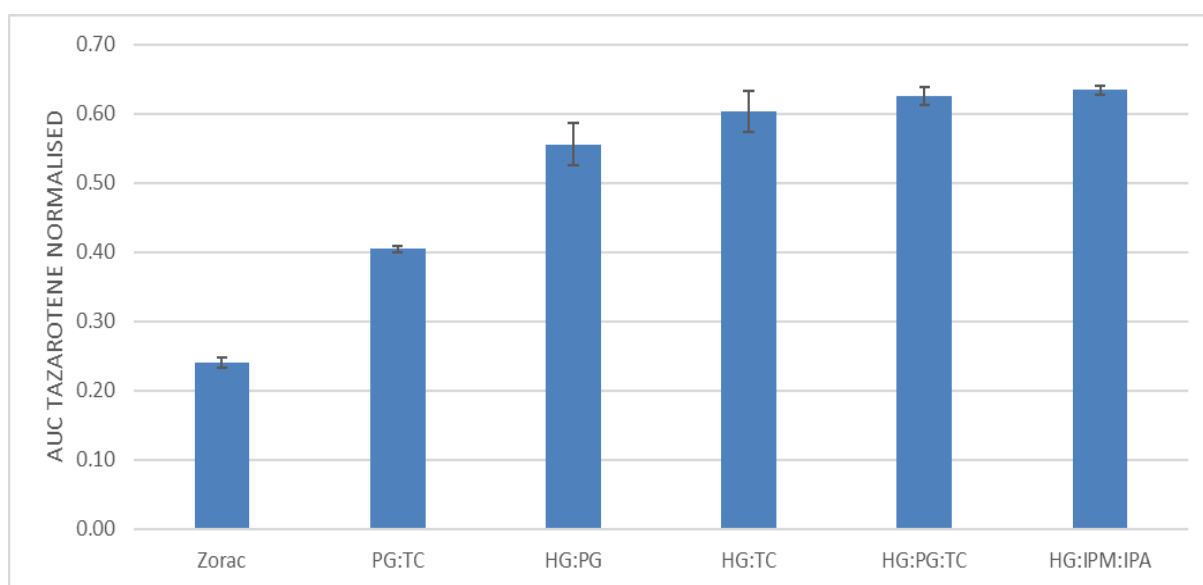


Figure 3.11 Normalised AUC of tazarotene in the skin from the commercial Zorac[®] gel formulation, HG:TC, PG:TC, HG:PG, HG:PG:TC and HG:IPM:IPA, mean ± SD, n=5

Figure 3.11 illustrates the normalised AUC of tazarotene depth profiles in the SC calculated from figure 3.8. Both HG:IPM:IPA and HG:PG:TC showed the greatest AUC for tazarotene with a value of 0.63 ± 0.01 followed by HG:TC (0.60 ± 0.03), HG:PG (0.56 ± 0.03), PG:TC (0.40 ± 0.01) and the Zorac[®] gel formulation ($0.24 \pm$

0.01). Statistical analysis of the normalized AUC of tazarotene profiles identified a significant variance ($p < 0.01$) between the population means. Further statistical analysis revealed a significantly higher ($p < 0.05$) AUC of tazarotene in the skin from solutions HG:TC, HG:PG, PG:TC, HG:PG:TC and HG:IPM:IPA compared with the Zorac[®] gel formulation. A significantly higher ($p < 0.05$) AUC of tazarotene from solutions HG:TC, HG:PG, HG:PG:TC and HG:IPM:IPA compared to the PG:TC was also observed. There was no significant difference ($p < 0.05$) between the normalised AUC of tazarotene in the skin from either binary or ternary HG containing formulations HG:TC, HG:PG, HG:PG:TC or HG:IPM:IPA.

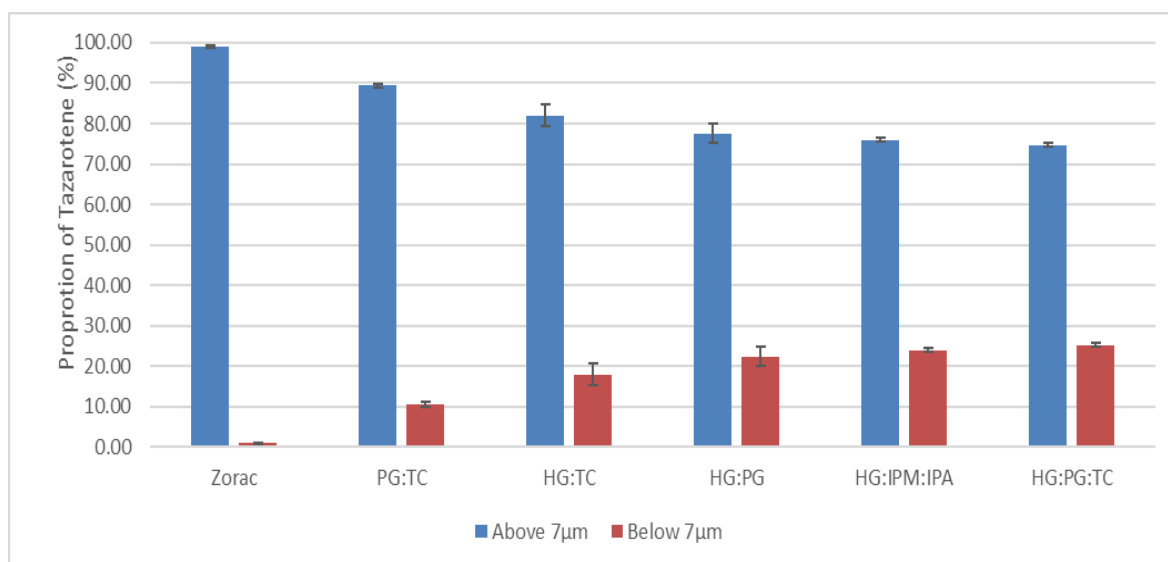


Figure 3.12 Proportion of tazarotene above and below a skin depth of 7 μ m from the commercial Zorac[®] gel formulation, HG:TC, HG:PG, PG:TC, HG:PG:TC, and HG:IPM:IPA, mean \pm SD, n=5

To show the penetration and delivery of tazarotene more clearly into the skin, relative proportions were calculated. Figure 3.12 illustrates the proportion of tazarotene identified as a percentage in the skin above and below 7 μm of the SC. Error bars represent the variation in the amount of tazarotene found in the skin. The greatest proportion of tazarotene found below 7 μm was delivered from HG:PG:TC (25.25 \pm 0.41% followed by HG:IPM:IPA (24 \pm 0.54%), HG:PG (22.43 \pm 2.3%), HG:TC (18 \pm 2.7%), PG:TC (10.63 \pm 0.53%) and the smallest proportion was delivered for the Zorac[®] gel formulation (0.96 \pm 0.21%).

Statistical analysis identified significant variance ($p < 0.01$) between the population means of Zorac[®] gel, HG:TC, HG:PG, PG:TC, HG:PG:TC and HG:IPM:IPA below 7 μm . The proportion of tazarotene below a depth of 7 μm showed that a significantly higher ($p < 0.05$) proportion was delivered from solutions HG:TC, HG:PG, PG:TC, HG:PG:TC and HG:IPM:IPA compared to the Zorac[®] gel formulation. There was a significant difference ($p < 0.05$) between the proportion of tazarotene below 7 μm delivered from solutions HG:TC, HG:PG, HG:PG:TC and HG:IPM:IPA compared to the PG:TC solution. There was also no significant difference ($p < 0.05$) between the proportion of tazarotene below 7 μm delivered from solutions HG:TC, HG:PG, HG:PG:TC or HG:IPM:IPA.

Hexylene glycol in the stratum corneum

Using the reference spectra previously generated in figure 3.1, it was possible to track the deposition of the CPEs driving tazarotene delivery into the skin through Fick's law of diffusion.

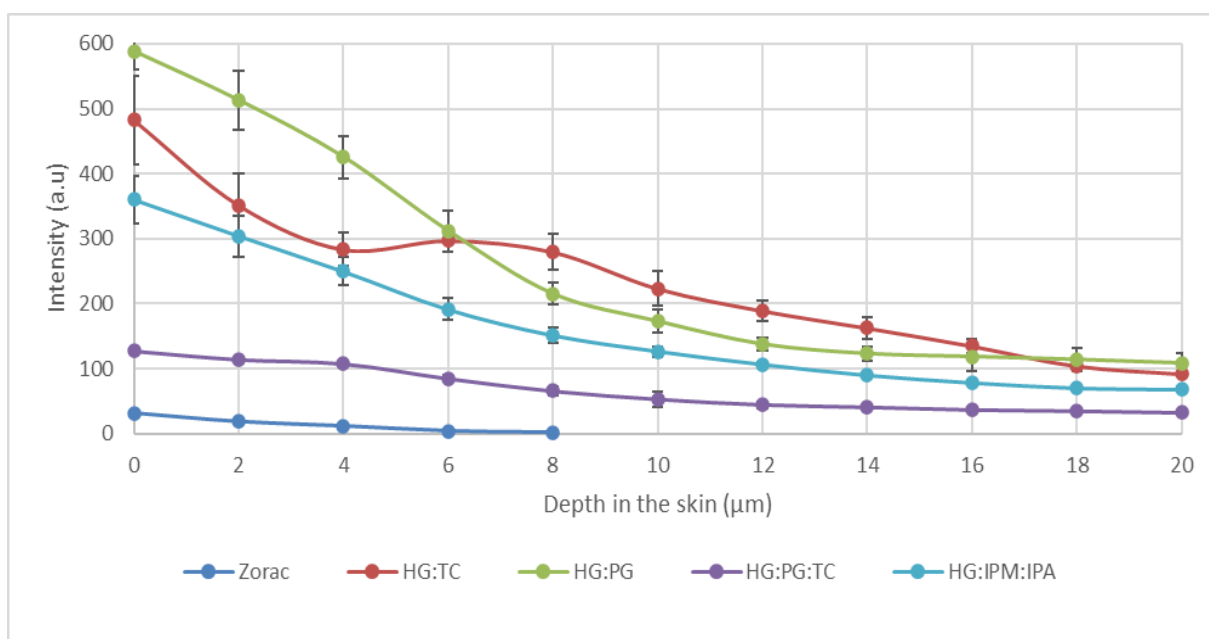


Figure 3.13 Semi-quantitative depth profiles of HG in the commercial Zorac[®] gel formulation, HG:TC, HG:PG, HG:PG:TC, and HG:IPM:IPA, mean \pm SD, n=5

Figure 3.13 illustrates the semi-quantitative depth profiles of HG in solutions HG:TC, HG:PG, HG:PG:TC, HG:IPM:IPA and in the commercial Zorac[®] gel formulation. HG in Zorac[®] gel was the least effective in penetrating the skin and could not be detected below a depth of 8 μm . HG on the other hand in all the solutions examined HG:TC, HG:PG, HG:PG:TC and HG: IPM:IPA could be detected below 20 μm . These results follow the same trend seen in figure 3.7 with tazarotene.

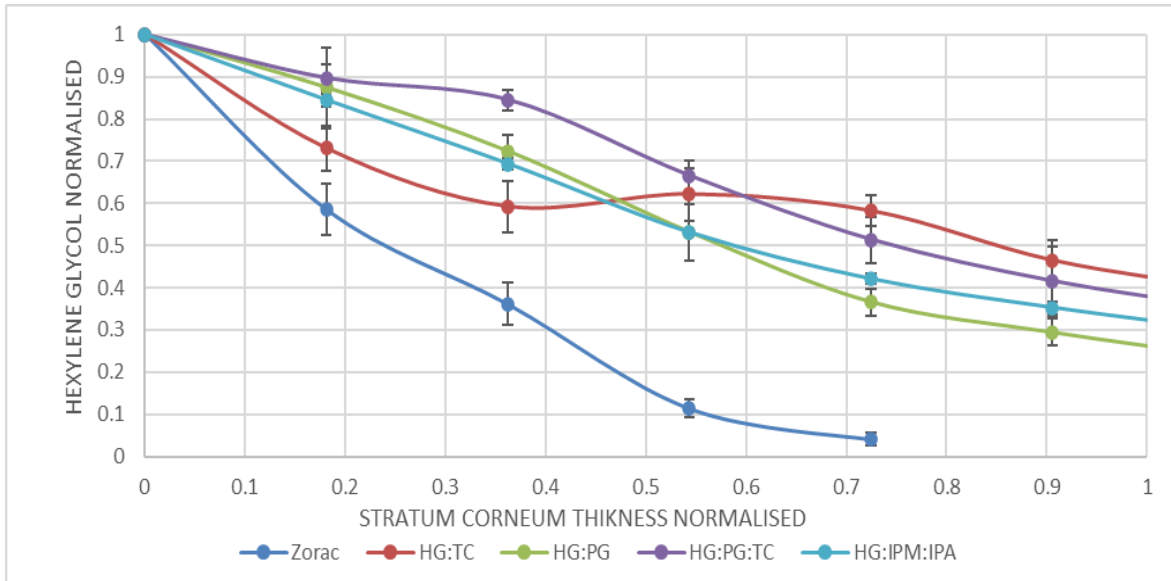


Figure 3.14 Normalised depth profiles of HG in the commercial Zorac® gel formulation, HG:TC, HG:PG, HG:PG:TC and HG:IPM, mean ± SD, n=5

Looking at the normalised depth profiles illustrated in figure 3.14, HG in the Zorac® gel formulation could not bypass the SC layer as it could only be faintly detected just over halfway through the SC. On the other hand, HG in all the solutions examined bypassed the SC layer and could be detected in the viable epidermis, similar to tazarotene in the same solutions previously seen in figure 3.8.

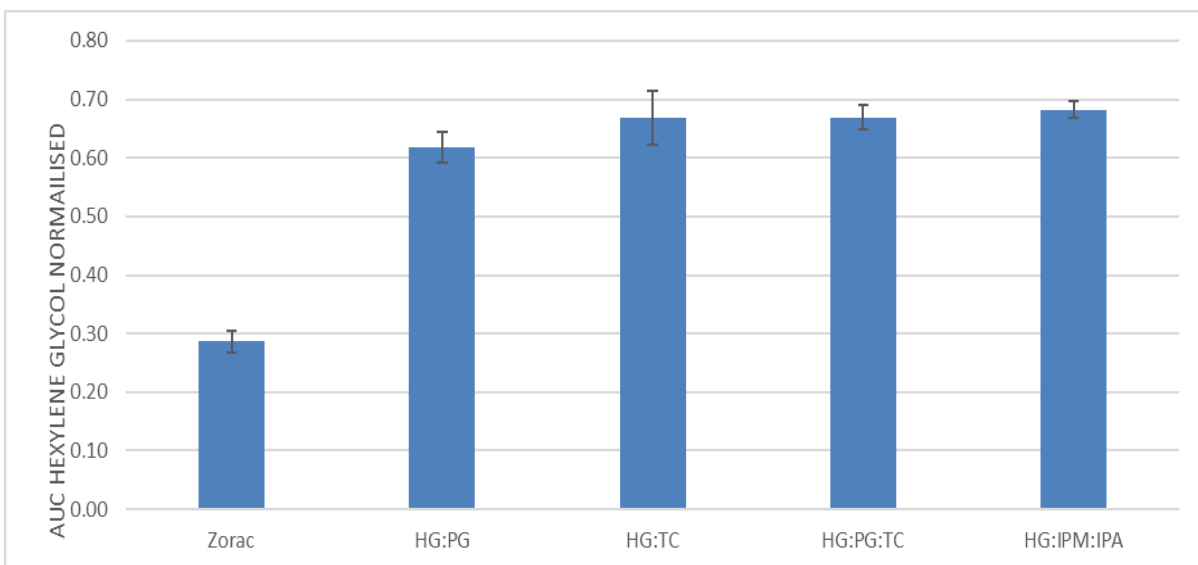


Figure 3.15 Normalised AUC of HG in the SC from the commercial Zorac® gel formulation, HG:TC, HG:PG, PG:TC, HG:PG:TC and HG:IPM:IPA, mean ± SD, n=5

HG:TC (0.67 ± 0.05), (HG:PG:TC 0.67 ± 0.02), (HG:PG 0.62 ± 0.03) and lastly the Zorac[®] gel formulation (0.29 ± 0.02). Statistical analysis of the normalized AUC of HG profiles identified a significant variance ($p < 0.01$) between the population means of Zorac[®] gel, HG:TC, HG:PG, HG:PG:TC and HG:IPM:IPA. A significantly higher ($p < 0.05$) amount of HG was delivered into the skin from solutions HG:TC, HG:PG, HG:PG:TC and HG:IPM:IPA compared with the Zorac[®] gel formulation. There was no significant difference ($p < 0.05$) between the normalized AUC of HG in the skin delivered from either HG:TC, HG:PG, HG:PG:TC or HG:IPM:IPA.

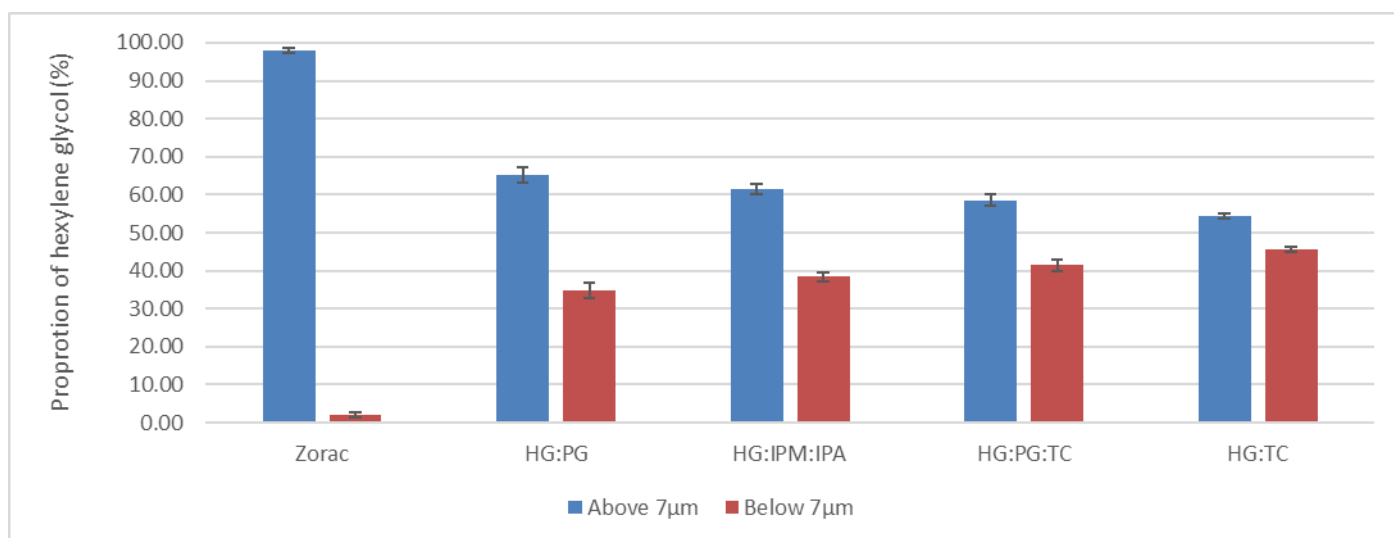


Figure 3.16 Proportion of HG above and below a skin depth of 7 μm from the commercial Zorac[®] gel formulation, HG:TC, HG:PG, HG:PG:TC and HG:IPM:IPA, mean \pm SD, n=5

Figure 3.16 illustrates the proportion of HG identified as a percentage in the skin above and below 7 μm of SC. Error bars represent the variation in the amount of HG found in the skin. The greatest proportion of HG found below 7 μm was delivered

from HG:TC ($45.63 \pm 0.75\%$) followed by HG:PG:TC ($41.43 \pm 1.52\%$), HG:IPM:IPA ($38.49 \pm 1.21\%$), HG:PG ($34.93 \pm 2.05\%$), and with the smallest proportion delivered the Zorac[®] gel formulation ($1.93 \pm 0.71\%$).

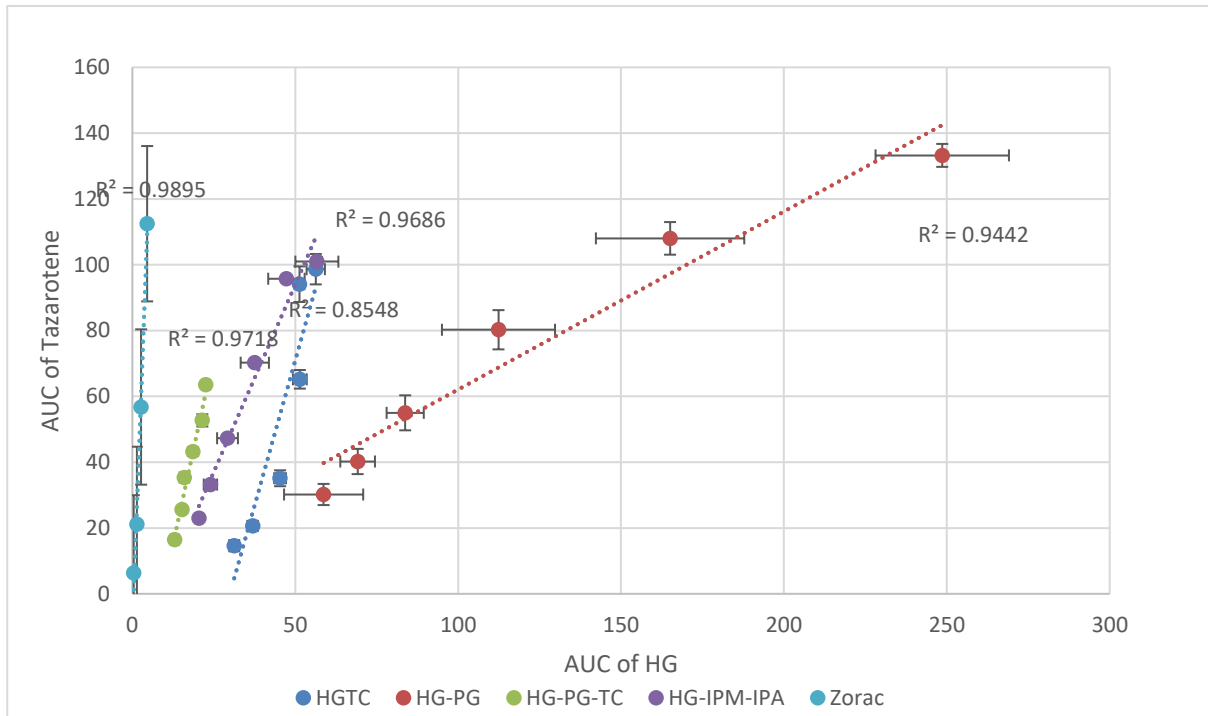


Figure 3.17 Correlations between the amount of tazarotene and HG found in the SC, mean \pm SD, n = 5

Statistical analysis identified significant variance ($p < 0.01$) between the population means of Zorac[®] gel, HG:TC, HG:PG, HG:PG:TC and HG:IPM:IPA below $7 \mu\text{m}$. Error bars in the x-axis and y-axis represent the variation in the amount of HG and tazarotene found in the skin respectively. The proportion of HG proportion below a depth of $7 \mu\text{m}$ showed a significantly higher ($p < 0.05$) amount was delivered from solutions HG:TC, HG:PG, HG:PG:TC and HG:IPM:IPA deeper into the skin

compared to the Zorac[®] gel formulation. No significant difference ($p < 0.05$) was found between the proportion of HG below 7 μm delivered from HG containing formulations HG:TC, HG:PG, HG:PG:TC or HG: IPM:IPA solutions.

The normalised depth profiles of HG and tazarotene in the SC show similarities in shape and penetration into the skin. To identify any trends between vehicle and API, the AUC for each normalised depth was calculated and compared with one another. The calculation of the AUC is directly proportional to the total amount of the analyte present in the SC at any given depth. Figure 3.17 illustrates the calculated AUC of both HG and tazarotene in the SC plotted agent at each depth.

A linear regression was performed on the plotted data where a correlation coefficient (R^2) was calculated for Zorac[®] gel, $R^2 = 0.99$, HG:TC, $R^2 = 0.85$, HG:PG, $R^2 = 0.94$, HG:PG:TC, $R^2 = 0.97$ and HG:IPM:IPA, $R^2 = 0.97$ indicating a very strong positive correlation between the normalised AUC of both HG and tazarotene. This positive trend suggests that as the amount of HG in the SC increases, so does the amount of tazarotene being delivered. The results presented here show that there is a critical relationship between the API and the CPE used to facilitate its delivery into the skin.

Propylene glycol in the stratum corneum

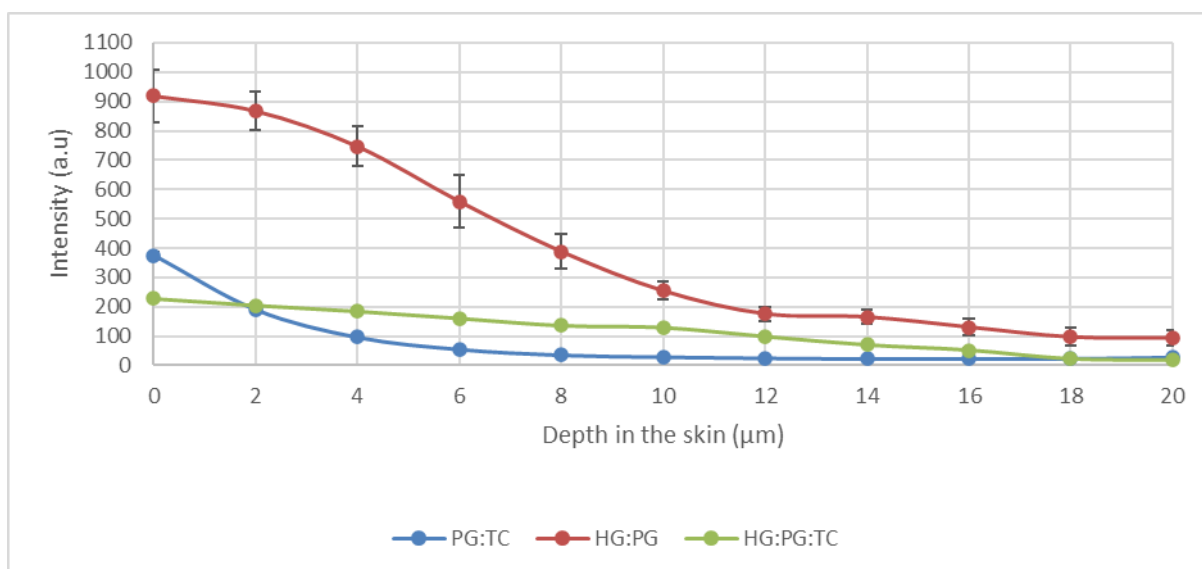


Figure 3.18 Semi-quantitative depth profiles of PG in PG:TC, HG:PG, and HG:PG:TC, mean \pm SD, n=5

Figure 3.18 illustrates the semi-quantitative depth profiles of PG in solutions PG:TC, HG:PG and HG:PG:TC. Like HG in figure 3.13, PG in all the solutions examined could be detected below 20 μm which again follows the same trend as tazarotene seen in figure 3.7.

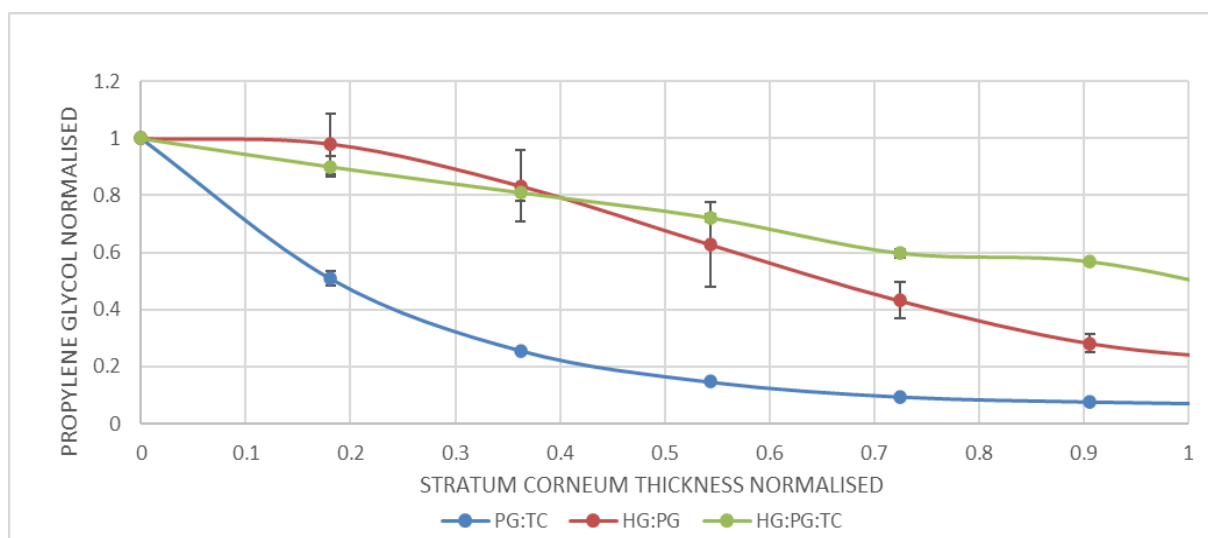


Figure 3.19 Normalised depth profiles of PG in PG:TC, HG:PG, and HG:PG:TC, mean \pm SD, n=5

Normalised depth profiles of PG in the SC illustrated in figure 3.19 show that PG was able to bypass the SC layer in PG:TC, HG:PG and HG:PG:TC similar to tazarotene in the same solutions from figure 3.8. The same trends can be seen with HG and tazarotene in figures 3.14 and 3.8 showing the relationship between CPE and API. The less CPE found in the skin the less tazarotene can be detected in the skin.

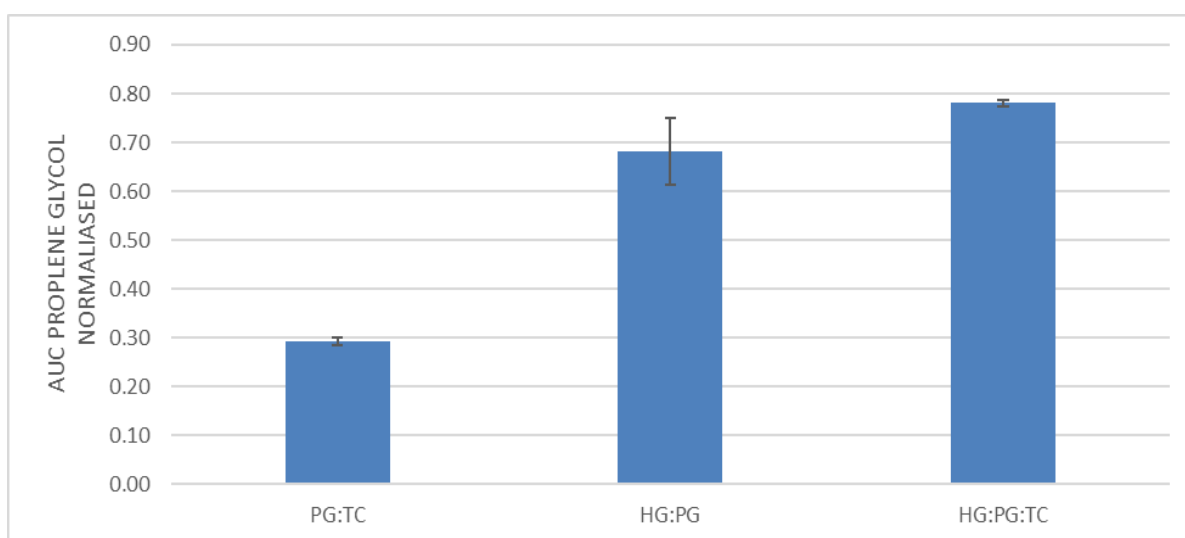


Figure 3.20 Normalised AUC of PG in the SC from PG:TC, HG:PG, and HG:PG:TC, mean \pm SD, n=5

Using figure 3.19 the normalised AUC of PG depth profiles in the SC was calculated which is illustrated in figure 3.20. HG:PG:TC showed the greatest AUC (0.78 ± 0.01) followed by HG:PG (0.68 ± 0.07) and PG:TC (0.29 ± 0.01). Statistical analysis of the normalised AUC profiles revealed significant variance ($p < 0.01$) between the population means of HG:PG:TC, HG:PG and PG:TC. A significantly higher ($p < 0.05$) amount of PG in the skin was observed for HG:PG:TC compared to HG:PG and

PG:TC. A significantly higher ($p < 0.05$) amount of PG was also calculated for HG:PG compared to PG:TC.

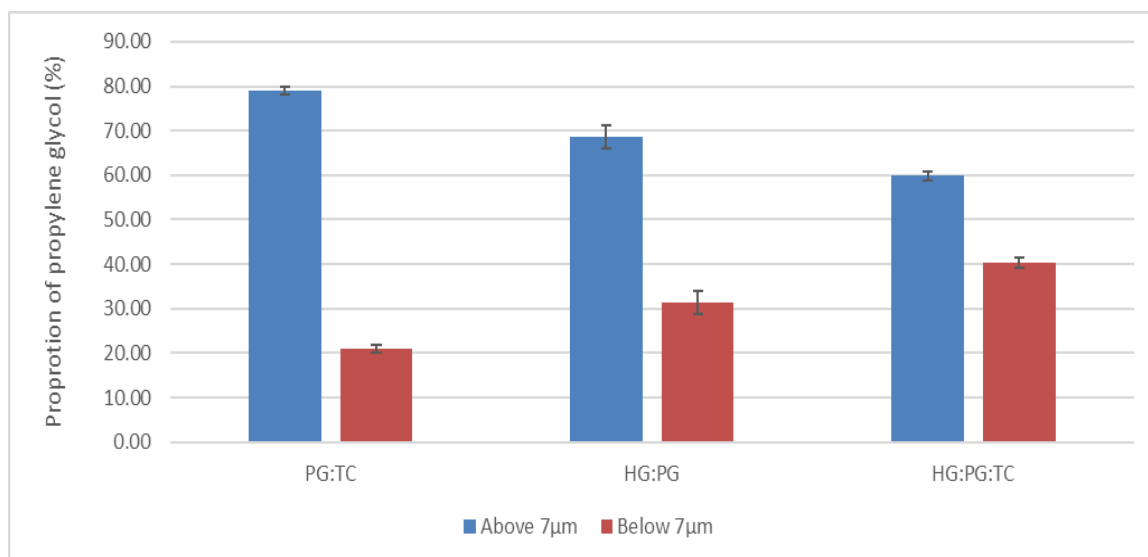


Figure 3.21 Proportion of PG above and below a skin depth of 7 µm from PG:TC, HG:PG and HG:PG:TC, mean \pm SD, n=5

Figure 3.21 illustrates the proportion of PG identified as a percentage in the skin above and below a depth of 7 µm of the SC. Error bars represent the variation in the amount of PG found in the skin. The greatest proportion of PG found below 7 µm was delivered from HG:PG:TC ($40.19 \pm 1.15\%$) followed by (HG:PG $31.41 \pm 2.69\%$), and PG:TC ($20.90 \pm 0.87\%$). Statistical analysis identified a significant variance ($p < 0.01$) between the population means of PG:TC, HG:PG and HG:PG:TC below 7 µm. The PG proportion below a depth of 7 µm showed a significantly higher ($p < 0.05$) proportion delivered into the skin from HG:PG:TC when compared to HG:PG

and PG:TC. A significantly higher ($p < 0.05$) proportion of PG was again also delivered further into the skin from solution HG:PG compared to PG:TC.

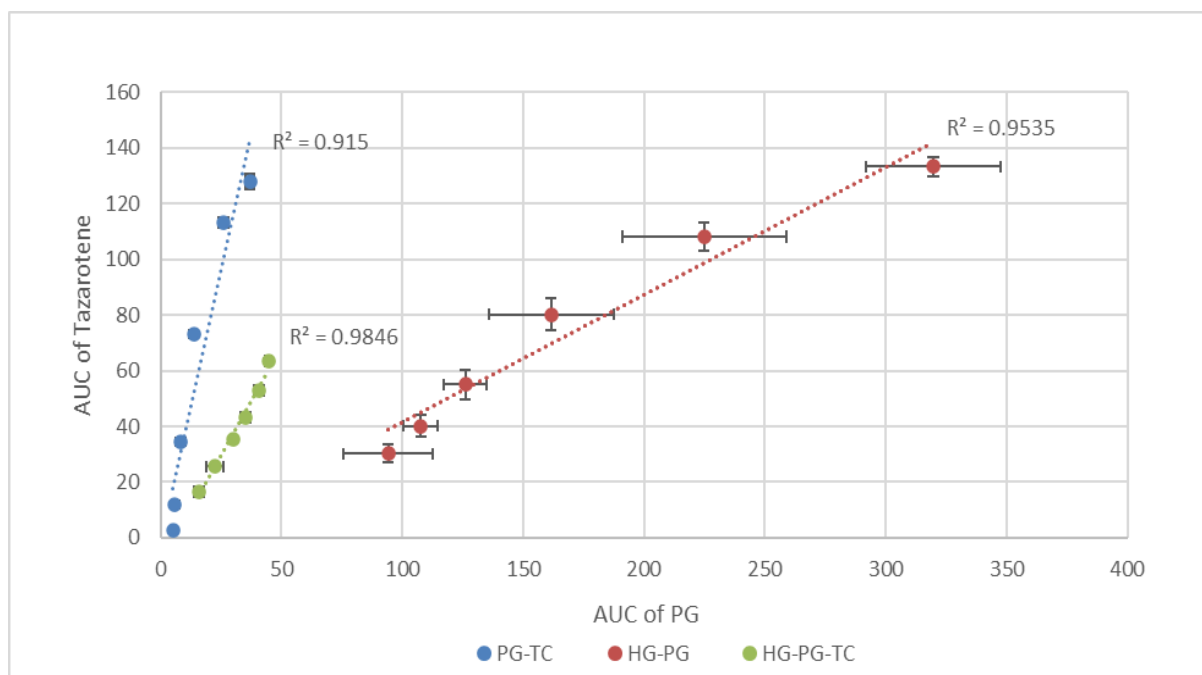


Figure 3.22 Correlation between normalised AUC of PG and tazarotene vehicle depth profiles, mean \pm SD, n=5

The depth profiles of PG and tazarotene in the SC show similarities in shape and penetration depth into the skin. Figure 3.22 illustrates the correlation between the calculated AUC of both PG and tazarotene in the SC. Error bars in the x-axis and y-axis represent the variation in the amount of PG and tazarotene found in the skin respectively. The linear regression of the plotted data has shown PG:TC, $R^2 = 0.92$, HG:PG, $R^2 = 0.95$, and HG:PG:TC, $R^2 = 0.98$ indicating again a very strong positive correlation between PG and tazarotene. These positive trends are further evidenced

alongside figure 3.17 suggesting that tazarotene deposition in the skin accompanies its CPE.

3.4 Conclusions

CRS is a novel technique that can be used for the non-invasive determination of molecular concentration profiles in the skin. CRS has proven its ability to simultaneously detect the active retinoid tazarotene and penetration enhancer vehicles HG and PG in porcine skin delivered from a range of formulations to examine differences in drug penetration. This chapter has demonstrated that water concentration profiles can be measured across the skin to identify the border between the SC and viable epidermis. Using CRS water concentration profiles of porcine skin were successfully collected which were then used to calculate SC thickness. CRS revealed significant differences in tazarotene penetration depth compared to the commercial Zorac[®] gel formulation. Tazarotene was detected throughout the SC up to a depth of 20 μm from all solvent systems examined while the commercial Zorac[®] gel formulation only reached a depth of 8 μm which was not enough to penetrate the SC. Not only was tazarotene detected throughout the SC from all the solvent systems examined, but both HG and PG could also be detected throughout the SC up to a depth of 20 μm . A very strong correlation was shown to exist between the amount of tazarotene, HG and PG delivered into the skin

suggesting tazarotene delivery is dependent on the CPE penetration. The method presented here enables the quantification of tazarotene in the skin through a unique calibration process that utilises the Raman signal intensities and mass ratios of different concentrations of tazarotene. Moreover, the use of CRS has shown that tazarotene was able to penetrate deeper into the skin in greater amounts from all simple solvent systems when compared to the commercial Zorac[®] gel formulation. From the binary solvent systems HG:TC delivered the most amount of tazarotene into the skin while HG:PG:TC delivered the most amount of tazarotene into the skin from the ternary solvent systems examined. These results confirm what was observed from *in-vitro* Franz diffusion cell studies in the previous chapter where HG:TC and HG:PG:TC significantly both performed the commercial Zorac[®] gel formulation the most when compared to all other solvent systems tested. Interestingly not only did tazarotene penetrate the skin the greatest from HG:TC and HG:PG:TC, but both HG and PG also penetrated the skin the most from HG:TC and HG:PG:TC compared to the other solvent systems studied as well. What is thought to be happening is HG and PG can modify the diffusion of tazarotene through the SC by interacting with the hydrophobic regions of the intercellular SC lipids increasing the lamellar phase distance. The results in this chapter reveal the transport dependence of tazarotene on HG and PG which highlights the importance of the relationship between API and CPE.

Chapter Four:

In-vitro LC-MS Evaluation of Topical Tazarotene Formulations

Chapter Four

In-vitro LC-MS evaluation of topical tazarotene formulations

4.1 Introduction

Since its inception over 30 years ago, Mass Spectrometry has emerged as an indispensable analytical tool, able to perform routine bioanalysis in a variety of laboratories around the world for a wide range of applications. It has proven to be an extremely powerful qualitative and quantitative analytical technique that offers several advantages over techniques such as HPLC and GC. Triple-quadrupole mass spectrometry (MS/MS) can offer additional benefits. Some of the major analytical advantages typically include having a more extensive linear dynamic range for the detection, improved lower limits of detection within the nano range, and higher accuracy and precision, especially when analysing large amounts of samples over extended periods. The use of liquid chromatography-mass spectrometry (LC-MS) for *in-vitro* permeation studies has been used to study aqueous solutions of ammonium perfluorooctanoate (APFO) applied to human epidermal membranes. Under infinite dose occlusive conditions, the steady-state penetration, permeability coefficient (K_p) and the cumulative amount of APFO were all calculated with increasing low sensitivity of detection (Fasano, Kennedy et al. 2005). *In-vitro* permeation studies with porcine and human skin were conducted to analyse chromium (Cr) species by

using capillary electrophoresis hyphenated to inductively coupled plasma–sector field mass spectrometry (CE–ICP–SFMS) to separate and quantify very small amounts of Cr in the receptor fluid. Cr(VI) species was shown to readily pass through the skin and could absorb more efficiently in the skin than Cr(III) species (Van Lierde, Chery et al. 2006). *In-vitro* permeation studies with human skin were used to analyse gold nanoparticles (AuNPs) by Inductively Coupled Plasma-Mass Spectrometry (ICP-MS) to assess very small amounts of absorption into damaged and intact human skin. The studies showed that AuNPs could permeate the skin in greater amounts than other NPs like silver but could not release Au ions in physiological conditions like some other metal NPs (Filon, Crosera et al. 2011). Sil et al used LC-MS to examine extremely small amounts of niacinamide (NIA) by-products during *in-vitro* skin permeation studies. Analysis and characterisation of NIA by-products using LC-MS resulted in the identification of different molecular entities with similar structures to NIA that were not previously detected during prior stability studies using HPLC alone (Sil, Moore et al. 2018). CPEs can change the way drugs are delivered to and through the skin. Megrab et al showed that by increasing the saturation of the lipophilic drug oestradiol (OE) in different PG:WATER systems the penetration and solubility of both OE and PG into human skin could be enhanced by way of increased thermodynamic activity of the formulations (Megrab, Williams et al. 1995). TC has been shown to enhance drug permeation of the skin by diffusing into

the SC and modifying the solubility parameter of the intercellular lipid domains (Harrison, Watkinson et al. 1996). Mohammed et al. previously showed that the amount of niacinamide in a range of vehicles that permeated through the skin *in-vitro* detected by HPLC was linearly proportional to the CRS intensity signal of niacinamide detected in the SC *in-vivo*. This author was also able to show a good correlation between the signal intensities of selected vehicles and niacinamide signal intensity (Mohammed, Matts et al. 2014). In this chapter an LC-MS method was developed and validated to quantify the third-generation retinoid tazarotene for finite-dose *in-vitro* permeation studies with human skin. The best solvent system was further developed into an in-house gel formulation, which was again examined through finite dose *in-vitro* permeation studies. The in-house gel was also examined by DVS and compared to the commercial Zorac[®] gel to evaluate the residence time of both gel formulations.

4.2 Material and methods

4.2.1 Materials

Zorac[®] gel 0.1% supplied by Allergan pharmaceuticals (IRL).

Tazarotene was supplied by Insight Biotechnology (UK).

HG, PG, IPA, UHPLC grade water, UHPLC grade methanol, formic acid and benzyl alcohol were supplied by Fisher Scientific (UK).

TC gifted by Gattefossé (UK).

IPM, BrijO20[®], Parafilm[®], Eppendorf centrifuge tubes, UHPLC amber glass vials, 200ml vial inserts, UHPLC Accucore column and grad were supplied by Sigma-Aldrich (UK).

Dulbecco PBS (pH = 7.3 ± 0.2 at 25°C) was supplied by Oxoid (UK).

High vacuum grease was supplied by Dow Corning (USA).

Carbomer 974P was supplied by Lubrizol (UK).

Franz diffusion cells were supplied by SES GmbH (UK).

Human skin was ethically sourced from a tissue bank.

4.2.2 LC-MS method development and validation for tazarotene analysis

The following method was developed and validated:

HPLC conditions

Column	C ₁₈ , 100 x 2.1 mm, 2.6 μm (Accucore, UK)
Mobile phase	80% MeOH UHPLC grade 20% Water UHPLC grade + 0.1% formic acid
Temperature	25 °C
Flow rate	2.0 mL/min
Run time	3 min
Injection volume	10 μL

MS and Ion Source Conditions

Ion mode	Positive Electrospray (H-ESI) Mode
Vaporizer Temperature	325 °C
Ion Transfer Tube Temperature	250 °C
Sheath Gas	70 psi
Aux Gas	20 psi
Sweep Gas	1 psi
Spray Voltage	Positive Ion:4000 V
Q1/Q2 Resolution	0.7/0.7 FWHM
Cycle time	0.8 sec
CID Gas	2 psi
Chromatographic Peak Width	6 sec

Analysis was conducted at 25°C using a Accucore ® column with dimensions C18, 100 x 2.1 mm, and a 2.6 μm stationary phase, fitted with a C8 4 × 3 mm, 5 μm guard cartridge and a 5 μm SecurityGuard™ ULTRA (Phenomenex, USA). Degassed mobile phases consisting of MeOH, and UHPLC grade water with 0.1% formic acid

were delivered by a binary pump at a total combined flow rate of 2 mL min⁻¹. The sample injection volume was 10 µL and samples were prepared in 1.5 mL amber glass vials containing 250 µL glass inserts and 8 mm screw caps with rubber septa. The method run time was 3 mins and the retention time of tazarotene was 1.46 mins. The LC system was coupled with an Agilent 6400 triple quadrupole mass spectrometer with an ion spray source operating in positive ESI mode.

Quantification was performed with multiple reaction monitoring (MRM). The ion spray voltage was 4000 V with a turbo heater temperature of 250 °C and vaporizer temperature of 325 °C. Sheath gas, auxiliary, sweep gas and collision-induced dissociation gas were kept at 70 psi, 20 psi, 1 psi and 2 psi respectively. A 0.8 second cycle time was selected with a 6 second chromatographic peak width.

Method reproducibility was evaluated, and validation is shown in this chapter. Stock standard solutions of tazarotene for calibration were prepared in MeOH at a concentration of 1 mg/mL and stored at -20°C. Working standard solutions of tazarotene were prepared by dilution of stock solutions in methanol and stored at -20°C. The working solutions of tazarotene for calibration curves were prepared at concentrations of 10, 90, 200, 400, 800, 1500 and 3000 ng/mL by spiking blank MeOH with the working standard to make up 100 µL. The samples were transferred to injection vials, and 10 µL were injected into the LC-MS system for analysis.

4.2.3 Tazarotene formulation preparation

All formulations were made fresh as required. The appropriate mass of tazarotene was weighed in a 2 mL plastic Eppendorf with a locking lid. For binary and ternary formulations, a total of 1 mL of the required solution was pipetted into a 2 mL Eppendorf containing the pre-weighed amount of tazarotene to give a final concentration of 0.1% (w/w). Eppendorfs were then locked, wrapped in Parafilm[®] and placed into an incubating orbital mini shaker (VWR, sK) at 800 RPM and 25 °C \pm 1°C for approximately 3 hours to ensure complete solubilisation of the tazarotene.

Binary and ternary vehicle ratios were as follows: PG:TC (4:1), HG:TC (4:1), HG:IPM: IPA (8:1:1), HG:PG:TC (2:2:1). For the gel formulation, HG and TC were pipetted into a 2mL Eppendorf containing the pre-weighed amount of tazarotene at a ratio 4:1 up to a volume of 500 μ L followed by 490 μ L of HPLC grade water, 10 μ L of benzyl alcohol and the addition of 15 mg of Carbomer 974P. Eppendorfs were then locked, wrapped in Parafilm[®] and placed into an incubating orbital mini shaker (VWR, UK) at 800 RPM and 25 °C \pm 1 °C until a homogeneous formulation was produced. All formulation constituents were weighed using an analytical balance (Mettler Toledo, UK). The concentration of tazarotene in all the solutions prepared was measured via LC-MS.

4.2.4 Human skin preparation

Human abdominal tissue obtained with the appropriate ethical approval was removed from a -20°C storage freezer and thawed at room temperature for approximately 3 h. All excess subcutaneous fat from the skin was carefully removed using a scalpel. 3 L of HPLC grade water was then heated to 60 °C \pm 1 °C in a large glass beaker using a magnetic stirrer hotplate (IKA, Germany). Using blunt forceps, the human tissue was completely submerged in the water for 45 s before being removed and the human SC membrane side was placed face up on No.1 filter paper (Whatman, UK).

To separate the human SC membrane from the epidermis, a corner of the upper surface was gently rubbed between the thumb and forefinger. As the human SC membrane began to separate, one hand was used to hold down the epidermis using a slight tension while the other hand peeled the human SC membrane away from the epidermis in a single unbroken sheet. The separated human SC membrane was then placed face-up in a stainless-steel basin filled with HPLC-grade water and completely uncoiled.

No.1 filter paper (Whatman, UK) was placed underneath the human SC membrane and slowly removed with the flattened human SC membrane attached before excess water was blotted from the surface. A second piece of filter paper was placed on top

of the human SC membrane, wrapped in aluminium foil, and then placed in a polythene bag along with a small piece of cardboard to ensure the human SC membrane remained flat before being stored at $-20\text{ }^{\circ}\text{C} \pm 1\text{ }^{\circ}\text{C}$ until needed. Before *in-vitro* permeation studies, sections of the frozen human SC membrane were cut and placed in a basin filled with HPLC-grade water. The human SC membrane sections were then mounted on a separate piece of filter paper and cut into approximately 15 mm in diameter pieces to be clamped onto Franz diffusion cells.

4.2.5 Receptor fluid preparation

PBS tablets were dissolved in the appropriate volume of UHPLC grade water with BrijO20[®] to a concentration of 6% in a duran bottle using a Nuova II magnetic stirrer (Thermolyne, USA). The receptor fluid was then degassed in an ultra-sonication bath (Thermolyne, USA) for 15 minutes. Until the receptor fluid was required, it was placed in a Nova thermostatic water bath (Grant Instruments, UK) at $32\text{ }^{\circ}\text{C} \pm 1\text{ }^{\circ}\text{C}$.

4.2.6 Human skin integrity measurements

The human SC membrane integrity was measured by an electrical impedance meter (UCL School of Pharmacy, UK). Donor compartments were filled with 1 mL of PBS. A first stainless-steel electrode was inserted into the receptor compartment arm filled with receptor fluid. The donor compartment was filled with 1 mL PBS and a second

stainless steel electrode was inserted into the PBS solution. The human SC membrane was considered intact if impedance was measured to be greater than 20 k Ω at 50 Hz. The PBS from the donor compartment was removed after being measured and dried with a cotton bud to ensure the skin was completely dry before formulation application.

4.2.7 *In-vitro* finite dose permeation studies of topical tazarotene formulations

All permeation studies were conducted with glass Franz diffusion cells. Both receptor and donor compartments were matched up according to their internal diameters measured by vernier callipers (Fischer Scientific, UK). The compartments with the smallest internal diameter were used to calculate the diffusion area of permeation. A thin, even layer of high vacuum grease (Dow Corning, USA) was spread on the contact surfaces of both the receptor and donor compartments to help them stick to the skin.

The cut human SC membrane was placed over the receptor compartment, then the donor compartment was aligned on top before both were fastened together with metal clamps. Empty Franz cells were first accurately weighed using an analytical balance (Mettler Toledo, UK) and then inverted to be filled with receptor fluid using a 10mL syringe before the total mass of the filled Franz cell was reweighed to calculate the exact volume of receptor fluid in each. A 5 mm PTFE coated magnetic

stir bar was inserted into the sampling arm on the receptor compartment and then placed into a custom-made acrylic Franz cell holder positioned over a submersible magnetic stir multi-plate (Thermo Scientific, USA).

To prevent evaporation of the receptor fluid, Franz cell sampling arms were capped with Parafilm®. Franz cells were left in a thermostatic water bath at a temperature of $32^{\circ}\text{C} \pm 1^{\circ}\text{C}$ for about 1 hour before dose application. Integrity measurements were conducted on the human SC membrane before dosing. The temperature on the membrane surface was measured using a TM-22 digital thermometer (Digitron, UK) to ensure the human skin surface was $32 \pm 1^{\circ}\text{C}$. Once the human skin had reached equilibrium, a 5 μL finite dose of each formulation was evenly applied to the skin surfaces.

At designated time points, 200 μL aliquots of receptor fluid were sampled. Receptor fluid samples were withdrawn from the sampling arm using polyvinyl chloride tubing (Thermo Scientific, USA) mounted to a 200 μL pipette plastic tip. All samples were analysed for tazarotene content using LC-MS and then normalised to diffusion area and receptor volume. All experiments were conducted in triplicates for statistical analysis.

4.2.8 Mass balance of topical tazarotene formulations

At the end of the permeation experiment, the receptor fluid was removed and then discarded. Using 100% UHPLC grade methanol, the skin surface was washed five consecutive times in 1 mL volumes and then dried with a cotton swab. All washes and swabs were transferred into a 2 mL Eppendorf tube. Franz cells were disassembled, and human SC membrane was removed from the receptor compartment and then placed into 2 mL Eppendorf tubes filled with 1 mL of UHPLC grade methanol for tazarotene extraction. All tubes were sealed with Parafilm® and placed into an orbital mini shaker (VWR, UK) at 8000 rpm for approximately 24 hours at 25°C. All washes and extractions were centrifuged at 12000 rpm for 15 min at 25°C then the supernatant was filtered through a 0.22 µm filter into glass vials before LC-MS analysis. All experiments were conducted in triplicates for statistical analysis.

4.2.9 Residence time studies of topical tazarotene gel formulations

Dynamic vapour sorption (DVS) (Surface Measurement Systems, UK) was conducted to monitor the change in the mass of formulations under controlled conditions. 15 mm quartz glass pans were hung from wires connected to an ultra-sensitive microbalance, accurate to ± 0.0001 mg, used for sample and reference chambers. Relative humidity (RH) was set at 50% achieved by mass flow of water vapour saturated nitrogen gas set at $32 \pm 1^\circ\text{C}$ for 24 hours. 5 µL of the formulation

was placed on the pan in the sample chamber and data was recorded in 10 s intervals. All experiments were conducted in triplicates for statistical analysis.

4.2.10 Data collection and statistical analysis of *in-vitro* results

Chromatogram data were integrated using Agilent ChemStation® for UHPLC systems (Agilent Technologies, USA). Microsoft® Excel Office 2018 (Microsoft, USA) was used to analyse and graph the data. Parametric statistical tests, ANOVA and t-tests were conducted to investigate statistical differences using GraphPad Prism® 6 (Dotmatics, USA). All results, unless stated otherwise, are presented as mean ± standard deviation (SD).

4.3 Results and discussion

4.3.1 LC-MS method developed & validation for tazarotene analysis

Linearity

The linearity of the LC-MS method was demonstrated by preparing six standard solutions between 3200ng/ml – 80ng/ml to cover the finite dose target tazarotene concentration on the skin surface, within the skin membrane and receptor medium.

Due to the detection limitations of the previously developed HPLC method in Chapter 2, finite dose studies of formulations containing 0.1% of tazarotene were not possible.

Table 4.1 LC-MS peak areas of tazarotene at different concentrations

Concentration (ng/ml)	Peak area
3120	613944
1560	306972
780	162888
390	88614
200	47228
90	19155

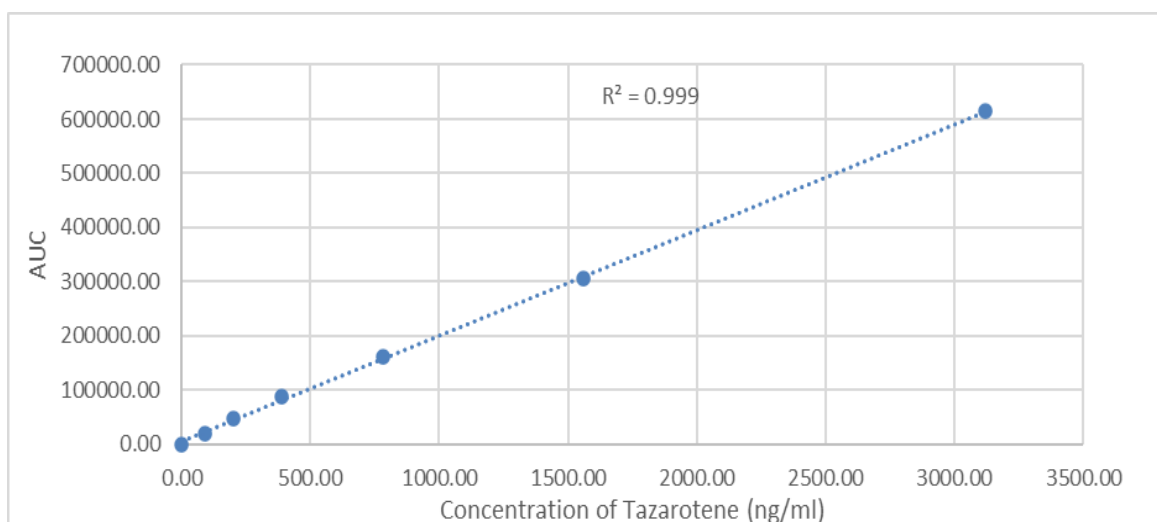


Figure 4.1 LCMS Linear calibration curve of tazarotene, mean \pm SD n=3

Figure 4.1 illustrates the linear regression of the LC-MS method. The linear equation representing the calibration curve was $y = 194.14x + 7794.9$. As part of this equation, 194.14 represents the slope of the line and 7794.9 the y-intercept. A correlation coefficient (R^2) value of 0.99 was obtained for this method indicating excellent linearity of the calibration curve to ensure accurate quantification of tazarotene (Green 1996).

Accuracy

A recovery study was performed by spiking tazarotene in blank samples at three concentration levels. Accuracy was reported as the percentage of tazarotene recovered in a sample that was examined with any deviation from its true expected value assessed. The accuracy of the LC-MS method for tazarotene was assessed in triplicates at high (3120 ng/ml), medium (1560 ng/ml) and low (200 ng/ml) concentrations, shown in table 4.2.

Table 4.2 LC-MS accuracy results for tazarotene

Theoretical concentration (ng/ml)	Measured concentration (ng/ml)*	Recovery (%)	R.S.D (%)
3120	3119.32 ± 2.88	99.98	0.09
1560	1559.87 ± 2.94	99.66	0.19
200	196.66 ± 0.44	97.47	0.23
		mean 99.15	mean 0.17

*mean ± SD (n=3)

Table 4.2 shows that the recovery values for the three different concentrations, were $99.98 \pm 0.09\%$, $99.66 \pm 0.19\%$ and $97.47 \pm 0.23\%$. The mean value of recovery was $99.15 \pm 0.17\%$. The recovery values were in the acceptable range between 95% to 105% for the recovery of drug substances in a mixture and therefore deemed sufficiently accurate (Green 1996).

Repeatability and Precision

The precision and repeatability of the LC-MS method was assessed by intra-day and inter-day measurements over one week using three solutions at high (3120 ng/ml), medium (1560 ng/ml) and low (200 ng/ml) concentrations. Similar to accuracy measurements, the percentage of tazarotene recovered in a sample was calculated from the deviation from its true expected value.

Table 4.3 LC-MS Intra-day variability results for tazarotene

Theoretical concentration (ng/ml)	Intra-day measured concentration(ng/ml)*					
	day 1		day 2		day 3	
	Mean ± SD	% R.S.D	Mean ± SD	% R.S.D	Mean ± SD	% R.S.D
3120	3123.71 ± 2.88	0.09	3110.08 ± 2.16	0.06	3120.92 ± 2.33	0.07
1560	1561.36 ± 2.94	0.19	1559.87 ± 2.27	0.14	1554.82 ± 2.71	0.17
200	198.54 ± 0.59	0.30	198.49 ± 0.57	0.29	196.34 ± 0.67	0.33

*mean ± SD (n=3); Intra-day precision was determined from three different runs over 1 week

Table 4.4 LC-MS Inter-day variability results for tazarotene

Theoretical concentration (ng/ml)	Inter-day measured concentrations(µg/ml)*	
	Mean ± SD	%R.S.D
3120	3124 ± 16.98	0.54
1560	1562 ± 15.11	0.97s
200	195 ± 3.62	1.87

* mean ± SD (n=12)

Tables 4.3 and 4.4 show that intra-day variability ranged between 0.07% to 0.33% and inter-day variability ranged between 0.57% to 1.86% which was within the acceptable $\pm 2\%$ variation range. The LC-MC method was considered to be satisfactory for precise experimental quantification of tazarotene (Green 1996).

Robustness

The robustness of the LC-MS method was evaluated through slight changes in method conditions by simultaneously varying flow rates, injection volume, temperature and mobile phase ratios.

Table 4.5 Robustness results for varied LC-MS conditions

Method	Flow Rate (ml/min)	Injection volume (μ l)	Temperature ($^{\circ}$ C)	Mobile phase H ₂ O + 0.1% FA: MeOH (v/v)	R ²	Recovery (%)
1	0.5	5	30	15:85	0.99	99.34
2	0.5	15	25	20:80	0.99	99.83
3	1	5	30	15:85	0.99	99.74
4	1	15	25	20:80	0.99	99.43
5	1.5	15	30	15:85	0.99	99.62

Table 4.5 shows the results from the varied chromatographic conditions for each experiment. No differences in the chromatograms were observed when specific modifications were made in each experiment. The correlation coefficients (R²) of the

calibration curves were all ≥ 0.99 and the recovery ranged between 99.34% and 99.83%. The results obtained have established that the LC-MS method is robust enough to analyse tazarotene (Green 1996).

Limit of Detection (LOD) & Limit of Quantification (LOQ)

In this LC-MS validation method, the standard deviation and slope determination methods were used with the LOD and LOQ determined to be 0.0313ng/ml and 0.1 ng/mL respectively, which shows excellent sensitivity for detecting and quantifying tazarotene (Green 1996).

System suitability

The system suitability was determined with six replicate injections from standard solutions of tazarotene at a concentration of 3120ng/ml and chromatogram parameters compared by peak shape, width, and baseline resolution.

Table 4.6 LC-MS System suitability results for tazarotene

	Mean \pm SD*	%R.S.D
peak area	612563 \pm 453	0.07
retention time(min)	1.46 \pm 0.01	0.03
symmetry	0.920 \pm 0.05	0.09

*n=6

Table 4.6 shows an excellent resolution of the tazarotene peak with a high degree of symmetry indicating the analytical system setup is suitable to examine tazarotene (Green 1996).

4.3.2 Mass balance of topical tazarotene formulations

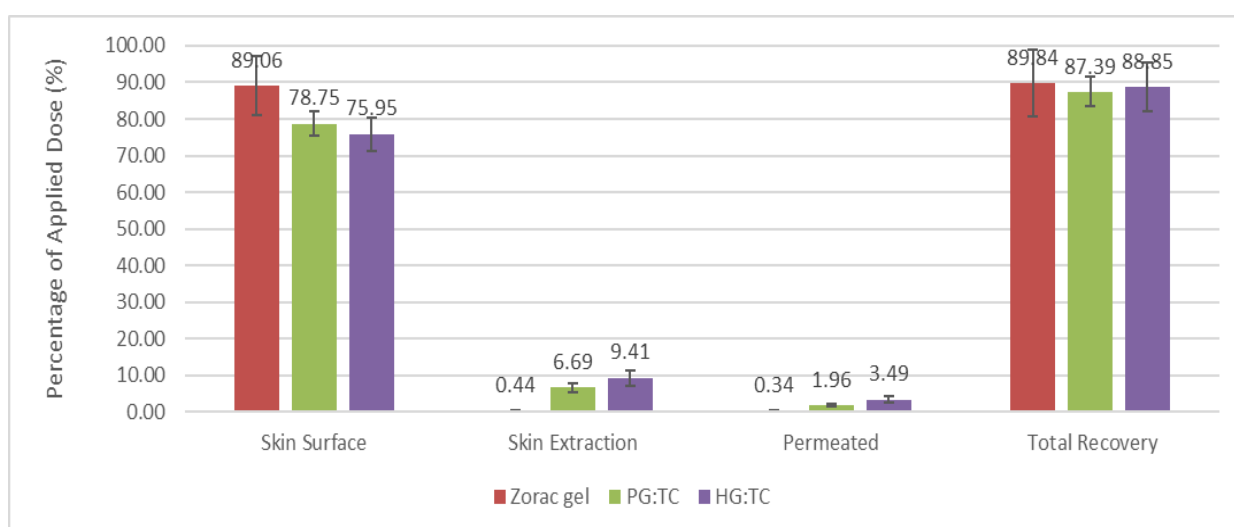


Figure 4.2 Finite dose mass balance study of binary solvent systems containing tazarotene compared with the commercial Zorac[®] gel formulation from human SC membrane after 24 h permeation experiments, mean \pm SD, n=5

The finite dose mass balance study in figure 4.2 shows the comparison of Zorac[®] gel with two binary solvent systems PG: TC (80:20) and HG: TC (80:20). Zorac[®] gel by far performed the worst with only $0.44 \pm 0.23\%$ of tazarotene extracted out of the skin and $0.34 \pm 0.12\%$ permeating through the skin with the vast majority of $89.06 \pm 8.05\%$ remaining on the skin surface.

By contrast, both binary solvent systems, PG: TC and HG: TC, performed better than Zorac[®] gel. From the PG: TC formulation $6.69 \pm 1.19\%$ of tazarotene was extracted

from the skin while $1.96 \pm 0.34\%$ penetrated through the skin and $78.75 \pm 3.20\%$ remained on the skin surface. From the HG:TC formulation, $9.41 \pm 2.14\%$ of tazarotene was found in the skin with $3.49 \pm 0.82\%$ penetrating through the skin and $75.95 \pm 4.56\%$ remaining on the skin surface. A significantly higher ($p < 0.05$) amount of tazarotene was delivered into the skin from PG:TC and HG:TC compared to Zorac[®] gel with HG:TC performing the best out of the binary systems.

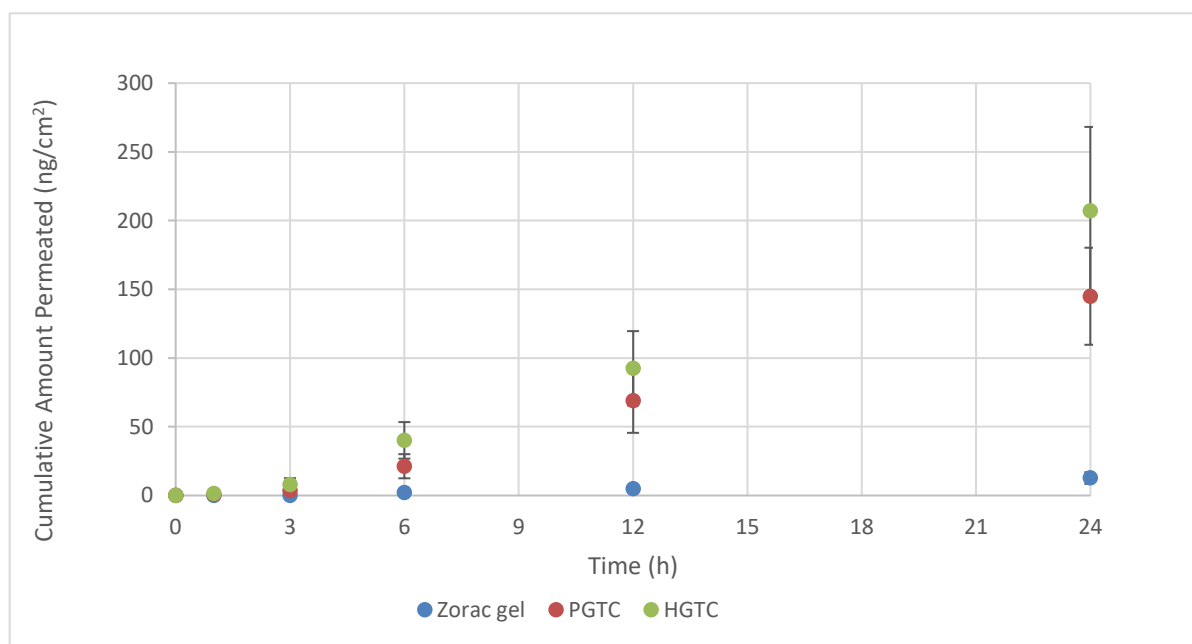


Figure 4.3 Permeation profile of tazarotene from the commercial Zorac[®] gel formulation and binary solvent systems PG:TC and HG:TC after application to human SC membrane, mean \pm SD, n=5

The cumulative amounts of tazarotene permeated through the skin from the commercial Zorac[®] gel formulation and binary solvent systems PG:TC and HG:TC are shown in figure 4.3. Statistical analysis shows a significantly higher ($p < 0.05$) cumulative amount of tazarotene passed through the skin from PG:TC and HG:TC

binary solvent systems compared to the commercial Zorac[®] gel, with HG:TC delivering the greatest amount over 24 h. These results correspond to what was seen in figure 4.2 where both PG:TC and HG:TC delivered a greater amount of tazarotene into the skin compared with the commercial formulation.

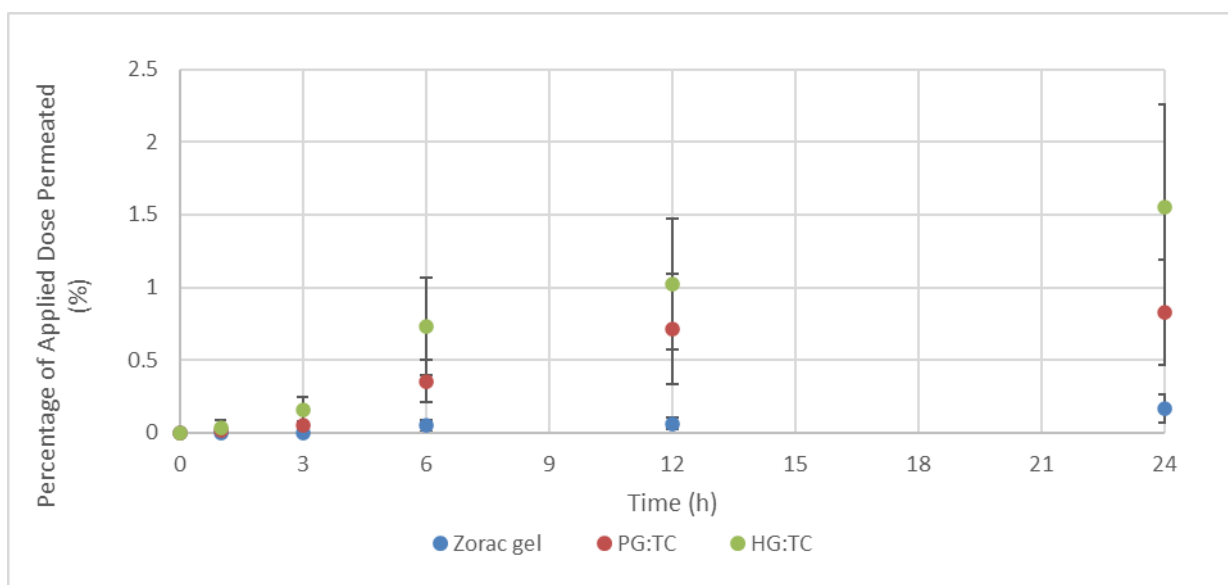


Figure 4.4 Percentage of tazarotene permeated through the skin from the commercial Zorac[®] gel formulation and binary solvent systems PG:TC and HG:TC after application to human SC membrane, mean \pm SD, n=5

The percentage of the applied dose of tazarotene permeated through the skin from the commercial Zorac[®] gel formulation and binary solvent systems PG:TC and HG:TC are shown in figure 4.4. A very small percentage, between $0.05 \pm 0.03\%$ - $1.55 \pm 0.71\%$, of the applied dose was detected over a 24 h period which could be expected due to the lipophilic nature of tazarotene. HG:TC delivered a significantly higher ($p < 0.05$) amount of tazarotene from the applied dose than PG:TC and Zorac[®] gel.

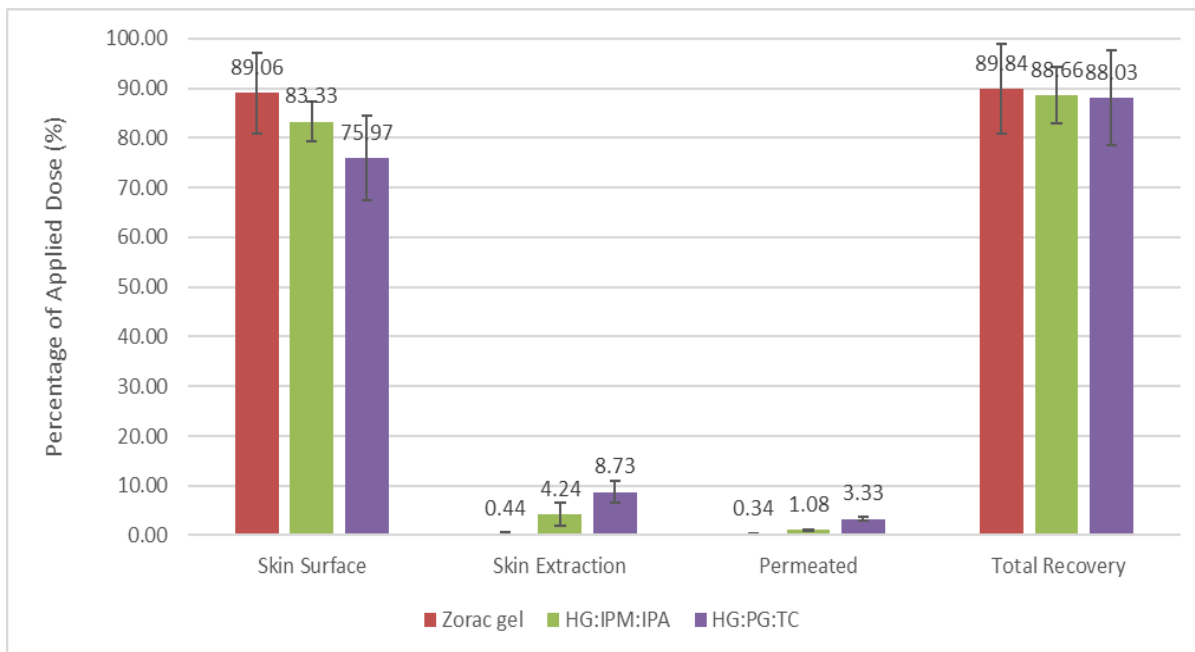


Figure 4.5 Finite dose mass balance study of ternary solvent systems containing tazarotene compared with the commercial Zorac[®] gel formulation from human SC membrane after 24 h permeation experiments, mean \pm SD, n=5

The finite dose mass balance study in figure 4.5 shows the comparison of Zorac[®] gel with two ternary solvent systems HG:IPM:IPA and HG:PG:TC. Compared to the ternary solvent systems, Zorac gel[®] again performed the worst. From the HG:PG:TC formulation $8.73 \pm 2.22\%$ tazarotene was extracted from the skin and $3.33 \pm 0.44\%$ tazarotene penetrated the skin while $75.97 \pm 8.46\%$ tazarotene remain on the skin surface. From the HG: IPM:IPA formulation $6.41 \pm 1.13\%$ tazarotene was extracted from the skin and $1.08 \pm 0.16 \%$ penetrated through the skin and $83.33\% \pm 4.07\%$ remained on the skin surface. A significantly higher ($p < 0.05$) amount of tazarotene was delivered into the skin from HG:PG:TC and HG:IPM:IPA compared to Zorac[®] gel with HG:PG:TC performing the best out of the ternary systems.

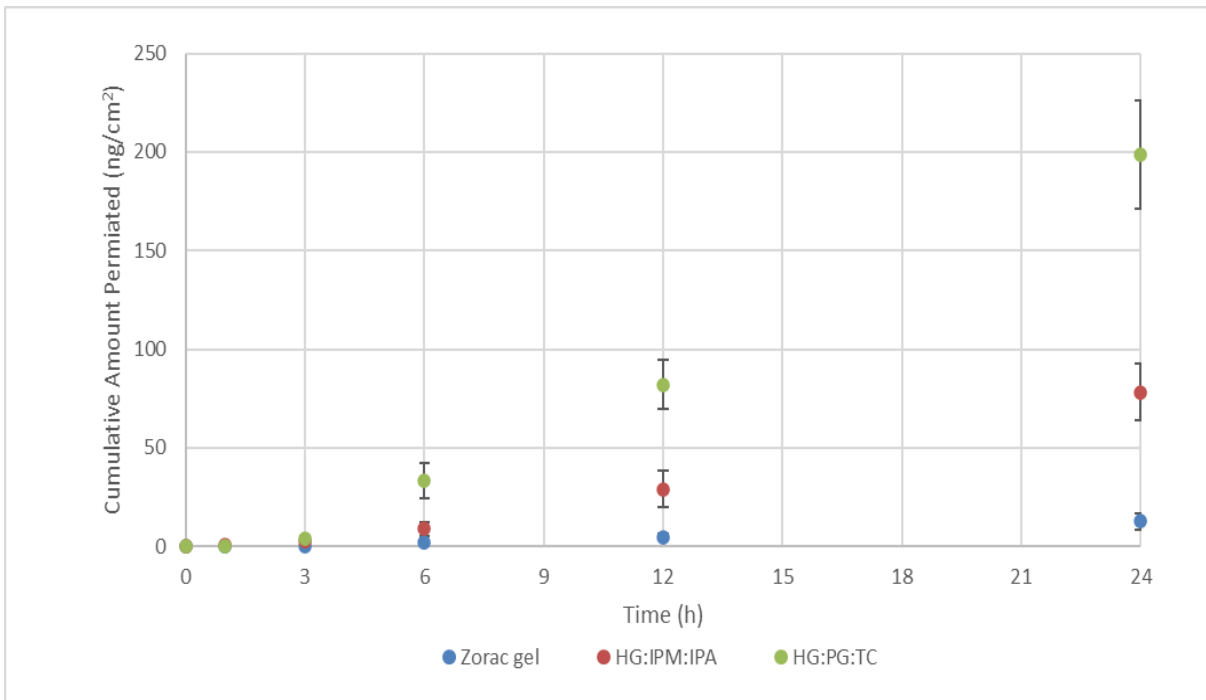


Figure 4.6 Permeation profile of tazarotene from the commercial Zorac® gel formulation and ternary solvent systems after application to human SC membrane skin, mean \pm SD, n=5

The cumulative amounts of tazarotene that permeated through the skin from the commercial Zorac® gel and ternary solvent systems HG:IPM:IPA and HG:PG:TC are shown in figure 4.6. Statistical comparisons of performance over 24 h show a significantly higher ($p < 0.05$) cumulative amount of tazarotene passed through the skin from HG:IPM:IPA and HG:PG:TC formulations compared to the commercial Zorac® gel. These results again correspond to what was seen in figure 4.5 where both HG:PG:TC and HG:IPM:IPA delivered a greater amount of tazarotene into the skin compared to Zorac® gel.

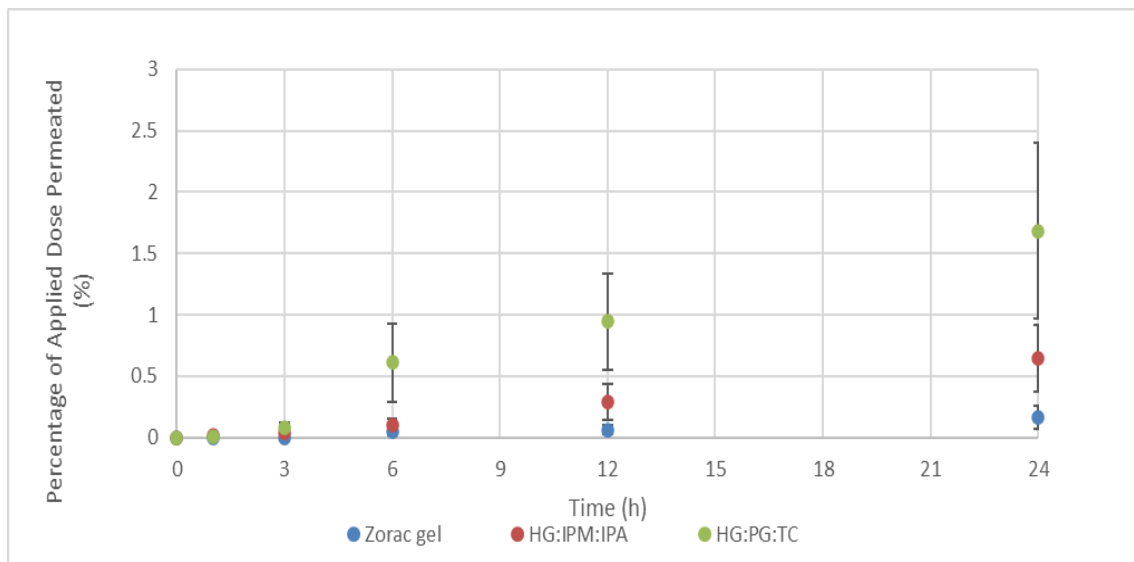


Figure 4.7 Percentage of tazarotene permeated through the skin from the commercial Zorac[®] gel formulation and ternary solvent systems HG:IPM:IPA and HG:PG:TC after application to human SC membrane, mean \pm SD, n=5

The percentages of tazarotene that permeated through the skin from the commercial Zorac[®] gel formulation and ternary solvent systems HG:IPM:IPA and HG:PG:TC are shown in figure 4.7. Again, as anticipated, due to the lipophilic nature of tazarotene only a small amount, between $0.08 \pm 0.04\%$ – $1.68 \pm 0.72\%$, of the applied dose, was detected over 24 h. A significantly higher percentage ($p < 0.05$) of tazarotene was delivered through the skin from HG:PG:TC compared to HG:IPM:IPA and Zorac[®] gel.

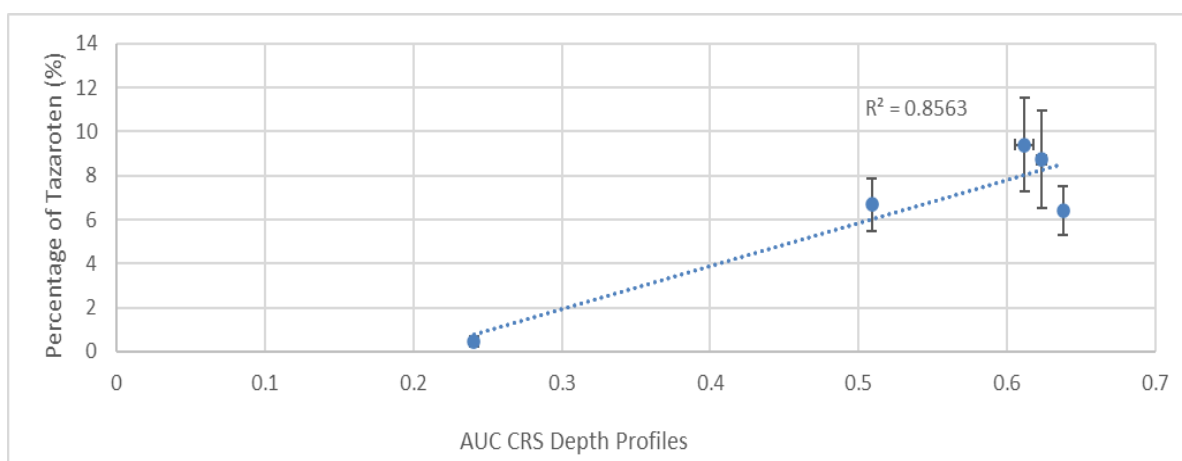


Figure 4.8 *In-vitro* correlation of LC-MS extractions and non-invasive CRS depth profiles

Figure 4.8 illustrates the comparison between *in-vitro* LC-MS and CRS analysis of tazarotene found in the skin from the commercial Zorac[®] gel, PG:TC, HG:TC, HG:PG:TC and HG:IPM:IPA solutions. The graph shows that as the percentage of tazarotene detected by the LC-MS in the skin from each formulation increases, the amount of tazarotene non-invasively detected by CRS in the SC is greater. A linear regression of the data reveals a strong correlation $R^2 = 0.86$ between both analytical techniques. This evidence helps strengthen and support the use of the CRS for the non-invasive analysis of skin penetration.

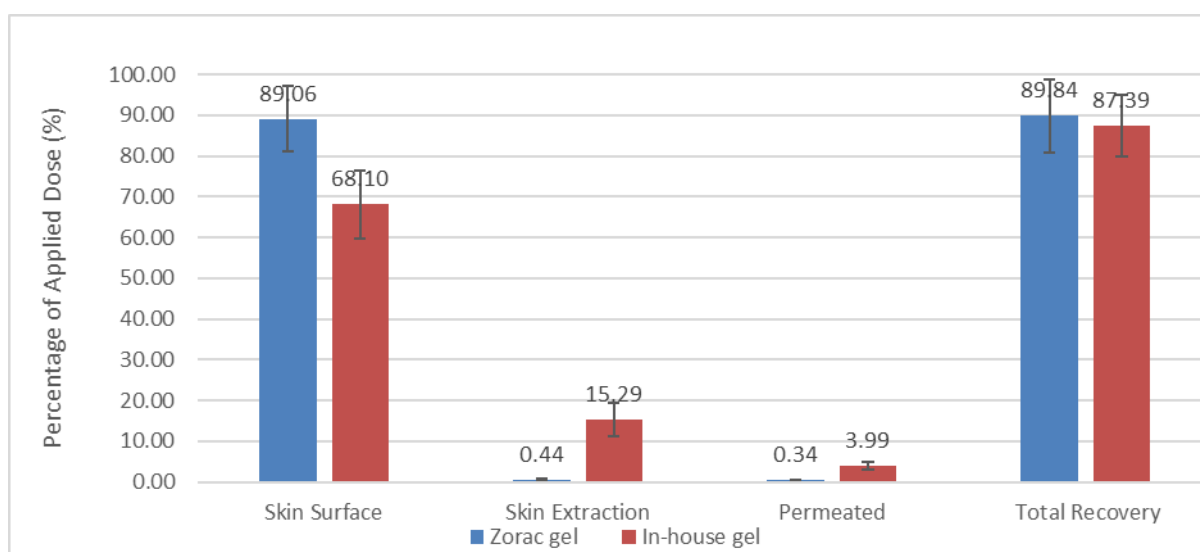


Figure 4.9 Finite dose mass balance study of an in-house gel containing HG:TC and tazarotene compared with the commercial Zorac[®] gel formulation from human SC membrane after 24 h permeation experiments, mean + SD, n=5

The finite dose mass balance study in figure 4.9 illustrates the percentage of tazarotene delivered to the skin from the in-house gel and commercial Zorac[®] gel formulations. The in-house gel delivered $15.29 \pm 4.23\%$ into the skin and $3.99 \pm$

0.94% through the skin, while $68.10 \pm 8.34\%$ remained on the skin surface.

Statistical analysis shows that the in-house gel significantly outperformed ($p < 0.05$)

the commercial gel by delivering 14.85 % more tazarotene into the skin over 24 h.

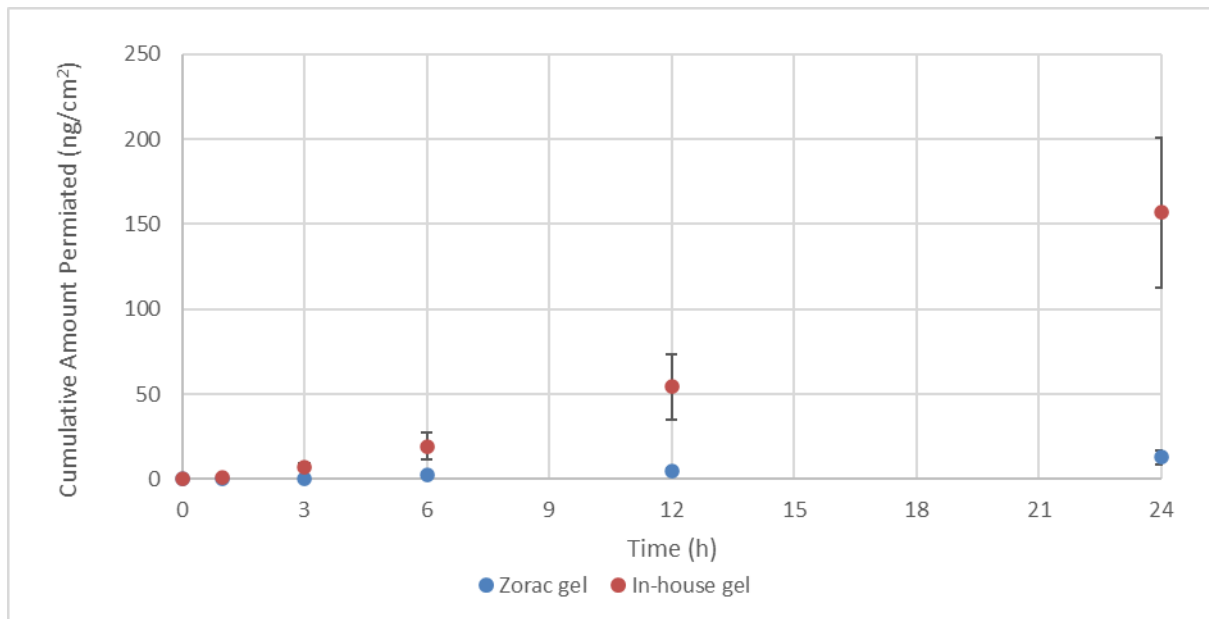


Figure 4.10 Permeation profile of tazarotene from the commercial Zorac® gel formulation and in-house gel formulations after application to human SC membrane, mean \pm SD, n=5

The cumulative amount of tazarotene that permeated through the skin from the commercial Zorac® gel and in-house gel formulations is shown in figure 4.10.

Statistical comparisons performed over 24 hours show a significantly higher ($p < 0.05$) cumulative amount of tazarotene passed through the skin from the in-house gel formulation compared to the commercial Zorac® gel formulation which corresponds to what was seen in figure 4.9 with the in-house gel delivering a significantly greater ($p < 0.05$) amount of tazarotene into the skin.

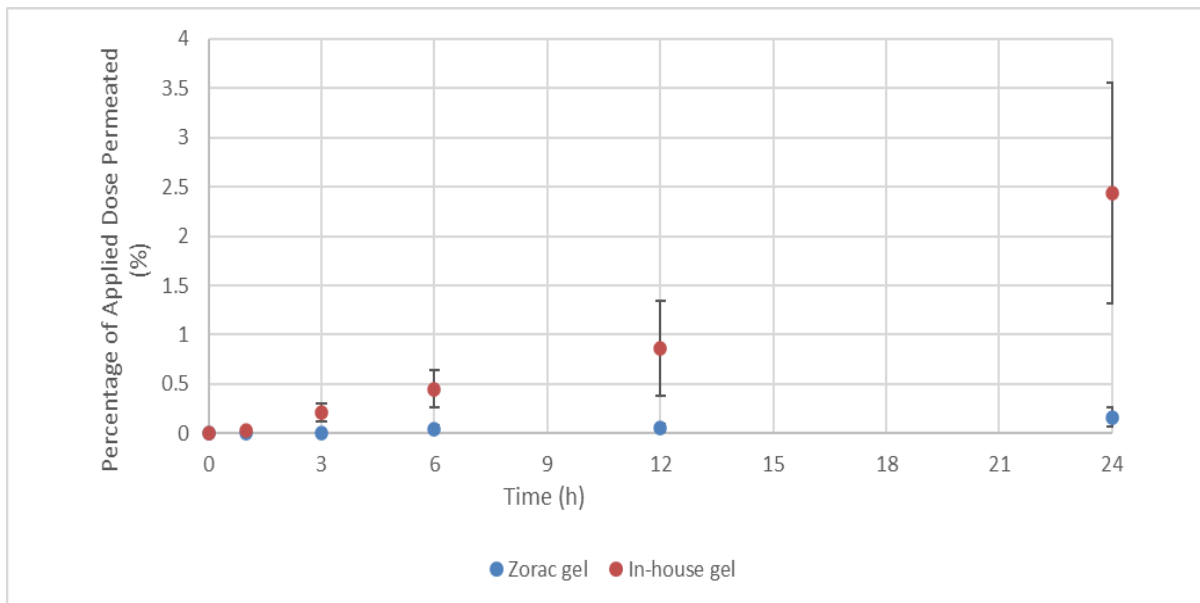


Figure 4.11 Percentage of tazarotene permeated through the skin from the commercial Zorac® gel formulation and in-house gel formulations after application to human SC membrane, mean \pm SD, n=5

The percentage of tazarotene that permeated through the skin from the commercial Zorac® gel and in-house gel formulations is shown in figure 4.11. As seen previously, only a small percentage, between $0.21 \pm 0.09\%$ – $2.44 \pm 1.16\%$ of the applied doses was detected over 24 h due to the lipophilic nature of tazarotene. A significantly higher ($p < 0.05$) percentage of tazarotene from the applied dose passed through the skin by the in-house gel formulation compared to the commercial Zorac® gel formulation.

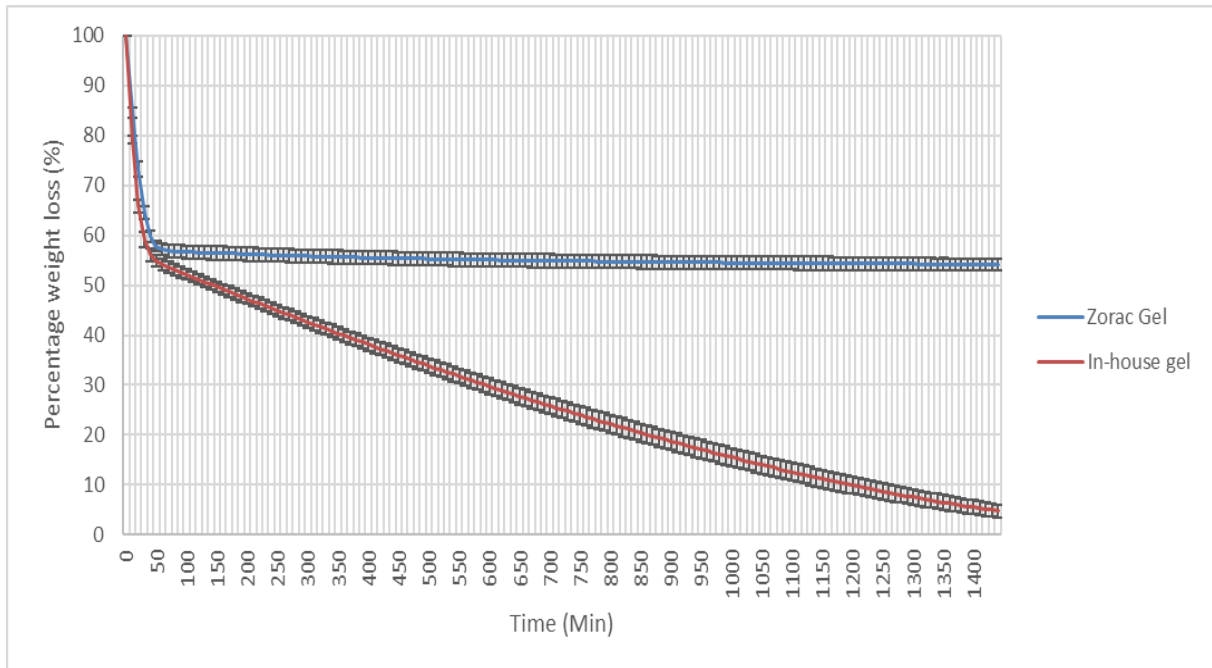


Figure 4.12 Percentage weight loss of the commercial Zorac® gel formulation and in-house gel under static conditions 50% RH and 32°C after application of 5µL on a quartz pan over 24 hours, mean ± SD, n=3

To evaluate the loss of vehicle from the residual phase evaporation studies using dynamic vapour sorption (DVS) were conducted on the commercial Zorac® gel and in-house gel illustrated in figure 4.12. An identical mass loss rate can be seen for both the commercial Zorac® gel and in-house gel for the first 40 min after which point the formulations begin to show two very distinct profiles. The mass loss appears to halt for the commercial Zorac® gel formulation after 40 min with a constant mass observed between 40 -1440 min, which resulted in a total mass loss of about 45.9% after 24 h. The in-house gel, on the other hand, showed a very slow mass loss rate between 40 – 1440 min and unlike the commercial Zorac® gel formulation, it did not

stop evaporating throughout the entire experiment, resulting in a total mass loss of about 95.2% after 24 h.

The rate of evaporation of a formulation is thought to be directly related to its vapour pressure and in this instance, it appears that the in-house gel produced a substantially higher vapour pressure than the commercial Zorac[®] gel under the same experimental conditions, resulting in the in-house gel having a slow but steady continuous mass loss over the entire examination period. If the delivery vehicle continuously evaporates on the skin surface, as seen with the in-house gel, the relative tazarotene concentration in the formulation increases, resulting in a higher thermodynamic activity at the skin surface, which enhances the delivery of tazarotene into the skin. On the other hand, if the delivery vehicle completely evaporates, as seen in the case of Zorac[®] gel, most of the tazarotene trying to penetrate the skin recrystallises on the skin surface, putting a halt to any penetration into the skin.

4.4 Conclusions

To conduct any permeation study, reproducible quantitative recovery of the compound being examined must be achieved to accurately evaluate the data being collected. In a finite dose study, only a small amount, between 5 – 10 μL , of a formulation is applied to best resemble *in-vivo* conditions where a formulation completely evaporates on the skin surface. Studying formulations containing 0.1% tazarotene in finite doses, however, posed a major challenge, as the limit of quantification achieved by the previously developed HPLC method was not low enough to perform a mass balance study. To overcome this limitation, a new LC-MS method was developed and validated to substantially lower the current limit of detection. The LC-MS method used HPLC to separate tazarotene from samples and mass spectrometry (MS) to identify the structure of tazarotene with a very high degree of sensitivity and molecular specificity. The LC-MS method developed was validated and showed excellent linearity, reproducibility, precision and robustness. The limit of quantification for the new LC-MS was significantly more ($p > 0.05$) sensitive than the previous HPLC method and ideal for finite-dose studies with formulations containing 0.1% tazarotene. The binary and ternary solvent systems all showed the ability to deliver tazarotene into the human SC in stark contrast with the commercial Zorac[®] gel formulation which was again unable to deliver any significant amount of

tazarotene into the SC. HG:TC and HG:PG:TC were able to deliver the most amount of tazarotene into the skin from the binary and ternary solvent systems examined. The work presented here confirms what was seen in previous chapters: combining a relatively small amphipathic excipient HG with the slightly larger miscible hydrophilic excipient TC is the best combination to significantly enhance the delivery of tazarotene, an extremely hydrophobic molecule, into the skin. Combinations of HG and TC are thought to enhance drug permeation of tazarotene through the solubilising properties of TC coupled with the partitioning, penetration and carrier properties of glycols through the interaction with intercellular SC lipids. Taking the best-performing solvent system HG:TC and formulating it into a gel did not lead to a decrease in skin penetration. In fact, by adding carbomer as a gelling agent and benzoyl alcohol as a preservative alongside HG:TC, the new in-house gel formulation further enhanced the delivery of tazarotene into human epidermal skin. Thermodynamic examination of the in-house gel and Zorac[®] gel by DVS revealed two very distinct profiles. Zorac[®] gel stopped evaporating after a short period, resulting in the recrystallisation of tazarotene out of the formulation, while the in-house gel evaporated continuously over the entire examination period, causing the concentration of tazarotene in the formulation to gradually increase over time. This increased thermodynamic activity created by the in-house gel is also thought to be a major contributor to the enhanced penetration of tazarotene into the skin over the

commercial Zorac[®] gel formulation. When comparing LC-MS skin extraction data in this chapter with the non-invasive CRS depth profile data generated in chapter 3, a strong correlation can be seen between both methods of skin analysis for all five formulations examined, helping to establish a proof-of-concept for the use of CRS for non-invasive analysis of skin penetration.

Chapter Five:

In-vivo LC-MS & CRS Evaluation of Topical Tazarotene Formulations

Chapter Five

In-vivo LC-MS & CRS evaluation of topical tazarotene formulations

5.1 Introduction

In-vitro Franz cell studies using human tissue are accepted as the most appropriate model to assess skin permeation. However, the experiments themselves may not fully represent the true complexity of what a formulation would encounter in real life. Studies on a variety of human volunteers give a more accurate representation of formulation efficacy concerning the population at large as opposed to using a single skin donor sample. Also, although the receptor medium of a Franz cell does provide sink conditions throughout the entire experiment, it is unable to model the true vasculature of human skin that influences skin permeation. Despite these differences, the relationship between the *in-vitro* and *in-vivo* permeation studies is one of great importance. *In-vitro* data is essential to help guide formulation development and predict the *in-vivo* performance of a formulation. A meta-analysis that collated data for thirty model permeants from thirty studies with ninety-two data sets revealed a strong positive correlation between the *in-vitro* and *in-vivo* permeation studies (Lehman, Raney et al. 2011). *In-vivo* studies are by far the best means of studying the percutaneous absorption of pharmaceutical actives.

Arguably, the most common *in-vivo* technique for skin-related studies is the well-established use of tape stripping, where sequential layers of the skin are stripped with the use of adhesive tape. The contents of the tape strips are usually extracted with an appropriate solvent and analytes are quantified by a suitable technique. Tape stripping studies have been widely used in dermatological research as a minimally invasive technique to study drug penetration into the epidermis, avoiding the need for skin biopsies (Escobar-Chavez, Merino-Sanjuan et al. 2008). Pellanda et al. used tape stripping to study the effects dose and application frequency have on triamcinolone acetonide (TACA) penetration into the human SC. They showed that TACA amounts would be retained within SC irrespective of dose or application frequency while low doses of TACA applied once are favoured over a high dose which might promote greater systemic exposure (Pellanda, Ottiker et al. 2006). Alberti et al. studied the penetration of terbinafine from isopropyl myristate and ethanol-containing formulations into human skin by tape stripping that revealed similar diffusion parameter amounts in all formulations examined but drug partitioning into the SC was significantly higher with ethanol-containing formulations (Alberti, Kalia et al. 2001). The development of the non-invasive, non-destructive technique of CRS in the field of dermatology has begun to revolutionise the way human skin is examined. The combined use of Raman scans taken in the fingerprint and the high wavenumber region allows detailed information about the skin to be

acquired with analyte and water depth profiles able to be constructed. The correlation between well-established analytical techniques with less established techniques such as CRS is critically important to help validate and support their potential future use. Some studies have already helped provide further evidence for the use of CRS to study drug disposition in the skin. Mateus et al. used CRS to study the penetration and deposition of salicylic acid (SA) into human skin and were able to show a strong positive *in-vitro* – *in-vivo* correlation between the cumulative amounts of SA that permeated through the skin and CRS signal of SA found in the skin (Mateus, Moore et al. 2014). More recently Patel et al. studied the permeation of ibuprofen (IBU) in selected solvent systems following the finite dose application to human skin *in-vitro* using HPLC to analyse the samples and *in-vivo* through the non-invasive use of CRS. In these studies, a comparison of both *in-vitro* and *in-vivo* data again revealed a strong positive correlation between the cumulative amount permeated of IBU *in-vitro* and the total amount of IBU that penetrated the SC *in-vivo*. Clear similarities and differences could be seen between the solvents under examination established by the two analytical methods (Patel, Iliopoulos et al. 2021). Draelos et al. developed an LC-MS method to quantify the amount of tazarotene on tape strips to investigate drug penetration into the skin. They found that tazarotene penetrated the skin and could be detected throughout the SC successfully with

concentration decreasing as penetration depth increased (Draelos and Draelos 2021).

Melot et al. used CRS for *in-vivo* analysis of trans-retinol in PG/ethanol and MYRITOL[®]318 following application to the skin. They were able to calculate the SC thickness using the same linear process of diffusion water gradient integrations revealing a similar average SC thickness. Significant differences in the delivery of trans-retinol were also shown between formulations with the type of penetration enhancer influencing delivery into the skin (Pudney, Melot et al. 2007, Melot, Pudney et al. 2009). Krombholz et al. studied the drug deposition of retinol by tape-stripping and CRS showing comparable skin penetration profiles and drug concentrations particularly within the first 10 μm up to a total penetration depth of around 15 μm into the skin (Krombholz, Fressle et al. 2022). More recently, Iliopoulos et al. studied the delivery of diclofenac sodium (DFNa) into the skin from the commercial Diclac[®] Lipogel and Primofenac[®] emulsion gel formulations through both tape stripping and CRS. CRS and tape stripping both showed similar depth and distribution profiles of DFNa in the SC with both techniques able to differentiate between formulations to establish similar conclusions (Iliopoulos, Goh et al. 2022). In this chapter *in-vivo* experiments were performed on human volunteers using an HG:TC binary solution and the previously developed in-house gel formulation. Tape stripping was

conducted on six healthy volunteers and CRS on one healthy volunteer with correlations between both *in-vivo* techniques being examined.

5.2 Materials and methods

5.2.1 Materials

Standard D-Squame[®] tape (2.2 cm in diameter, 3.8 cm²) was supplied by CuDerm (USA).

Zorac[®] gel 0.1% supplied by Allergan pharmaceuticals (IRL).

Tazarotene was supplied by Insight Biotechnology (UK).

HG, PG, IPA, UHPLC grade water, UHPLC grade methanol, formic acid and benzyl alcohol were supplied by Fisher Scientific (UK).

TC gifted by Gattefossé (UK).

IPM, BrijO20[®], Parafilm[®], Eppendorf centrifuge tubes, UHPLC amber glass vials, 200ml vial inserts, UHPLC Accucore column and guard column were supplied by Sigma-Aldrich (UK).

Carbomer 974P was supplied by Lubrizol (UK).

5.2.2 Volunteer recruitment

To investigate the effects of tazarotene on the SC, 7 healthy volunteers aged between 22 – 45 years were recruited (3 males, 4 females; 3 Caucasian and 4 Asian subjects) The research protocol was approved by the UCL Research Ethics Committee (Reference 15709/001).

A participant information leaflet was supplied to all the volunteers before the studies. None of the volunteers had any history of skin disease and were asked, apart from daily washing, not to apply any moisturiser or cosmetic product 2 days before the study.

5.2.3 Tazarotene formulation preparation

Formulations were made fresh as required. The appropriate mass of tazarotene was weighed in a 2 mL plastic Eppendorf with a locking lid. For the HG:TC formulation, a total of 1 mL of the required vehicle was pipetted into a 2 mL Eppendorf containing the pre-weighed amount of tazarotene to give a final concentration of 0.1% (w/w). For the gel formulation, HG and TC were pipetted into a 2mL Eppendorf containing the pre-weighed amount of tazarotene at a ratio 4:1 up to a volume of 500 μ L followed by 490 μ L of HPLC grade water, 10 μ L of benzyl alcohol and the addition of 15 mg of Carbomer 974P. Eppendorfs were then locked, wrapped in Parafilm M[®] and placed into an incubating orbital mini shaker (VWR, UK) at 800 RPM and 25 °C \pm 1 °C until a homogeneous formulation was produced. All formulation constituents

were weighed using an analytical balance (Mettler Toledo, UK). The concentration of tazarotene in all the solutions prepared was measured via LC-MS.

5.2.3 Application of topical tazarotene formulations

Circular areas of the forearm were marked with a water-resistant felt tip pen before a finite dose of 5 µl of each formulation was applied to the skin via an Eppendorf multiple dispenser pipette. A plastic rod was then used to evenly spread the formulations within the designated area. Volunteers were asked to keep the area under examination clear and undisturbed for 3 h before tape stripping.

5.2.4 Tape stripping procedure

Standard D-Squame[®] tape was applied to the forearm with the application of a constant pressure of 225g/cm² using a D-Squame[®] pressure instrument for 5 seconds. The tape was then removed and placed in a standard D-Squame[®] tape rack. To investigate the baseline measurement, 4 tape strips were collected from a different forearm area. However, to observe depth profiling, 15 consecutive tape strippings were performed on the site. To minimise variation, the procedure was always conducted by the same operator. The interval between the stripping was 1 ± 0.5 min.

5.2.5 TEWL measurements

TEWL was measured using an Aquaflux[®] AF103 (Biox Systems, London, U.K.) Volunteers were allowed to acclimatise for at least 15 min before the measurements to adapt to the room conditions and for the sweat glands to be inactive. TEWL was then measured at ambient conditions of 20 ± 1 °C and $45 \pm 1\%$ relative humidity (RH) (Voegeli, Heiland et al. 2007). TEWL measurements were taken before formulation application to establish a baseline, and subsequently after every 5 tape strips.

5.2.6 SC Protein content measurements

Protein content was measured directly from the tape strips using infrared densitometry. The method has previously been validated using the conventional bicinchoninic acid colourimetric technique to determine protein content (Voegeli, Heiland et al. 2007).

$$C_{\text{protein}} (\mu\text{g}/\text{cm}^2) = 1.366 \times \text{Absorption} (\%) - 1.557 \quad (5.1)$$

Protein absorption was determined at 850 nm using an infrared densitometer SquameScan[®] A850 (Heiland Electronic, Wetzlar, Germany). The amount of protein was subsequently quantified using Equation 5.1 as described by Voegeli et al.

5.2.8 LC-MS quantification of tazarotene on tape strips

All tape strips were placed in 2 mL Eppendorf tubes in addition to 1 mL of the UHPLC grade methanol. Tubes were sealed with Parafilm[®] placed in an incubating mini shaker (VWR, UK) and held at $32 \pm 1^\circ\text{C}$ for 12 h at 800 RPM. After 24 h, tubes were placed in a 5415R microcentrifuge (Eppendorf, Germany), pre-warmed to 32°C and centrifuged at 13200 rpm for 15 min. The supernatant was removed, and samples were centrifuged again at 13200 rpm for an additional 15 min. The samples were finally filtered through a $0.22\mu\text{m}$ millipore syringe filter. The LC-MS method developed and validated in chapter 4 was used to quantify the amount of tazarotene on each tape strip.

5.2.9 CRS instrument

CRS measurements were conducted using a River Diagnostics gen2-SCA Skin Analyser equipped with two fibre-coupled diode-pumped lasers operating at two wavelengths, 671 nm ($2500 - 4000\text{ cm}^{-1}$) and 785 nm ($400 - 2000\text{ cm}^{-1}$, fingerprint region). Skin water content measurements were obtained using the 671 nm laser with a $1\mu\text{m}$ spot of $\leq 20\text{ mW}$ power. The fingerprint region spectra of the skin were obtained from the 785 nm laser with a $1\mu\text{m}$ spot of $\leq 20\text{ mW}$ power.

The laser light was focused on the skin via an oil-immersion microscope (NA 0.86, focal length 5.8 mm, working distance 1.5 mm). The depth of the laser that

penetrates the skin is controlled by a high-precision piezoelectric focusing drive. The scattered light formed by the tissue is collected through the same objective. The Raman scattered light is focused onto an optical fibre, which is 25 μm in diameter and acts as the confocal pinhole that rejects signals from out-of-focus regions. The Raman signals are detected by an air-cooled, high-sensitivity back-illuminated, deep-depletion CCD camera (1024 x 128 pixels) at a 5 cm^{-1} spectral resolution out to 1000 nm.

5.2.10 Data collection and statistical analysis of the *in-vivo* results

CRS depth profile spectra were obtained at a step size of 2 μm with a ten-second laser exposure time per depth in one frame using the 785 nm laser collecting data in the fingerprint region (400–2000 cm^{-1}). Raman water profile spectra were obtained at a step size of 2 μm with a ten-second exposure time per depth in one frame, using the 671 nm laser collecting data in the high wavenumber region (2400 – 4000 cm^{-1}). The calibration of tazarotene and reference spectra of PG and HG in chapter 3 were used for qualitative and quantitative analysis. All CRS data were acquired using RiverIcon[®] v.3.0013 and analysed with Skin Tools[®] v.3.0 programs (River Diagnostics, The Netherlands).

Chromatogram data were integrated using Agilent ChemStation[®] for HPLC systems (Agilent Technologies, USA). Microsoft[®] Excel Office 2018 (Microsoft, USA) was

used to analyse and graph the data. Parametric statistical tests, ANOVA and t-tests were conducted to investigate statistical differences using GraphPad Prism® 6 (Dotmatics, USA). All results, unless stated otherwise, are presented as mean \pm standard deviation (SD).

5.3 Results and discussion

5.3.1 Tape stripping of topical tazarotene formulations

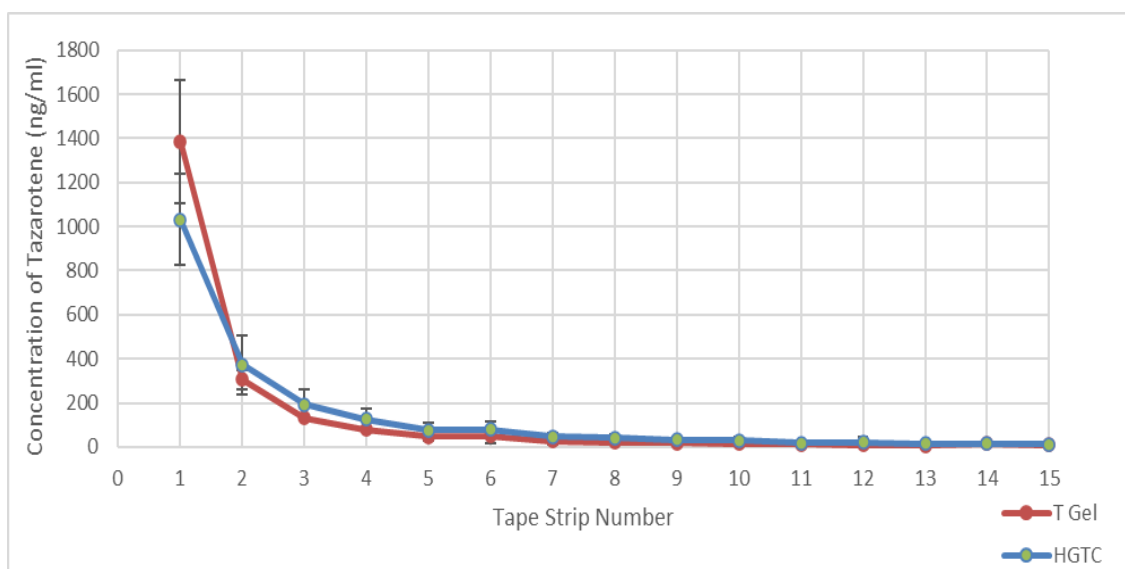


Figure 5.1 Concentration of tazarotene delivered into the SC from HG:TC solution and in-house gel, mean \pm SD, n=6

Figure 5.1 illustrates the concentration of tazarotene detected on each tape strip from the forearm of healthy volunteers. The results reveal tazarotene delivered from both the HG:TC solution and in-house gel could be detected throughout the SC after 3 hrs with concentrations decreasing with depth. A statistically significant ($p < 0.05$)

difference in the amount of tazarotene on each tape strip delivered from the HG:TC solution and in-house gel formulation was not observed. The results show the in-house gel and HG:TC solution is both able to enhance the delivery of tazarotene into the skin in a similar manner, even though the proportion of HG:TC incorporated in the in-house gel formulation is less than 50% of the pure HG:TC solution.

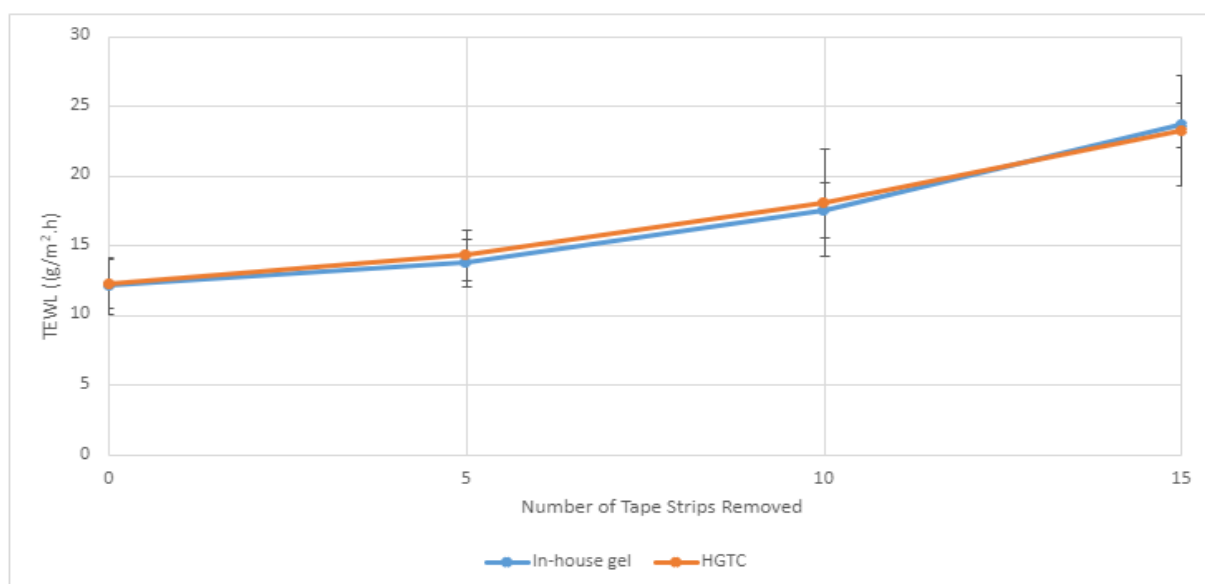


Figure 5.2 Changes in TEWL of tape-stripped healthy volunteers' forearms after application of the HG:TC solution and in-house gel, mean \pm SD, n=6

TEWL values measured following the application of both the HG:TC solution and in-house gel and tap stripping are illustrated in figure 5.2. As expected TEWL values for both formulations increased with an increasing number of tape strips removed. All volunteers lost a similar amount of water regardless of the formulation being examined, indicating that the loss of barrier function for both the HG:TC solution and

the in-house gel was roughly the same. There was not a statistically significant difference ($p < 0.05$) observed between HG:TC and in-house gel TEWL values, suggesting all volunteers lost water in a similar fashion, which indicates that the loss of barrier function for all the volunteers was the same throughout the investigation.

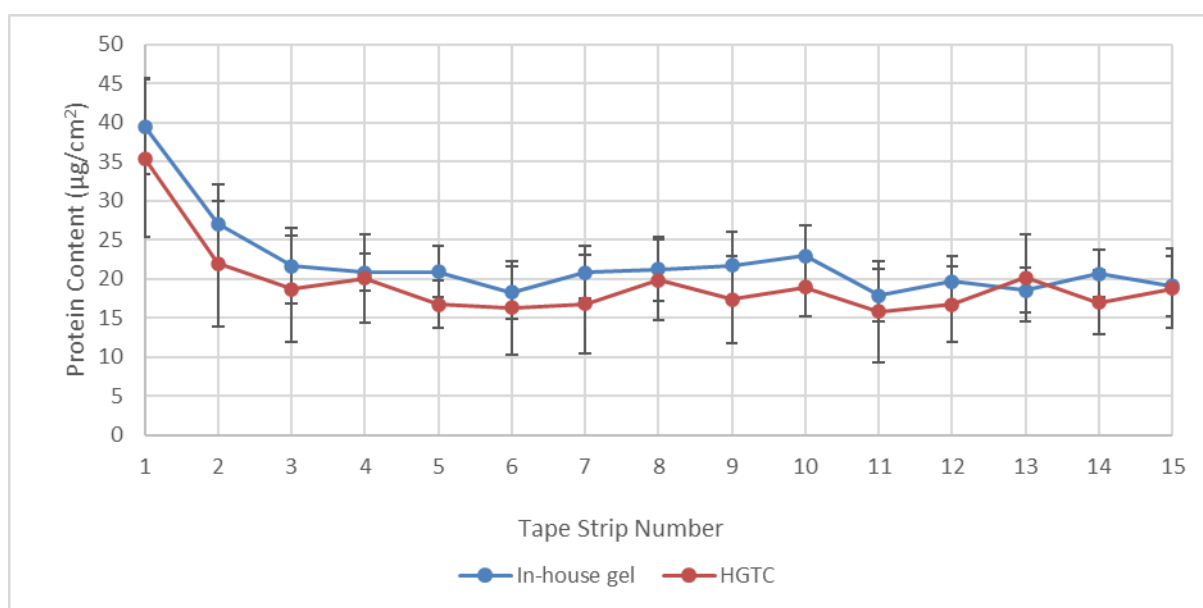


Figure 5.3 Amount of SC protein removed from the forearm of healthy volunteers after application of HG:TC solution and in-house gel, mean \pm SD, n=6

Figure 5.3 illustrates the protein content in the SC collected following tape stripping of the forearm area of healthy volunteers. Looking at the graph, it is clear that most of the protein removed by each tape strip was greater with the in-house gel than with the pure HG:TC solution. By comparison, protein content removed by each tape strip from the in-house gel area was significantly higher ($p < 0.05$) than the area where the HG:TC solution was applied. The concentration of tazarotene detected by LC-MS was roughly the same on each tape strip for both formulations, however, the amount

of protein removed by each tape strip was consistently larger for the in-house gel, suggesting that the amount of tazarotene throughout the SC was greater for the in-house gel, which shows that it was able to outperform the pure HG:TC solution by delivering more tazarotene into the skin.

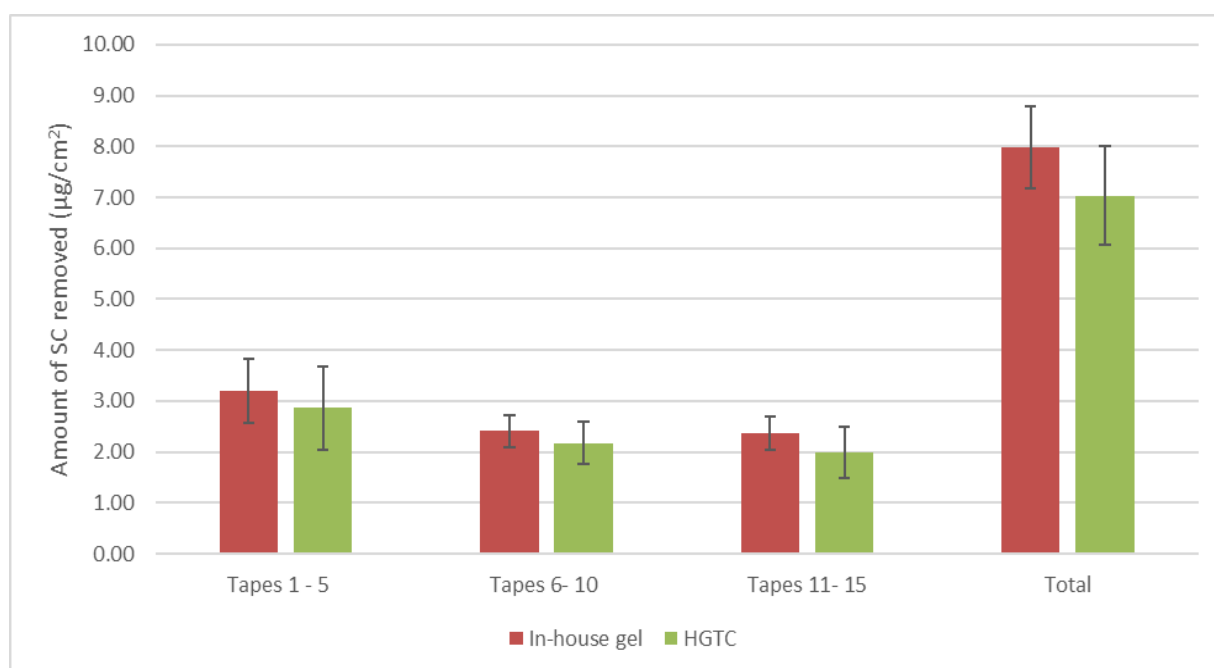


Figure 5.4 Pooled amount of SC removed from the forearm of healthy volunteers after application of HG:TC solution and in-house gel, mean \pm SD, n=6

Figure 5.4 illustrates the pooled amount of SC protein removed from the forearm area of healthy volunteers. In this graph, it is evident that the total amount of protein removed in the SC was greater with the in-house gel than with the pure HG:TC solution. Again, comparing the two formulations reveals that the area where the in-house gel was applied removed a significantly higher ($p < 0.05$) amount of SC than the area where the HG:TC solution was applied.

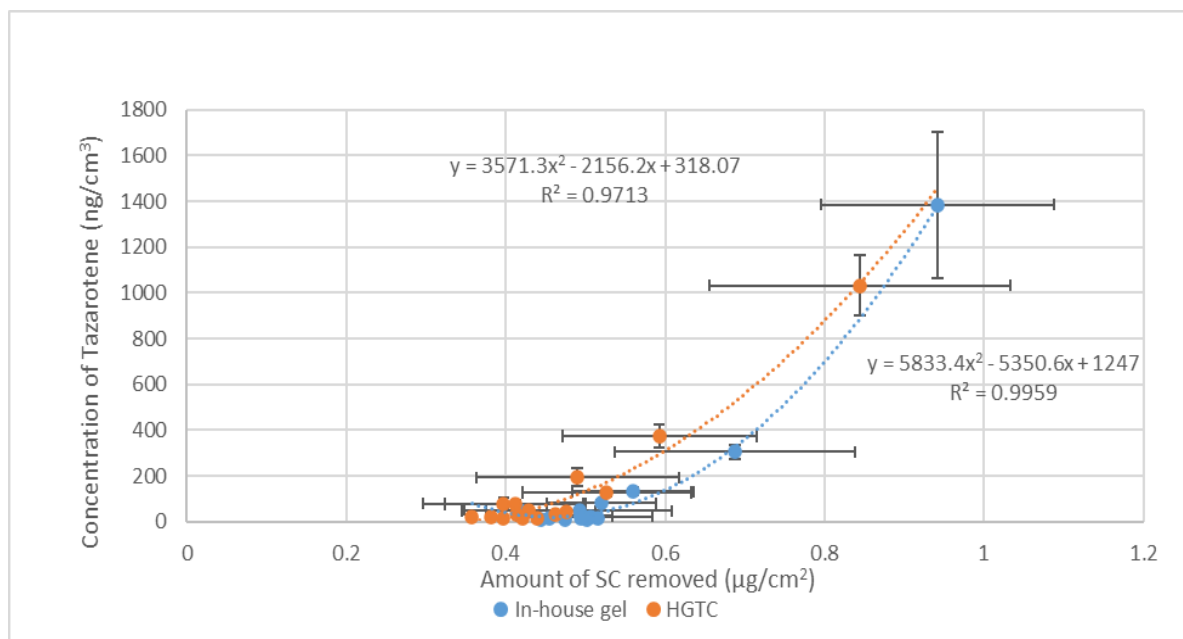


Figure 5.5 Correlation between the concentration of tazarotene and amount of SC removed from the forearm of healthy volunteers after application of HG:TC solution and in-house gel, mean \pm SD, n=6

Figure 5.5 illustrates the concentration of tazarotene over the amount of SC removed from the skin on each tape strip. The graph shows that as the amount of SC being removed decreases, the amount of tazarotene in the skin also substantially decreases, suggesting that both formulations penetrated deep into the SC after the 3-hour application. The x-axis error bars represent the variation in concentration on each tape strip while the y-axis error bars represent the variation in SC removed from each tape strip.

A strong polynomial correlation was observed for both the in-house gel ($R^2 = 0.96$) and HG:TC solution ($R^2 = 0.97$) while, statistically, analysis reveals that the in-house gel delivered significantly more ($p < 0.05$) tazarotene deeper into the skin compared to the pure HG:TC solution within the same time frame. This correlates well with *in-vitro*

data from chapter 4 that indicated that the in-house gel outperforms the HG:TC binary solution as well as all other formulations examined, including the commercial Zorac[®] gel.

5.3.2 CRS of topical tazarotene formulations

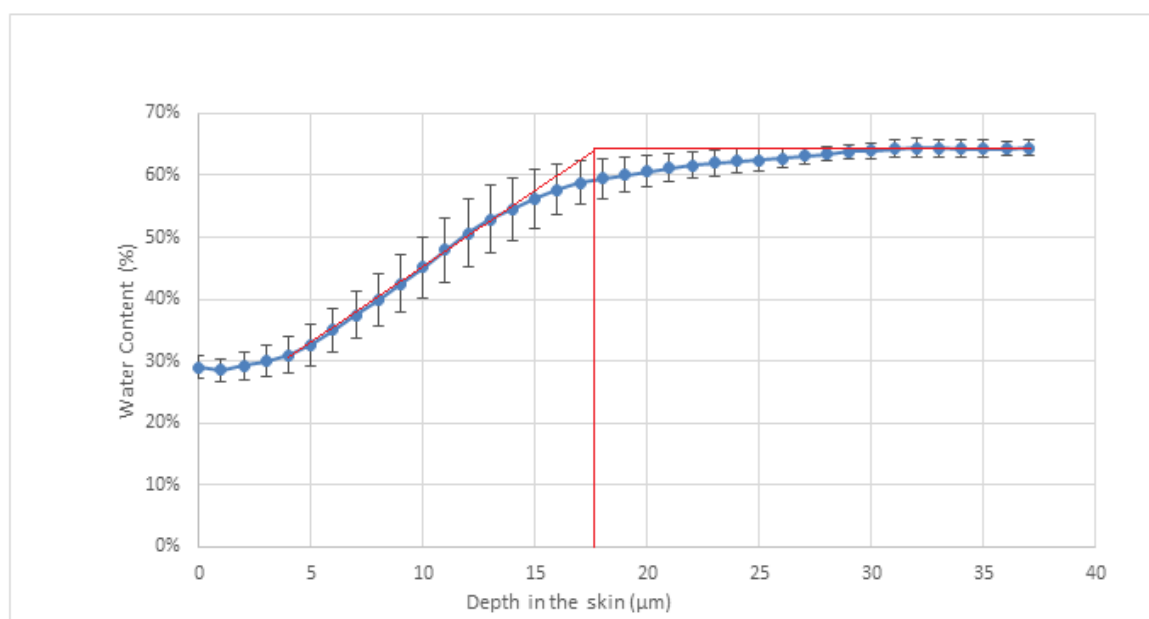


Figure 5.6 Water content profile from the forearm of a healthy volunteer with model fitting to calculate SC thickness. mean + SD. n=5

Figure 5.6 illustrates the water content profile and intersection between the lower boundary of the SC and viable epidermis. Water-protein band ratios were measured from the forearm skin of a human volunteer at sequential depth increments via CRS to construct a water concentration profile. A linear process of diffusion was imposed for the increasing and plateau phases of the graph, with the intersection of the two gradients establishing the SC thickness.

Water concentration profiles were taken before and after formulation application to ascertain whether any changes in SC thickness could be observed. There was no significant difference ($p < 0.05$) in SC thickness before and after formulation application. SC thickness values measured after formation application were used to normalise all depth profiles. The average SC thickness of the skin used in this study was calculated to be $18 \mu\text{m} \pm 0.2 \mu\text{m}$.

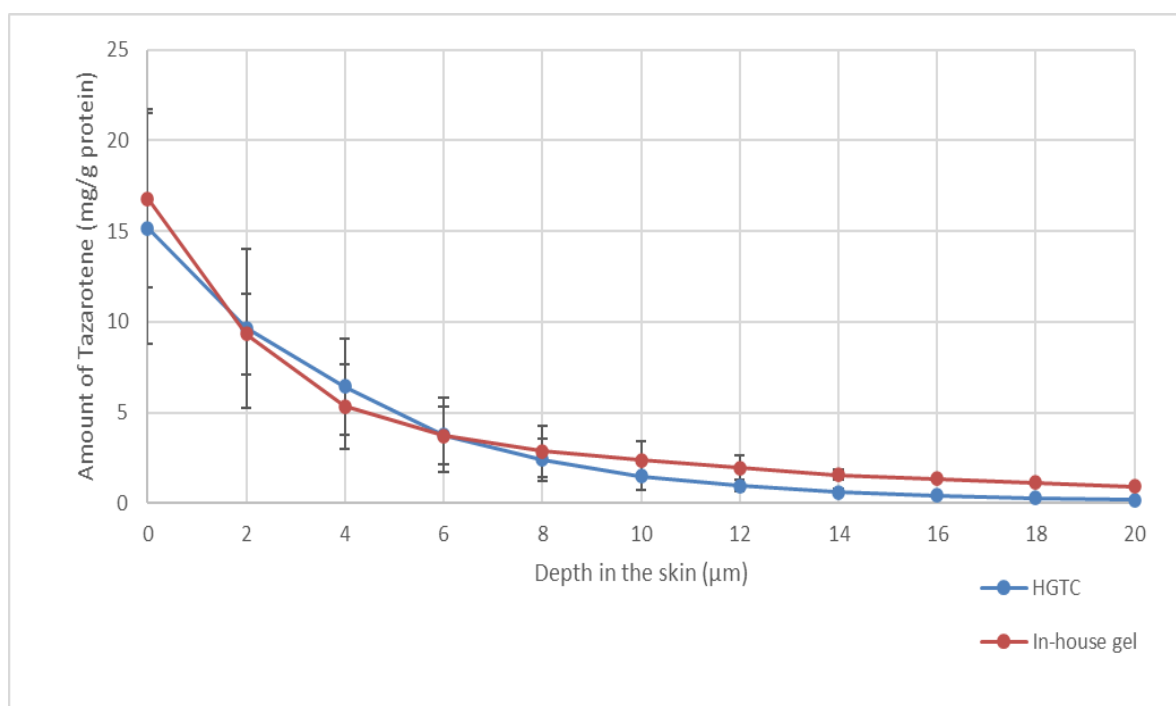


Figure 5.7 Quantitative depth profiles of tazarotene for the HG:TC solution and in-house gel collected from the forearm of a healthy volunteer, mean \pm SD, n=5

Figure 5.7 illustrates the quantitative mass ratio $m_{\text{tazarotene}}/m_{\text{protein}}$ (mg/g protein) depth profiles of tazarotene in the HG:TC solution and in the in-house gel delivered into the skin. This was calculated using the previously determined proportionality constant

$C_{\text{tazarotene:protein}}^{-1}$ in chapter 3 and measured Raman ratios $\frac{R_{\text{Tazarotene}}}{R_{\text{protein}}}$ at each depth

from this study. Figure 5.7 shows that both formulations can be detected up to 20 μm into the skin. Statistical comparison of the two formulations reveals that the in-house gel delivered a significantly higher amount ($p < 0.05$) of tazarotene per gram of protein deeper into the skin than the HG:TC solution. These results agree with tape stripping data that also showed that the in-house gel outperformed the pure HG:TC solution.

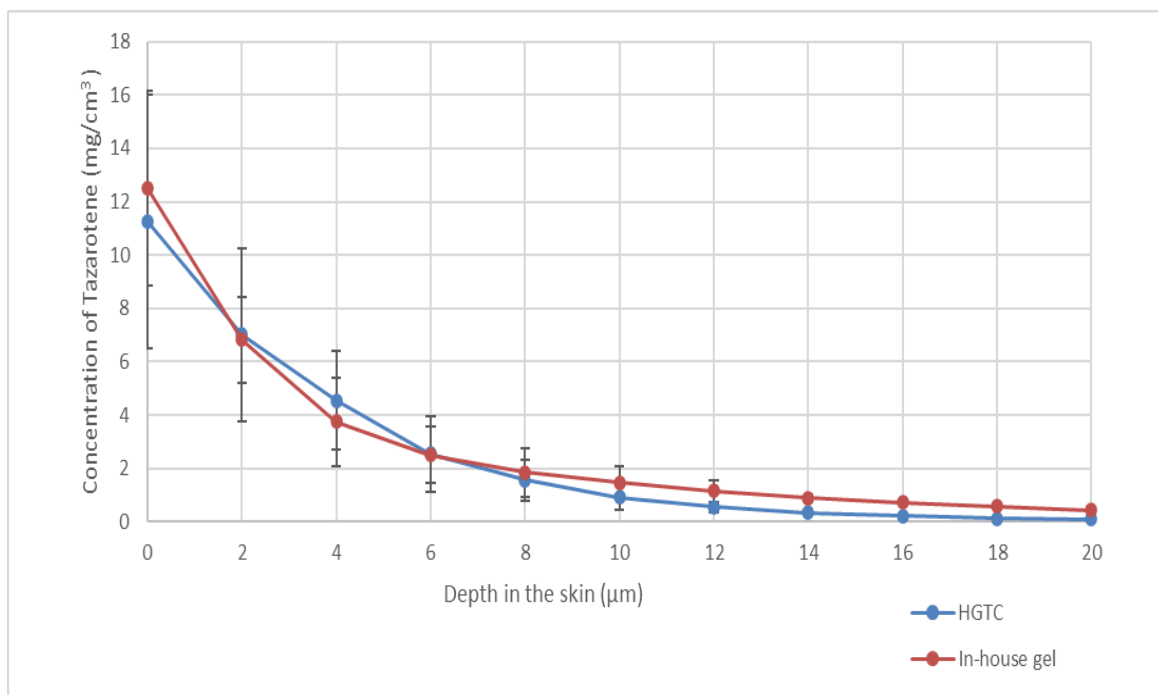


Figure 5.8 Concentration depth profiles of tazarotene in the HG:TC solution and in-house gel from the forearm of a healthy volunteer, mean \pm SD, $n=5$

Figure 5.8 illustrates the concentration of tazarotene following application in the HG:TC solution and in-house gel as mg/cm^3 calculated by using the mass ratio $m_{\text{tazarotene}}/m_{\text{protein}}$ (mg/g protein) depth profiles in figure 5.7 with equations 3.5 and 3.6

from chapter 3. The graph shows that the concentration of tazarotene from both formulations decreased with depth over the entire 20 μm of skin examined. Statistical comparison of the two formulations again revealed that the in-house gel delivered a significantly higher amount ($p < 0.05$) of tazarotene per cm^{-3} deeper into the skin than the HG:TC solution.

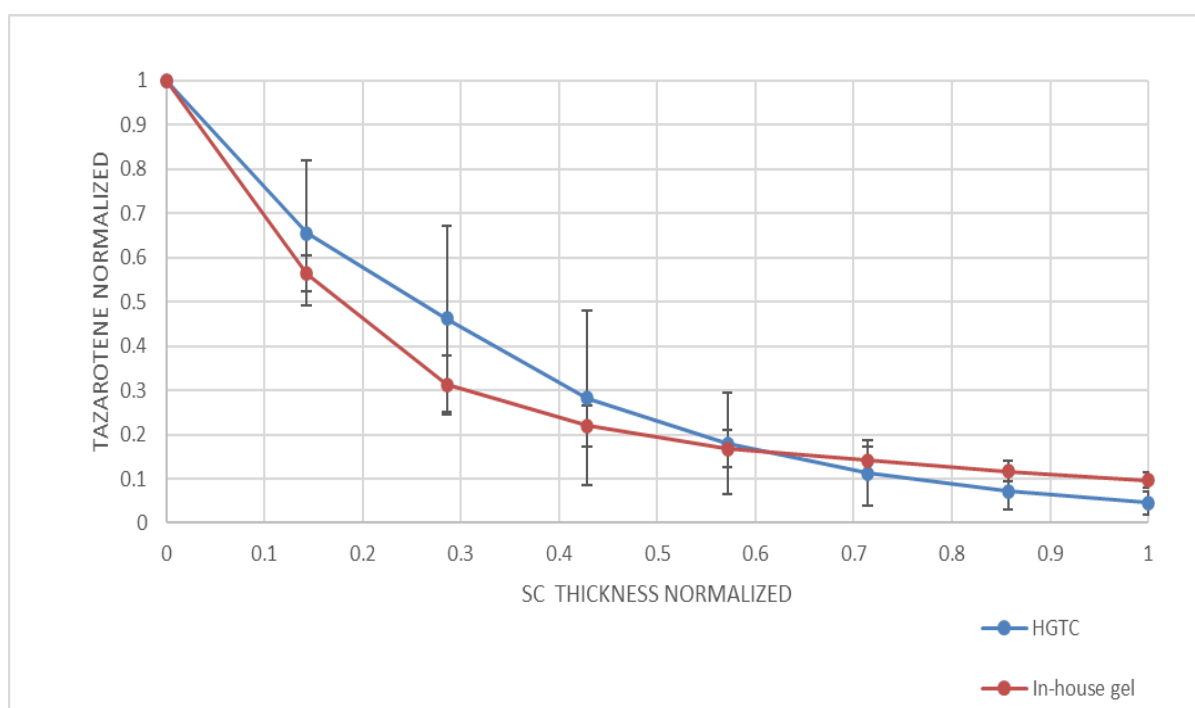


Figure 5.9 Normalised depth profiles of tazarotene following application in the HG:TC solution and in-house gel from the forearm of a healthy volunteer, mean \pm SD, n=5

Figure 5.9 illustrates the normalised depth profiles of the HG:TC solutions and in-house gel from the absolute Raman intensities of tazarotene and SC thickness calculated from the water content profile. The graph shows that both formulations were detected throughout the entire SC. The in-house gel was able to deliver a

significantly higher amount ($p < 0.05$) of tazarotene into the SC than the HG:TC solution. These results agree with both *in-vitro* data from Chapter 4 and tape stripping data in this chapter, which indicate that the in-house gel outperformed the pure HG:TC solution.

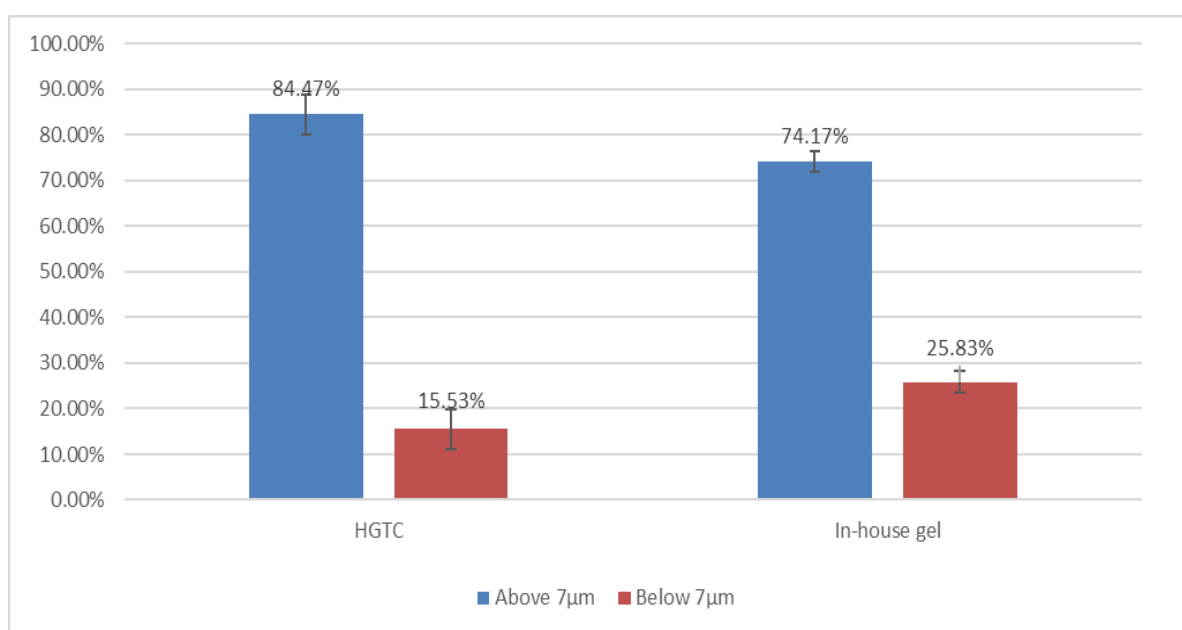


Figure 5.10 Proportion of tazarotene above and below a skin depth of 7 μm in the HG:TC solution and in-house gel from the forearm of a healthy volunteer, mean ± SD, n=5

Figure 5.10 illustrates the proportion of tazarotene quantified in the skin as the percentage above and below a depth of 7 μm. The greatest proportion of tazarotene found below 7 μm was delivered from the in-house gel with a value of $25.83 \pm 2.37\%$ while the HG:TC solution delivered 10.30% less tazarotene, $15.53 \pm 4.41\%$, below 7 μm into the skin. Statistical analysis of the two formulations reveals that the in-house gel delivered a significantly higher ($p < 0.05$) total amount of tazarotene deeper into the skin compared to the HG:TC solution. These results are consistent with Figure

5.9 which indicated the in-house gel was able to deliver more tazarotene into the SC than the HG:TC solution.

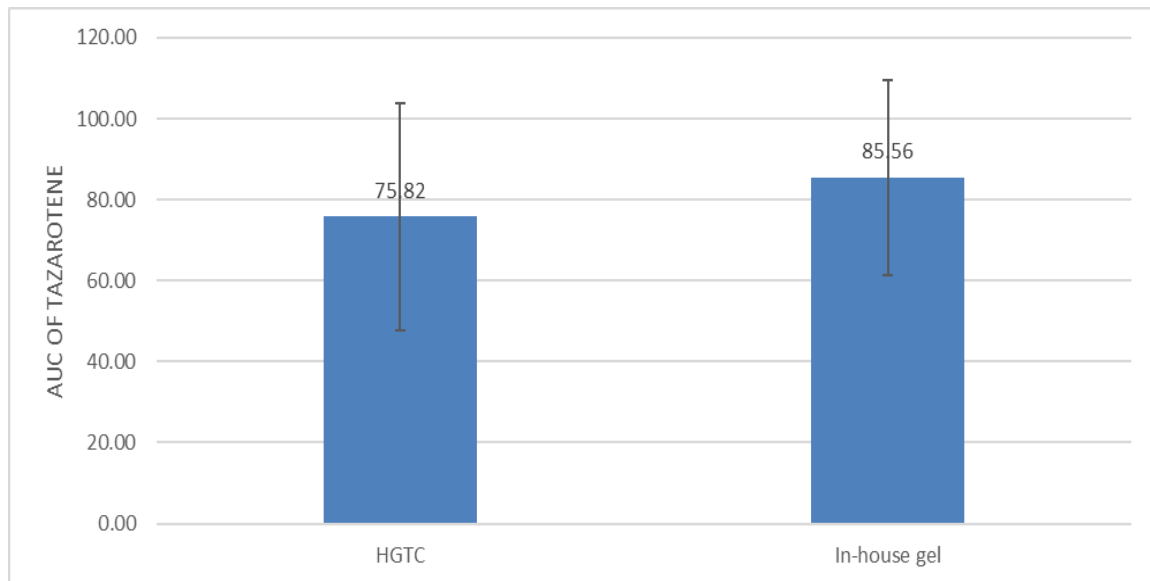


Figure 5.11 Total AUC of tazarotene delivered into the forearm of a healthy volunteer from the HG:TC solution and in-house gel, mean \pm SD, n=5

Figure 5.11 illustrates the total AUC of tazarotene measured in the skin from the HG:TC solution and in-house gel after 3 hours. The greatest amount of tazarotene found in the skin was delivered by the in-house gel with 85.56 ± 24.11 mg/cm² while the HG-TC solution delivered less tazarotene, 75.82 ± 28.14 , into the skin over the same period. Statistical comparison of the two formulations reveals that the in-house gel delivered a significantly higher amount ($p < 0.05$) of tazarotene into the skin overall. These results are again consistent with *in-vitro* data from Chapter 4 and tape

stripping data, which showed that the in-house gel was able to deliver the most tazarotene into the skin compared to the HG:TC solution.

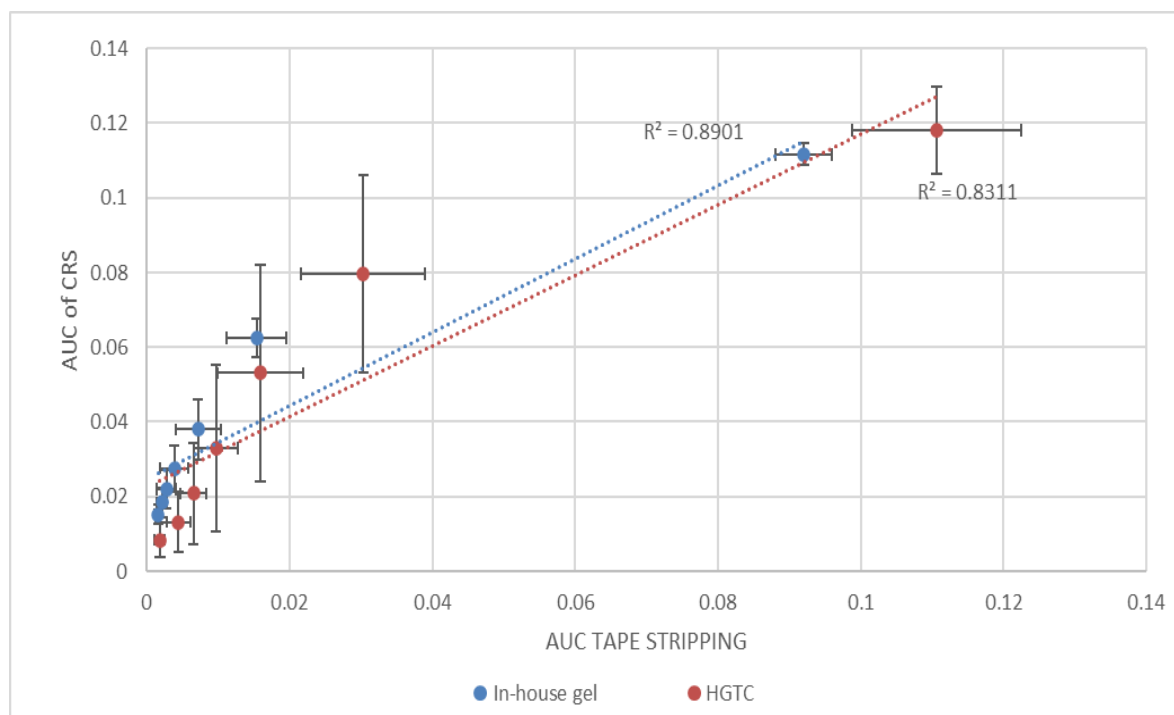


Figure 5.12 Correlation between the AUC of tazarotene in the SC detected *in-vivo* by CRS and LC-MS delivered from the HG:TC solution and in-house gel, mean + SD, n=5

Figure 5.12 illustrates the comparisons between the AUC of tape stripping depth profiles and the AUC of CRS depth profiles of tazarotene in the skin. The graph shows that, as the amount of tazarotene detected by LC-MS on each tape strip decreased, the amount of tazarotene non-invasively detected by CRS at each skin depth also decreased. A strong linear correlation can be seen between the decreasing AUC of tazarotene detected by LC-MS and CRS in the skin delivered from the in-house gel ($R^2 = 0.89$) and HG:TC solution ($R^2 = 0.83$) indicating both

analytical techniques are in agreement with one another. Statistical analysis between LC-MS and CRS data from both in-house gel and HG:TC solution depth profiles did not reveal a significant difference ($p < 0.05$) between the two analytical techniques. These results provide further evidence for the use of CRS in the non-invasive analysis of drug penetration into the skin.

5.4 Conclusions

In-vivo experiments play a vital role in establishing the true efficacy of any formulation under development. In this chapter, LC-MS and CRS were used to first detect and then quantify finite doses of tazarotene applied to the forearm of healthy volunteers. The LC-MS analysis of tape-stripped skin was able to show the penetration of tazarotene into the skin from a binary solution of tazarotene in HG:TC and an in-house gel formulation containing the HG:TC carrier vehicle. As the number of tape strips removed increased, so did the TEWL measurements going from approximately 12g/m²h to 23 g/m²h for both the in-house gel and HG:TC solution indicating an identical loss of barrier function for all the healthy volunteers irrespective of the formulation applied to the skin. When comparing protein content the amount of protein removed from tape strips with the in-house gel formulation was significantly higher than that of the HG:TC formulation suggesting tazarotene penetrated further into the skin from the in-house gel. Additionally, the amount of SC removed from the tape strips with the in-house gel was also greater than from the HG:TC solution. A very strong correlation was observed between the amount of tazarotene measured by LC-MS and SC protein content calculated by densitometry on each tape strip for both the in-house gel and HG:TC solution. As the amount of SC removed increased the concentration of tazarotene decreased with a significant

amount of drug found deep within SC for both in-house gel and HG:TC solution suggesting successful penetration into the skin. In this work, non-invasive CRS analysis was used to measure water content throughout the SC and epidermis to calculate SC thickness by identifying water gradients in the skin through a linear process of diffusion. CRS depth profiles revealed a similar trend to tape stripping data as the in-house gel was shown to penetrate further into the skin in greater amounts than the HG:TC solution. The in-house gel and HG:TC solution both bypassed the SC to penetrate the epidermis. The amount of tazarotene below 7 μm delivered into the skin from the in-house gel was also significantly greater than from the HG:TC solution. Tape-stripping and CRS have both revealed significant differences between the delivery of tazarotene from the pure HG:TC solution and in-house gel formulation with the in-house gel showing superiority. The CRS and tape-stripping data indicated that tazarotene applied in both the HG:TC solution and in-house gel penetrated the SC after a 3 h application period. Permeation of tazarotene is thought to be driven by HG integrating into the hydrophilic regions between intercellular lipids while simultaneously having TC alter the solubility parameter of intercellular lipid domains allowing tazarotene to diffuse through the SC more readily. A strong correlation was observed between the AUC of tazarotene detected *in vivo* by LC-MS and CRS

delivered into the skin by the in-house gel and HG:TC solution further strengthening the use of CRS for real-time drug tracking into the skin.

Chapter Six:

Overall Conclusions and Further Work

Chapter Six

6.1 Overall conclusions

The engineering of a formulation is an extremely important part of any drug development process, with a rational formulation design approach being fundamental to maximising the efficacy of an API. Retinoids are compounds that exert their effects by binding to the retinoic acid receptor (RAR), with the RAR- γ subunit being the primary molecular target for retinoid therapeutic action and located predominantly in the human epidermis. The use of topical retinoids has shown positive effects in several dermatological conditions including psoriasis, acne and photoaging, but the use of older non-specific first- and second-generation retinoids is associated with unwanted side effects such as erythema, dryness, and itching and even a stinging pain.

Tazarotene was developed as a third-generation selective retinoid able to target the RAR- γ subunit to enhance the cellular effects of retinoid therapy whilst reducing the occurrence or severity of unwanted side effects. Topical delivery of tazarotene into the epidermis, however, remains a major challenge for formulation scientists due to its lipophilic nature with the complex tightly packed SC structure acting as the main barrier and rate-limiting step for delivery into the skin.

In this thesis, passive enhancement strategies were used to study the effects different combinations of CPEs have on the delivery of tazarotene into the skin. both *in-vitro* and *in-vivo*. Molecular modelling of tazarotene and selected CPEs HG, PG, PGMC, PGDC, TC, DiPG, IPM, PGML and MTC was performed to theoretically calculate solubility parameters for comparison with actual saturation solubilities. To analyse samples containing tazarotene a HPLC method was successfully developed and then validated. The HPLC method was first used to quantify the amount of tazarotene at saturation in the selected CPEs through solubility studies. The saturation solubility of tazarotene in the CPEs selected compared well with the solubility parameters calculated by molecular modelling. Tazarotene did not show any stability issues during 24 h stability studies in the selected CPEs or solubilizing agents throughout the entire examination period and thus tazarotene did not need any stabilising agents for it to be examined further.

Miscibility studies demonstrated that all CPEs were completely miscible with one another, except PGDC and MTC which were completely immiscible with both HG and PG. *In vitro* infinite dose Franz diffusion cell studies using porcine skin revealed that from the CPEs selected, combinations of HG, PG, TC, IPM and IPA significantly enhance the delivery of tazarotene into the skin, compared to the commercial Zorac®

gel formulation, with the binary HG:TC solvent system, succeeding to deliver the most amount of active into the skin.

A CRS method was developed to non-invasively detect and then quantify the amount of tazarotene deposited into the skin. *In-vitro* CRS experiments were used to examine the deposition of tazarotene and CPEs into porcine skin as well as their relationship with one another. The water concentration profile of porcine skin was determined using CRS and SC thickness calculated from the distinct water gradients in the skin. CRS data revealed that tazarotene in all simple binary and ternary solvent systems examined could penetrate significantly deeper into the skin in greater amounts than the commercial Zorac[®] gel formulation, with the HG:TC, HG:PG:TC and HG:IPM:IPA solutions, outperforming it.

By comparing CRS depth profiles of tazarotene, HG and PG, a very strong correlation was observed between the AUC of API and CPE in the SC at different depths, suggesting tazarotene follows the CPE into the skin. To perform finite dose *in-vitro* permeation studies, a new LC-MS method was developed and validated to quantify extremely small amounts of tazarotene in samples. The LC-MS method developed was significantly more sensitive than the previous HPLC method and could quantify tazarotene within the low nanogram range. *In-vitro* finite dose permeation studies using human skin showed that HG:TC and HG:PG:TC performed

the best for tazarotene delivery while binary and ternary solvent systems examined outperformed the commercial Zorac® gel formulation.

The consistently best-performing solvent system HG:TC was used as the main carrier vehicle of tazarotene in a new in-house gel formulation that was tested again through *in-vitro* finite dose permeation studies. The in-house gel formulation was found to further enhance the delivery of tazarotene into the skin, showing it could significantly outperform not only the commercial Zorac® gel formulation but also the binary and ternary solvent systems. DVS studies revealed that the in-house gel would continually evaporate over time until full depletion, resulting in a steady increase in tazarotene concentration within the in-house gel formulation. The commercial Zorac gel formulation, on the other hand, would stop evaporating after a short timeframe, causing tazarotene to recrystallize out of the formulation extremely quickly. The increased thermodynamic activity created by the slow but steady saturation of tazarotene within the in-house gel is believed to be a major contributing factor to its enhanced delivery into the skin.

Comparing *in-vitro* LC-MS and CRS results suggests a strong correlation between the amount of tazarotene extracted from the skin and non-invasively detected in the skin for all formulations examined. *In-vivo* tape stripping experiments were conducted by applying the tazarotene in HG:TC solution and in-house gel to the

forearm of healthy volunteers. A strong correlation was observed between the amount of tazarotene and SC protein content on each tape strip throughout the SC. LC-MS and densitometry results suggest that tazarotene significantly penetrated the skin from both formulations investigated, with the in-house gel outperforming the HG:TC binary solution. *In-vivo* CRS analysis was used to non-invasively measure the SC thickness and amount of tazarotene deposited in the skin of a healthy volunteer. CRS results suggested the in-house gel formulation delivered more tazarotene further into the skin than the pure HG:TC binary solution with both formulations successfully able to deliver tazarotene through the SC after a 3 h application.

A strong correlation was observed between the amount of tazarotene detected by LC-MS on each tape strip and detected by CRS in the skin, adding further evidence for the use of CRS to non-invasively monitor penetration of APIs and excipients into the skin from topically applied formulations in real-time.

6.2 Future work

The long-term stability of tazarotene within the in-house gel could be examined through accelerated stability studies. The in-house gel can then be further developed to incorporate other excipients to prevent tazarotene degradation and to maintain its concentration, making it suitable for long-term storage use. The new gel formulations

could then be tested again through accelerated stability studies to assess and compare their shelf-life. Tazarotene deposition into the skin from the new gel formulations could be examined first *in-vitro* through Franz diffusion cell studies and then *in-vivo* by tape stripping using human volunteers.

Further work could also be done to better understand how both TC and HG enhance the delivery of tazarotene into the skin. LC-MS methods could be developed to detect and quantify both TC and HG in samples. The new methods can then be used to analyse both *in-vitro* and *in-vivo* samples from permeation and tape-stripping studies of the new gel formulations. Further *in-vivo* CRS studies could also be conducted to non-invasively track and quantify the deposition of tazarotene, HG and TC delivered into the skin from the new gel formulations in a larger sample size of healthy volunteers. Potential collaborations can be established with dermatology colleagues to initiate clinical trials to evaluate the efficacy of the in-house gel in treating dermatological conditions such as acne and psoriasis.

References

- Alberti, I., et al. (2001). "Effect of ethanol and isopropyl myristate on the availability of topical terbinafine in human stratum corneum, in vivo." International Journal of Pharmaceutics **219**(1-2): 11-19.
- Anigbogu, A. N. C., et al. (1995). "Fourier-transform Raman-spectroscopy of interactions between the penetration enhancer dimethyl sulfoxide and human stratum-corneum." International Journal of Pharmaceutics **125**(2): 265-282.
- Anja, T., et al. (2008). "Topical retinoids in acne – an evidence-based overview." JDDG: Journal der Deutschen Dermatologischen Gesellschaft **6**(12): 1023-1031.
- Barbero, A. M. and H. F. Frasch (2009). "Pig and guinea pig skin as surrogates for human in vitro penetration studies: A quantitative review." Toxicology in Vitro **23**(1): 1-13.
- Barry, B. W., et al. (1992). "Fourier transform Raman and infrared vibrational study of human skin: Assignment of spectral bands." Journal of Raman Spectroscopy **23**: 641-645.
- Benson, H. A. E. (2012). "Skin Structure, Function, and Permeation." Topical and Transdermal Drug Delivery. : 1-22.
- Bhate, K. and H. C. Williams (2013). "Epidemiology of acne vulgaris." British Journal of Dermatology **168**(3): 474-485.
- Blomhoff, R. and H. K. Blomhoff (2006). "Overview of retinoid metabolism and function." Journal of Neurobiology **66**(7): 606-630.
- Boehncke, W.-H. and M. P. Schön (2015). "Psoriasis." The Lancet **386**(9997): 983-994.
- Bogdanic (2006). "Group contribution methods for estimating the properties of polymer systems." Hemijaska industrija **60**: 11-12.
- Bommannan, D., et al. (1990). "Examination of stratum-corneum barrier function in vivo by infrared-spectroscopy." Journal of Investigative Dermatology **95**(4): 403-408.
- Bos, J. D. and M. Meinardi (2000). "The 500 Dalton rule for the skin penetration of chemical compounds and drugs." Exp Dermatol **9**(3): 165-169.

Brinkmann, I. and C. C. Muller-Goymann (2003). "Role of isopropyl myristate, isopropyl alcohol and a combination of both in hydrocortisone permeation across the human stratum corneum." Skin Pharmacology and Applied Skin Physiology **16**(6): 393-404.

Brinkmann, I. and C. C. Muller-Goymann (2005). "An attempt to clarify the influence of glycerol, propylene glycol, isopropyl myristate and a combination of propylene glycol and isopropyl myristate on human stratum corneum." Pharmazie **60**(3): 215-220.

Brouwers, J., et al. (2009). "Supersaturating Drug Delivery Systems: The Answer to Solubility-Limited Oral Bioavailability?" Journal of Pharmaceutical Sciences **98**(8): 2549-2572.

Bucks, D., et al. (2008). Percutaneous Penetration and Mass Balance Accountability: Technique and Implications for Dermatology.

Byrd, A. L., et al. (2018). "The human skin microbiome." Nature Reviews Microbiology **16**(3): 143-155.

Caspers, P. J., et al. (2000). "Automated depth-scanning confocal Raman microspectrometer for rapid in vivo determination of water concentration profiles in human skin." Journal of Raman Spectroscopy **31**(8-9): 813-818.

Caspers, P. J., et al. (2001). "In vivo confocal Raman microspectroscopy of the skin: Noninvasive determination of molecular concentration profiles." Journal of Investigative Dermatology **116**(3): 434-442.

Caspers, P. J., et al. (1998). "In vitro and in vivo Raman spectroscopy of human skin." Biospectroscopy **4**(5): S31-S39.

Caspers, P. J., et al. (1999). In vivo Raman spectroscopy of human skin: determination of the composition of natural moisturizing factor. Biomedical application of Raman spectroscopy proceeding of. **3608**: 99-102.

Caspers, P. J., et al. (2019). "Method to quantify the in vivo skin penetration of topically applied materials based on confocal Raman spectroscopy." Translational Biophotonics **1**(1-2): e201900004.

Chandraratna, R. A. (1996). "Tazarotene--first of a new generation of receptor-selective retinoids." Br J Dermatol **135** Suppl **49**: 18-25.

Chandraratna, R. A. S. (1998). "Rational design of receptor-selective retinoids." Journal of the American Academy of Dermatology **39**(4, Supplement): S124-S128.

Choi, P., et al. (1992). "Estimation of the three-dimensional solubility parameters of alkyl phenol ethoxylates using molecular dynamics." Journal of Colloid and Interface Science **150**(2): 386-393.

Darvin, M. E., et al. (2009). "In vivo distribution of carotenoids in different anatomical locations of human skin: comparative assessment with two different Raman spectroscopy methods." Exp Dermatol **18**(12): 1060-1063.

de Lera, A. R., et al. (2017). "Design of selective nuclear receptor modulators: RAR and RXR " Nature Reviews Drug Discovery **6**(10): 811-820.

Dias, M., et al. (2007). "Influence of membrane-solvent-solute interactions on solute permeation in model membranes." International Journal of Pharmaceutics **336**(1): 108-114.

Dick, I. P. and R. C. Scott (1992). "Pig ear skin as an in-vitro model for human skin permeability." Journal of Pharmacy and Pharmacology **44**(8): 640-645.

Downing, D. T., et al. (1987). "Skin lipids - An update " Journal of Investigative Dermatology **88**(3): S2-S6.

Draelos, Z. D. and M. M. Draelos (2021). "Development of a Tape-Stripping Liquid Chromatography-Mass Spectrometry Method for Evaluating Skin Deposition of Topical Tazarotene." Journal of Drugs in Dermatology **20**(10): 1105-1111.

Escobar-Chavez, J. J., et al. (2008). "The tape-stripping technique as a method for drug quantification in skin." Journal of Pharmacy and Pharmaceutical Science **11**(1): 104-130.

Fabian, H. and P. Anzenbacher (1993). "New developments in Raman-spectroscopy of biological systems." Vibrational Spectroscopy **4**(2): 125-148.

Fasano, W. J., et al. (2005). "Penetration of ammonium perfluorooctanoate through rat and human skin in vitro." Drug and Chemical Toxicology **28**(1): 79-90.

Filon, F. L., et al. (2011). "Human skin penetration of gold nanoparticles through intact and damaged skin." Nanotoxicology **5**(4): 493-501.

Franz, T. J. (1975). "Percutaneous absorption - relevance of in-vitro data." Journal of Investigative Dermatology **64**(3): 190-195.

Franz, T. J., et al. (1993). "Percutaneous penetration of n-nitrosodiethanolamine through human skin (in-vitro) - comparison of finite and infinite dose applications from cosmetic vehicles." Fundamental and Applied Toxicology **21**(2): 213-221.

Frasch, H. F. and A. M. Barbero (2009). "A paired comparison between human skin and hairless guinea pig skin in vitro permeability and tag time measurements for 6 industrial chemicals." Cutaneous and Ocular Toxicology **28**(3): 107-113.

Frasch, H. F. and A. M. Barbero (2018). "In vitro human skin permeation of benzene in gasoline: Effects of concentration, multiple dosing and skin preparation." Journal of Exposure Science and Environmental Epidemiology **28**(2): 193-201.

Friend, D. R. (1992). "In vitro skin permeation techniques." Journal of Controlled Release **18**(3): 235-248.

Frigoli, S., et al. (2005). "A Practical and Efficient Process for the Preparation of Tazarotene." Organic Process Research & Development **9**(5): 646-650.

Gioia, F. and L. Celleno (2002). "The dynamics of transepidermal water loss (TEWL) from hydrated skin." Skin Research and Technology **8**(3): 178-186.

Goldsmith, L. A. (1991). Physiology, biochemistry, and molecular biology of the skin, Oxford University Press.

Green, J. M. (1996). "Peer Reviewed: A Practical Guide to Analytical Method Validation." Analytical Chemistry **68**(9): 305A-309A.

Gregoriou, S., et al. (2014). "Use of tazarotene foam for the treatment of acne vulgaris." Clinical Cosmetic and Investigational Dermatology **7**: 165-170.

Hadgraft, J. (1989). Mathematical - models of skin absorption. Conf on Prediction of Percutaneous Penetration : Methods, Measurements, Modelling, Univ Manchester, Inst Sci & Technol, Manchester, England.

Hadgraft, J. (2001). Permeation routes through human skin. 10th Congress of the European-Academy-of-Dermatology-and-Venereology, Munich, Germany.

Hadgraft, J. (2004). "Skin deep." European Journal of Pharmaceutics and Biopharmaceutics **58**(2): 291-299.

Hadgraft, J. and M. E. Lane (2009). "Transepidermal water loss and skin site: A hypothesis." International Journal of Pharmaceutics **373**(1-2): 1-3.

Hadgraft, J. and M. E. Lane (2011). "Skin: the ultimate interface." Physical Chemistry Chemical Physics **13**(12): 5215-5222.

Hadgraft, J. and M. E. Lane (2012). "Skin penetration and formulation design." International Journal of Cosmetic Science **34**(4): 370-370.

Hadgraft, J. and K. Walters (1994). "Skin penetration enhancement." Journal of Dermatological Treatment **5**(1): 43-47.

Han, A., et al. (2014). "Photoaging." Dermatologic Clinics **32**(3): 291.

Hansen (1967). "The three-dimensional solubility parameter - key to paint component affinities: solvents, plasticizers, polymers, and resins. II. Dyes, emulsifiers, mutual solubility and compatibility, and pigments. III. Independent calculation of the parameter components" " Journal of Paint Technology **39**(511): 505-510.

Harrison, J. E., et al. (1996). "The relative effect of Azone(R) and Transcutol(R) on permeant diffusivity and solubility in human stratum corneum." Pharmaceutical Research **13**(4): 542-546.

Herkenne, C., et al. (2006). "Pig ear skin ex vivo as a model for in vivo dermatopharmacokinetic studies in man." Pharmaceutical Research **23**(8): 1850-1856.

Hildebrand, J. H. (1936). "Thermodynamic aspects of the theory of non-electrolytic solutions." Chemical Reviews **18**(2): 315-323.

Hughes, A. J., et al. (2021). "Tape strips in dermatology research." British Journal of Dermatology **185**(1): 26-35.

Iliopoulos, F., et al. (2022). "Dermal Delivery of Diclofenac Sodium-In Vitro and In Vivo Studies." Pharmaceutics **14**(10).

Jha, D. K., et al. (2021). "Effect of Hypromellose Acetate Succinate Substituents on Miscibility Behavior of Spray-dried Amorphous Solid Dispersions: Flory-Huggins Parameter Prediction and Validation." Carbohydrate Polymer Technologies and Applications **2**.

Joseph, M., et al. (1978). "Stability of pharmaceuticals." Journal of Pharmaceutical Sciences **67**(4): 443-465.

Jouyban, A., et al. (2011). "Solubility Prediction of Drugs in Mixed Solvents Using Partial Solubility Parameters." Journal of Pharmaceutical Sciences **100**(10): 4368-4382.

Kavassalis, T. A., et al. (1993). "The Calculation of 3D Solubility Parameters Using Molecular Models." Molecular Simulation **11**(2-4): 229-241.

Kezic, S., et al. (2008). "Loss-of-function mutations in the filaggrin gene lead to reduced level of natural moisturizing factor in the stratum corneum." Journal of Investigative Dermatology **128**(8): 2117-2119.

Koo, J., et al. (2003). "The efficacy of topical tazarotene monotherapy and combination therapies in psoriasis." Expert Opin Pharmacother **4**(12): 2347-2354.

Krueger, J. and A. Bowcock (2005). "Psoriasis pathophysiology: current concepts of pathogenesis." Annals of the Rheumatic Diseases **64**(Suppl 2): ii30-ii36.

Lam, H. (2004). Performance Verification of HPLC. Analytical Method Validation and Instrument Performance Verification: 173-185.

Lampe, M. A., et al. (1983). "Human epidermal lipids -characterization and modulations during differentiation." Journal of Lipid Research **24**(2): 131-140.

Lane, M. E. (2013). "Skin penetration enhancers." International Journal of Pharmaceutics **447**(1): 12-21.

Lane, M. E., et al. (2012). "Rational formulation design." International Journal of Cosmetic Science **34**(6): 496-501.

Lehman, P. A., et al. (2011). "Percutaneous Absorption in Man: In vitro-in vivo Correlation." Skin Pharmacology and Physiology **24**(4): 224-230.

Leopold, C. S. and B. C. Lippold (1995). "An attempt to clarify the mechanism of the penetration enhancing effects of lipophilic effects of lipophilic vehicles with differential scanning calorimetry (DSC)." Journal of Pharmacy and Pharmacology **47**(4): 276-281.

Leyden, J., et al. (2017). "Why Topical Retinoids Are Mainstay of Therapy for Acne." Dermatology and Therapy **7**(3): 293-304.

Liu, P., et al. (2009). "Effects of Isopropanol-Isopropyl Myristate Binary Enhancers on In Vitro Transport of Estradiol in Human Epidermis: A Mechanistic Evaluation." Journal of Pharmaceutical Science **98**(2): 565-572.

Lu, G. W., et al. (2004). "Raman scattering spectra of La₃Ga₅SiO₁₄ (LGS) crystals." Physica status solidi b-basic solid state physics **241**(2): 439-446.

Lucassen, G. W., et al. (1998). In vivo infrared- and Raman spectroscopy of human stratum corneum. Infrared Spectroscopy: New Tool In Medicine Proceedings of. **3257**: 52-61.

Lucassen, G. W., et al. (2000). Water content and water profiles in skin measured by FTIR and Raman spectroscopy. Controlling Tissue optical properties: application in clinical study. **4162**: 39-45.

Machui, F. and C. J. Brabec (2012). Solubility, Miscibility, and the Impact on Solid-State Morphology. Semiconducting Polymer Composites: 1-38.

Mahrhauser, D. S., et al. (2015). "Assessment of Raman spectroscopy as a fast and non-invasive method for total stratum corneum thickness determination of pig skin." International Journal of Pharmaceutics **495**(1): 482-484.

Makino, K., et al. (1992). "Membrane permeation under continuous elution of skin side of the membrane." Biophysical Chemistry **43**(1): 21-28.

MaoQiang, M., et al. (1996). "Optimization of physiological lipid mixtures for barrier repair." Journal of Investigative Dermatology **106**(5): 1096-1101.

Mateus, R., et al. (2013). "A new paradigm in dermatopharmacokinetics - Confocal Raman spectroscopy." International Journal of Pharmaceutics **444**(1-2): 106-108.

Mateus, R., et al. (2014). "Percutaneous absorption of salicylic acid - in vitro and in vivo studies." International Journal of Pharmaceutics **475**(1-2): 471-474.

Melot, M., et al. (2009). "Studying the effectiveness of penetration enhancers to deliver retinol through the stratum corneum by in vivo confocal Raman spectroscopy." Journal of Controlled Release **138**(1): 32-39.

Menon, G. K. (2002). "New insights into skin structure: scratching the surface." Advanced Drug Delivery Reviews **54**: S3-S17.

Menon, G. K., et al. (2012). "The structure and function of the stratum corneum." International Journal of Pharmaceutics **435**(1): 3-9.

Menter, A. (2000). "Pharmacokinetics and safety of tazarotene." Journal of the American Academy of Dermatology **43**(2): S31-S35.

Miles, R. B., et al. (2001). "Laser Rayleigh scattering." Measurement Science and Technology **12**(5): R33-R51.

Mitragotri, S., et al. (2011). "Mathematical models of skin permeability: An overview." International Journal of Pharmaceutics **418**(1): 115-129.

Mohamad, M., et al. (2012). Non Invasive Measurement of Skin Hydration and Transepidermal Water Loss in Normal Skin. 2012 IEEE Colloquium on Humanities, Science & Engineering Research (CHUSER 2012).

Mohammed, D., et al. (2014). "In Vitro-In Vivo Correlation in Skin Permeation." Pharmaceutical Research **31**(2): 394-400.

Mohammed, D., et al. (2012). "Comparison of gravimetric and spectroscopic approaches to quantify stratum corneum removed by tape-stripping." European Journal of Pharmaceutics and Biopharmaceutics **82**(1): 171-174.

Moser, K., et al. (2001). "Passive skin penetration enhancement and its quantification in vitro." European Journal of Pharmaceutics and Biopharmaceutics **52**(2): 103-112.

Ng, S. F., et al. (2010). "Validation of a Static Franz Diffusion Cell System for In Vitro Permeation Studies." AAPS Pharmscitech **11**(3): 1432-1441.

Norlen, L., et al. (1999). "Inter- and intra-individual differences in human stratum corneum lipid content related to physical parameters of skin barrier function in vivo." Journal of Investigative Dermatology **112**(1): 72-77.

Patel, A., et al. (2021). "In Vitro-In Vivo Correlation in Dermal Delivery: The Role of Excipients." Pharmaceutics **13**(4).

Pedersen, E. S., et al. (2019). Topical Retinoids for the Treatment of Photoaged Skin.

Pellanda, C., et al. (2006). "Topical bioavailability of triamcinolone acetonide: effect of dose and application frequency." Archives of Dermatological Research **298**(5): 221-230.

Petry, R., et al. (2003). "Raman Spectroscopy - A prospective tool in the life sciences." Chemphyschem **4**(1): 14-30.

Poon, F., et al. (2015). "Mechanisms and treatments of photoaging." Photodermatology Photoimmunology & Photomedicine **31**(2): 65-74.

Potts, R. O., et al. (1992). "Routes of Ionic permeability through mammalian skin." Solid State Ionics **53**: 165-169.

Pudney, P. D. A., et al. (2007). "An in vivo confocal Raman study of the delivery of trans-retinol to the skin." Applied Spectroscopy **61**(8): 804-811.

Puppels, G. J., et al. (1990). "A high-throughput Raman notch filter set." Review of Scientific Instruments **61**(12): 3709-3712.

Rawlings, A. V., et al. (1994). "Stratum-corneum moisturization at the molecular level." Journal of Investigative Dermatology **103**(5): 731-740.

Riahi, R. R., et al. (2016). "Topical Retinoids: Therapeutic Mechanisms in the Treatment of Photodamaged Skin." American Journal of Clinical Dermatology **17**(3): 265-276.

Roberts, M. S., Cross S.E., and Pellett M.A. (2002). Skin transport, in Dermatological and Transdermal Formulation, Marcel Dekker, Inc.: New York, Basel.

Robeson, L. M. (2007). Polymer blends : a comprehensive review. Munich ; Cincinnati, Hanser.

Savjani, K. T., et al. (2012). "Drug Solubility: Importance and Enhancement Techniques." ISRN Pharmaceutics **2012**: 195727.

Schmook, F. P., et al. (2001). "Comparison of human skin or epidermis models with human and animal skin in in-vitro percutaneous absorption." International Journal of Pharmaceutics **215**(1-2): 51-56.

Selzer, D., et al. (2013). "Finite and infinite dosing: Difficulties in measurements, evaluations and predictions." Advanced Drug Delivery Reviews **65**(2): 278-294.

Sil, B. C., et al. (2018). "Use of LC-MS analysis to elucidate by-products of niacinamide transformation following in vitro skin permeation studies." International Journal of Cosmetic Science **40**(5): 525-529.

Solanas, G. and S. A. Benitah (2013). "Regenerating the skin: a task for the heterogeneous stem cell pool and surrounding niche." Nature Reviews Molecular Cell Biology **14**(11): 737-748.

Stefanescu, D. M. (2015). Thermodynamic Concepts—Equilibrium and Nonequilibrium During Solidification. Science and Engineering of Casting Solidification. Cham, Springer International Publishing: 7-27.

Suhonen, T. M., et al. (1999). "Chemical enhancement of percutaneous absorption in relation to stratum corneum structural alterations." Journal of Controlled Release **59**(2): 149-161.

Tang-Liu, D. D., et al. (1999). "Clinical pharmacokinetics and drug metabolism of tazarotene: a novel topical treatment for acne and psoriasis." Clin Pharmacokinet **37**(4): 273-287.

Tanveer, M. A., et al. (2023). "Molecular basis of skin photoaging and therapeutic interventions by plant-derived natural product ingredients: A comprehensive review." Heliyon **9**(3): e13580.

Temova Rakuša, Ž., et al. (2021). "Retinoid stability and degradation kinetics in commercial cosmetic products." J Cosmet Dermatol **20**(7): 2350-2358.

Thielitz, A. and H. Gollnick (2008). "Topical retinoids in acne vulgaris: update on efficacy and safety." American Journal of Clinical Dermatology **9**(6): 369-381.

Touitou, E. (2002). "Drug delivery across the skin." Expert Opinion on Biological Therapy **2**(7): 723-733.

Tsai, J. C., et al. (1992). "Drug and vehicle deposition from topical application - use of in-vitro mass balance technique with minoxidil solutions." Journal of Pharmaceutical Sciences **81**(8): 736-743.

van de Kerkhof, P. C. M. (2006). "Update on retinoid therapy of psoriasis in: an update on the use of retinoids in dermatology." Dermatologic Therapy **19**(5): 252-263.

Van Lierde, V., et al. (2006). "In vitro permeation of chromium species through porcine and human skin as determined by capillary electrophoresis-inductively coupled plasma-sector field mass spectrometry." Anal Bioanal Chem **384**(2): 378-384.

Voegeli, R., et al. (2007). "Efficient and simple quantification of stratum corneum proteins on tape strippings by infrared densitometry." Skin Research and Technology **13**(3): 242-251.

Vonzglinicki, T., et al. (1993). "Water and ion distribution profiles in human skin." Acta Dermato-Venereologica **73**(5): 340-343.

Walters, K. A. (2002). Dermatological and transdermal formulations. New York, M. Dekker.

Warner, R. R., et al. (1988). "Electron-probe analysis of human skin element concentration profiles." Journal of Investigative Dermatology **90**(1): 78-85.

Warren, E. W. and U. Khanderia (1989). "Use of retinoids in the treatment of psoriasis." Clin Pharm **8**(5): 344-351.

Watkinson, A. C. and K. R. Brain (2002). "Basic mathematical principles in skin permeation (Reprinted from Dermatological and Transdermal Formulations, pg 61-88, 2001)." Journal of Toxicology-Cutaneous and Ocular Toxicology **21**(4): 371-402.

Weindl, G., et al. (2006). "Receptor-Selective Retinoids for Psoriasis." American Journal of Clinical Dermatology **7**(2): 85-97.

Weinstein, G. D. (1997). "Tazarotene gel: Efficacy and safety in plaque psoriasis." Journal of the American Academy of Dermatology **37**(2, Part 3): S33-S38.

Wertz, P. W. (2000). "Lipids and barrier function of the skin." Acta Dermato-Venereologica: 7-11.

Wickett, R. R. and M. O. Visscher (2006). "Structure and function of the epidermal barrier." American Journal of Infection Control **34**(10, Supplement): S98-S110.

Williams, A. C. and B. W. Barry (2001). "Raman spectroscopy (Reprinted from Percutaneous Adsorption, pg 499-514, 1999)." Journal of Toxicology - cutaneous and Ocular Toxicology **20**(4): 497-511.

Williams, A. C. and B. W. Barry (2004). "Penetration enhancers." Advanced Drug Delivery Reviews **56**(5): 603-618.

Williams, A. C. and B. W. Barry (2012). "Penetration enhancers." Advanced Drug Delivery Reviews **64**: 128-137.

Zasada, M. and E. Budzisz (2019). "Retinoids: active molecules influencing skin structure formation in cosmetic and dermatological treatments." Postepy Dermatol Alergol **36**(4): 392-397.

Zsikó, S., et al. (2019) Methods to Evaluate Skin Penetration In Vitro. Scientia Pharmaceutica **87**,
DOI: 10.3390/scipharm87030019